Dark Energy in Child Universes and Cold Dark Matter Detection

Thesis submitted in partial fulfillment
of the requirements for the degree of
Doctor of Philosophy

Submitted by
Idan Shilon

Supervisor
Prof. Eduardo Guendelman

אוניברסיטת
בן-גוריון בנגב

Department of Physics
Faculty of Natural Sciences
Ben-Gurion University of the Negev

November 6, 2011

Acknowledgements

First and most importantly, I am grateful to my supervisor, Eduardo Guendelman. Eduardo's work provided the foundation from which many of the ideas in this thesis were derived from. I thank him for encouraging me to carry out our joint work while allowing me to independently develop as a young scientist. I appreciate his polite and courteous manner with which he always treated me. And I am ever thankful for his everlasting patience during countless hours of fascinating discussions, where he guided and encouraged me through my first steps in science. For all these and much more I am forever indebted.

I also thank all my teachers at the department of physics, who enriched and broadened my physical understanding and knowledge, each from his own perspective, during classes as well as through stimulating discussions. I am mostly grateful to Ram Brustein, Aharon Davidson and Michael Gedalin.

I owe a great deal of gratitude to my collaborator, Stefano Ansoldi, with which it was a great experience and a pleasure to work. I also appreciate the kind hospitality he offered me during my visit to Udine University.

I greatly appreciate the hospitality, help, support and encouragement I received from all my collaborators at CERN. A particular mention includes Stephan Russenschuck, who agreed to supervise this unusual project and patiently taught me the basic concepts of magnet design; Alexey Dudarev, who supported my ideas about the analysis of the NGAH magnet and helped me carry them out; Igor Irastorza, who helped me to understand the practical requirements of the NGAH as a whole and to comprehend the big picture; Shlomo Caspi, for his patient explanations during many discussions and Biljana Lakic, for her constant support and encouragement. I am especially thankful to Konstantin Zioutas, who had faith in me and offered me the opportunity for this

amazing experience and for supporting me during all that time.

To the departmental administrative staff, Lili Ohayon and Aviva Friedman, for their willing to help in any matter, small as large, always in a kind, welcoming, willing and prompt manner.

I am also thankful to my colleagues at the department of physics, mostly to Shay Leizerovitch, Shimon Rubin, Ido Ben-Dayan and Ilya Gurwich, for advising, arguing, reading, criticizing, supporting and encouraging.

And last but not least, I wish to thank my family, Orit, Avi and Mor, who believed in me, supported me and accompanied me along the way.

Abstract

The work presented in this thesis deals with two fundamental subjects. One subject deals with cosmological physics and involves the study of two dimensional extended objects features and dynamics in general relativistic scenarios: The formation of domain walls can be caused, for example, by a spontaneous symmetry breaking of a discrete symmetry at a phase transition. This situation may be realized in the very early universe, when the universe has cooled down through some critical temperature and the scalar field dominating the universe acquired a non-zero value. Therefore, the study of creation and evolution of domain walls may be significant for understanding the evolution of the universe.

To that end, we use models of thin shells, where the thickness of the shell is much smaller than any other length scale in the system, in order to study the ways in which they can induce stabilization of thin shells when an electromagnetic field is present and also how vacuum bubbles trigger the creation of child universes out of an almost empty space. The methods and the techniques which will be in use are presented and explained. In particular, we study the properties of a system consisting of an uncharged spherically symmetric two-dimensional extended object which encloses a stationary point charge placed in the shell's center. We show that there can be a static and stable configuration for the neutral shell, using only the gravitational field of the charged source as a stabilizing mechanism. We also analyze the dynamical possibilities, including the possibility of child universe creation. Then, we examine the possibility of unsuppressed creation of child universes at an arbitrarily small energy cost, i.e. from an almost empty space, for a number of general scenarios.

The other research topic presented here, concerns axion-photon conversion in 2+1 dimensions. This study explores a continuous axion-photon duality symmetry to view the axion and the photon in terms of complex scalar particles and anti-particles.

This novel formalism allows one to analyze the scattering of axions in an external magnetic field in two spatial dimensions in a relatively simple manner and to view it in a way which resembles a Stern-Gerlach experiment. We have used the particle-anti-particle 2D scattering formalism to calculate the axion-photon conversion probability for external magnetic fields with cylindrical symmetry and also for the scattering of axions in a quadrupole magnetic field. The guideline in this research is to obtain the expected conversion probabilities in different possible terrestrial experiments.

In this study, we calculate the total cross section for the production of photons from the scattering of axions by different forms of inhomogeneous cylindrical magnetic fields which can approximately be produced by a solenoidal current. These theoretical results are used to estimate the axion-photon conversion probability which could be expected in a reasonable experimental situation. We also study the scattering at a resonance $E_{axion} \sim m_{axion}$, which corresponds to the scattering from a δ-function and gives the most enhanced results. Then, we analyze the 2D scattering of axions from an accelerator like quadrupole magnet using the eikonal approximation in order to learn whether or not such a setup could serve as a new possible method for detecting axions in terrestrial experiments.

Lastly, we discuss some basic technological aspects and requirements from a Next Generation Axion Helioscope (NGAH). In particular, we discuss the ideal design of the NGAH magnet's geometry. Inspired by the huge barrel toroid design of the ATLAS experiment at CERN, we analyze some aspects of possible designs with toroidal geometry.

Contents

Part I

Preface

My doctorate studies have been developing through the research of two topics: One concerning cosmological objects known as general relativistic shells and another one studying axion-photon conversion in external magnetic fields. Although the initial proposal of my doctorate concerned the study of thin general relativistic shells, during my studies my supervisor, Prof. Eduardo Guendelman, introduced a novel formalism to analyze the axion-photon system by means of a duality symmetry in the axion-photon phase space. This new formalism has attracted my attention as an advanced and new way to discover the speculated axion. For this reason, I decided to work in parallel on the subjects of general relativistic shells and axion-photon conversion. Furthermore, our study of the novel axion-photon formalism was proved to be very fruitful and lead to a collaboration with Prof. Konstantin Zioutas of Patras University and CERN. Following this joint work, I was offered by Prof. Zioutas to visit CERN as a project associate for a period of 6 months (which was extended by one more month during my visit). The goal of this visit was to conduct a conceptual design study and optimization of the Next Generation Axion Helioscope (NGAH) magnet as a future possible replacement of the CAST experiment at CERN. The reason behind this, perhaps peculiar, transition from theory to experimental/technological aspects of axions hunt is my motivation to go deeper into axions research and to learn and gain experience in different aspects of it. The strong mathematical and theoretical background, established by my theoretical work will complete and complement the comprehension and understanding of the experimental and technological side of axion research. Indeed, my post-doctoral studies will be held at CERN as part of the NGAH collaboration, which these days is being established and founded and will consider both the theoretical and experimental/technological aspects of axions search.

As the title of my PhD proposal ("Thin Shells and How They Induce Stable Solitons and Child Universes Production") reads, the original plan of my doctorate period was to study the dynamics of 2+1D topological defects. General relativistic thin shells provide a non-trivial gravitational system, whose dynamics can be described by a set of equations with a clear geometrical meaning. This allows one, for example, to consider a finite sized elementary particle like structure while taking into account the effects of gravity. In principle, the basic concept uses a static and stable brane. Imposing the approximation that the thickness of the brane is much smaller than any other length scale in the system means that we consider a static, stable, general relativistic shell. The idea of an elementary particle with a finite size is very appealing. Quoting Dirac, such an idea may be ?the most natural concept that makes the total energy of the Coulomb field of the electron finite?. Of course, it is known from experiment that up to a scale of 10^{-16} cm, quarks and leptons behave as point-like objects.

Usually, attempts to describe finite sized static and stable shells use additional matter terms constrained to the brane's surface. Nonetheless, we have brought up the interesting question of whether it would be possible to obtain a static and stable configuration by pure gravitational means. Of course, additional fields must be present and we apply them by placing a source of electric field within the shell. Although we describe a finite-sized static and stable we do not pretend to claim that our model may be a candidate for an elementary particle with a finite size. Rather, we concentrate on the question of what scenarios will allow for a static configuration of a brane.

Furthermore, another, perhaps more intuitive, use of general relativistic shells is within the context of cosmology. Cosmology, the study of the origin and evolution of our universe, greatly challenges our understanding of the laws of physics. Recent developments have enlightened the suggestive possibility that this challenge may be more concrete for us than we may have thought. Moreover, this may not be confined to the, remote in time, era when our universe was born. In general relativity, the dynamics of space-time is very rich. This, sometimes, pushes one to face situations which seem counterintuitive

when interpreted with a Newtonian mind. An example for such a situation is the realization of child universes. Child universes are regions of space-time that expand to an infinite radius without displacing, and in fact affecting in any way, the surrounding space-time. This situation is realized when the presence of wormhole is allowed in the global manifold. Then, the shell can expand by making its own space, provided it is located in the wormhole region of the global manifold. Various models of child universe creation realize, indeed, the possibility that the process could be taking place spontaneously in our vacuum at all times. Moreover, the additional possibility that it could also be realized as an induced effect in the laboratory compels us to a more detailed and in depth study of these models and their consequences. The child universe models are usually interesting in the inflationary models, where the shell can undergo an exponential growth, which recalls the exponential expansion of the early universe during the inflationary era.

However, current models of child universes feature a mass threshold which requires the shell to be massive enough in order to evolve into a child universe. This motivates us to ask if this threshold is inevitable, or would it be possible for a child universe to be realized when its mass is arbitrary. Then, the external observer, located in the surrounding space-time, would have a difficulty sensing the presence of this low-energy object. Therefore, in other words, we ask whether child universes may be emerged from an almost empty space. These solutions of child universe scenarios are intended in the broader sense of regions of space-time disconnecting from an ambient space and may be relevant also outside the inflationary scenario in common cosmology.

The Nobel prize in physics for 2011, was very recently awarded to Perlmutter, Schmidt and Riess for the discovery of the accelerating expansion of the universe through observations of distant supernovae. This accelerated expansion accounts for what we call today dark energy. Dark energy was originally introduced by Einstein and de-Sitter as the cosmological constant. In 1980, Alan Guth proposed that a negative pressure field, similar in concept to dark energy, could drive cosmic inflation in the very early

universe, as can also be realized by child universes in inflationary scenarios. It turns out that roughly 70% of the Universe is dark energy. Ordinary matter adds up to about 5% and dark matter makes up about 25%. Dark matter neither emits nor scatters light or other electromagnetic radiation and so cannot be directly detected via optical or radio astronomy. Its existence is inferred from gravitational effects on visible matter and gravitational lensing of background radiation. It was originally hypothesized to account for discrepancies between calculations of the mass of galaxies, clusters of galaxies and the entire universe made through dynamical and general relativistic means. Many experiments to detect dark matter through non-gravitational means are underway.

Light bosons, such as axions, are among the most promising candidates to solve the dark matter problem of cosmology as well as the strong CP problem in QCD. In addition, other axion like particles have been considered in order to solve puzzles related to the cosmic gamma ray background. While such particles play a central role in the very foundations of contemporary physics they, so far, have not been detected and therefore their existence is still speculative. In the work presented here, we seek new means to detect these particles, or at least to put better limits on their existence over a wider range of parameter space. More specifically, we shall extend and develop new means for axion detection via a beam splitting effect. This effect, which makes sense in at least 2 spatial dimensions, is evident from a novel formalism which introduces an axion-photon duality symmetry when an external magnetic field is present and when the axion mass is neglected. This symmetry allows one to examine the behavior of axions and photons in external magnetic fields in terms of an axion-photon complex field, as this complex field obtains the same scattering amplitude as the amplitude for axion-photon conversion.

Part II of this thesis deals with the analysis of general relativistic shell dynamics. Sections 1, 2 and 3 serve as an introduction and a review of the methods currently being used to study such a system. In particular, we shall explain more coherently and in greater detail the ways to obtain a child universe solution and also the necessary means to obtain a static and stable configuration. We shall explain and obtain Israel's junc-

tion conditions, which yield the equation of motion for an embedded brane, by using the Gauss-Codacci formalism and explain how these junction conditions are sufficient to provide a full description of the brane dynamics. Section 4 introduces a new way for achieving stabilization of a two dimensional extended object using the gravitational effects from a massive charged source on an *uncharged* spherical shell. Therefore, the stabilization is induced purely from gravitational effects. Section 5 analyzes the ways to obtain unsuppressed creation of child universes out of almost empty space.

Part III concerns new methods for the detection of axions (and axion like particles) using the novel particle-anti-particle formalism. In section 6 we present a thorough introduction of axion theory, starting with a discussion on the strong CP problem and its solution by Peccei and Quinn. We then discuss the different axion models relevant to this work and explain shortly the current bounds on invisible axion models. Section 7 introduces the new axion-photon duality symmetry, while in section 8 we use this formalism to obtain measurable quantities for a possible terrestrial experiments using magnetic field with solenoidal symmetry. In section 9 we obtain the axion-photon conversion probability from an accelerator like quadrupole magnet, as this setup was recently proposed as a possible experiment that will extend the current limits of axions search.

Part IV gives an introductory summary of the requirements from a Next Generation Axion Helioscope magnet. This part is a short and simple review of the work I have conducted at CERN. It may be viewed, perhaps, as an appendix which broadens Part III. However, it is presented as an independent part because of the technological nature of this subject. It is written so that merely general knowledge in physics is required to understand it since we have kept the more subtle issues like cold mass design, stress analysis along magnet's coils, cryogenics and protection systems, etc. out of this thesis.

Part II

Thin Shells and How They Induce Stable Solitons and Child Universes Production

1. INTRODUCTION

The formation of global or local topological defects, and in particular domain walls, is known to happen during a spontaneous symmetry breaking of a discrete symmetry at a phase transition, when a nontrivial topology exists. In the cosmological context, these objects are likely to occur in the very early universe, when the universe has cooled down through some critical temperature and the scalar field dominating the universe acquired a non-zero value. Therefore, domain walls might have important implications for the creation and evolution of our universe [1, 2].

Loosely speaking, domain walls exist when space-time has two or more regions. The common structure of the models we shall use to analyze the dynamics of domain walls is made of a spherically symmetric wall positioned at the radius $R(\tau)$, where τ is the proper time of an observer moving along with the domain wall. This shell of matter-energy Σ is the intersection of both space-time manifolds $\mathcal{M}_{\pm}$ (i.e. the interior and exterior, represented by the $-$ and $+$ subscripts, respectively), so that $\mathcal{M}_{-} \cap \mathcal{M}_{+} = \Sigma$. Furthermore, the thin-wall approximation, which considers the thickness of the wall to be infinitely small compared to all other length scales in the problem, is applied. In many models (particularly in the context of inflationary cosmology), the domain wall often encloses a false vacuum region in its interior $\mathcal{M}_{-}$ while the true vacuum region is at its exterior $\mathcal{M}_{+}$. Therefore, put more visually, these models are considering bubbles

of false vacuum. This system is also known as a thin general relativistic shell [3].
For definiteness, let us write the metric, which is static and adapted to the spherical symmetry (thus satisfying the relation $g_{rr}g_{tt} = -1$), in the two space-times (i.e. the interior and exterior of the bubble)

$$ds_{\pm}^2 = -A_{\pm}(r_{\pm})dt_{\pm}^2 + A_{\pm}^{-1}(r_{\pm})dr_{\pm}^2 + r_{\pm}^2 d\Omega_{\pm}^2 \ . \tag{1.1}$$

Due to the spherical symmetry, it is not restrictive to assume $\theta_- = \theta_+ = \theta$ and $\phi_- = \phi_+ = \phi$. Then, the shell can be described solely by its radius $R(\tau)$. Moreover, since we also have for the circumferential radius

$$R(\tau) = r_{\pm}|_{\Sigma} \ , \tag{1.2}$$

the continuity of the (induced) metric across Σ is realized. This allows for the dynamics of the shell to be analyzed by geometrical means, as we shall see in the following sections. Let us note that, equivalently, the induced metric on the brane will be well defined when the internal and external radii coincide on the brane (Eq. (1.2)). This is obtainable from the demand that the total area of the brane, as measured from both regions at the same proper time of the brane, will yield the same result. In addition to that, the time flow on either side of the domain wall has to satisfy

$$-A_+(R)dt_+^2 + A_+^{-1}(R)dR^2 = -A_-(R)dt_-^2 + A_-^{-1}(R)dR^2 \ . \tag{1.3}$$

The latter defines $-d\tau^2$ for an observer moving along with brane at fixed (θ, ϕ).
Several different models which apply the physical system we have just presented were suggested in the past. These models can generally be divided into two main categories: The first one analyzes the dynamics and evolution of the bubble, usually in the framework of inflationary cosmology. Many models of this category explore the creation of a "child

universe" (i.e. the process in which a new universe (the child universe) emerges from an existing one, usually referred to as the parent universe, in such a way that the structure of the parent universe is preserved) from a false vacuum bubble which detaches, classically or via tunneling, from the original space-time as it goes through an inflationary phase [4–9]. Models of the second category are looking for the possibility of obtaining a stable, elementary-particle-like, bubble. These models often utilize additional matter terms in the energy density of the domain wall or a negative surface tension (or both) [10–17].
The work presented in this part of the thesis is divided into two different branches, each of which can be related to one of the categories mentioned above. The first will explore the possibility of achieving a static and stable bubble purely from gravitational effects, while the second explores the interesting possibility of creating a child universe from an almost empty space.

1.1. Child Universes

The study of vacuum decay has began more than 30 years ago with the work of Callan and Coleman [18, 19]. In the following years interest in this subject has increased and the possible interplay of true vacuum bubbles with gravitation was also studied [20]. At the same time, and as opposed to the true vacuum bubble of Coleman et. al., false vacuum bubbles were also considered. The behavior of false vacuum bubbles with connection to gravity was first analyzed by Sato et. al. [21–24] and later also in [4] and [7]. In the original model, the universe was represented by an inner false vacuum core, surrounded by a shell-like true vacuum region, which was itself immersed in a false vacuum bulk. In this model the vacuum phase transition appears with an interesting and important connection to the formation of black holes and wormholes in the space-time structure (which is a crucial condition for the creation of child universes, as we shall see) [4, 25]. Not much later, a detailed analysis of the creation process of false vacuum bubbles appeared [22]. The relevance of thermal bubble nucleation, in conjunction with the

quantum production process, has also been emphasized, together with the important role that is played by primordial black/white holes and wormholes [23].

In inflationary cosmology, the consideration of the dynamics of an isolated false vacuum bubble leads to the concept of *child universes*. The latter is a common name for regions of space-time that expand up to an infinite size without displacing the surrounding space. For example, a natural and straightforward model of a false vacuum bubble is obtained by choosing a de Sitter space-time to describe the interior of the bubble and a Schwarzschild space-time to describe the exterior.

For a big enough bubble of false vacuum, the expansion to arbitrarily large values of the radius is inevitable despite the fact that the pressure difference (the false vacuum implies that the pressure in the interior is smaller than the pressure in the external region) and the existence of a positive surface tension on the domain prevent the bubble from expanding into the surrounding space. This, of course, is counterintuitive. Nevertheless, this scenario is indeed possible due to the presence of wormholes. The peculiar structure of the Kruskal extension makes it possible for the bubble to expand by making its own space, provided it is located in the wormhole region of the Schwarzschild space. When this situation is realized, the mechanical force that accelerates the wall, which is pushing from the outside to the inside, acts in the direction of *increasing* radius (i.e. towards the wormhole region in the Kruskal diagram) and supports the bubble's expansion. Then, as the bubble grows, the wormhole will get thiner until its throat will close entirely and the child universe will continue to grow disconnected from the parent space-time. Therefore, the growth of the child universe takes place without affecting in any way the evolution of the parent universe and the child universe is, in fact, growing by making its own space. In fact, the late time evolution of the child universe is classically hidden from an observer living in the parent universe by the presence of an event horizon. These observers will only witness the child universe's creation (at least classically) by looking into their very far past.

Often, models of the child universe scenario use a family of three parameters. These

parameters are the energy density inside the bubble Λ, a parameter describing the matter content on the surface of the bubble σ, and the total mass-energy as measured in the parent space-time M. Then, whether or not a child universe will be formed, depends on the values of these three parameters. For example, some generic choices of these parameters might not give birth to a child universe as there can be no solution where the bubble is small enough at earlier times and big enough at later times. This happens when, for instance, there is a potential barrier separating small bubble configurations from large ones. Put differently, a generic feature of the child universe models is the existence of the critical value M_{cr} for the total mass-energy in the parent space-time. When $M < M_{cr}$ the bubble will not be able to expand to infinity when starting from a small enough region. Thus, in order for a classical creation of a child universe to occur (i.e. tunneling is not taken into consideration in the process), M must be greater than the critical value M_{cr}. We will further discuss this subject in Sec. 3. However, as we will show in Sec. 5, models in which the mass threshold is avoided are also feasible and thus allow for the creation of a child universe from an almost empty space (i.e. for an arbitrarily small M).

1.2. Static and Stable Domain Walls

As mentioned before, the vacuum bubble will generally not be static and, in particular, spherical solutions of domain walls are usually unstable toward collapse. Nonetheless, prior studies have shown that some modifications of the effective surface tension (e.g radially dependent surface tension) [11, 12], as well as considerations of charged bubbles [13, 14], can yield a static and stable shell solution. However, this kind of stabilization takes place even before considering gravitational effects. Stable configurations of domain walls can give rise to many interesting physical models (e.g models for elementary particles). Hence, let us review and explain shortly the idea behind the possibility of obtaining a stationary domain wall.

Attempts to describe a stable elementary particle with a finite size began a long time ago (see for example the paper by Einstein from 1919 [15], where he proposed to describe an elementary particle as a bubble with an internal cosmological constant). The first brane model was suggested by Dirac in 1962 [16], where he thought of the electron as a charged conducting surface with a positive surface tension which balances the repulsive forces of the charge. However, in Dirac's paper, gravity was not considered. Yet, by using the so-called Israel junction conditions [3] (see Sec. 2) one can solve the corresponding problem with the presence of gravity.

As we will show in the next section, the equation of motion for a spherically symmetric domain wall is equivalent to the equation of motion of a particle moving in one dimension under the influence of a potential. Naturally, the dynamic coordinate is the trajectory of the bubble. If the surface tension of the bubble is constant, the effective potential will not have minima, and, therefore, one can not find a solution for a static and stable bubble. In order to obtain a local minimum in the effective potential, one should consider the more general case, where the surface tension of the domain wall σ is a function of the dynamic coordinate (i.e. $\sigma = \sigma(R)$). The radial dependence of the effective surface tension yields the possibility of obtaining a minimum value of the potential and, thus, a stable configuration.

There are many examples for ways to obtain a stable false vacuum bubble. Here, we shall shortly review the rather simple example of the model suggested by Guendelman and Portnoy (GP) [11]. In the GP model, one views an elementary particle as a 2+1 dimensional brane embedded in a 3+1 bulk. Next, a 2+1 gauge theory is introduced on the brane's surface. The action for the brane now takes the form

$$S = \sigma_0 \int \sqrt{-h} d^3y + \alpha \int \sqrt{-h} F_{ab} F^{ab} d^3y \ , \tag{1.4}$$

where a and b take the values 0,1,2 and $h = \det(h_{ab})$, where h_{ab} is the induced metric on the brane. For the spherically symmetric bubble, the simplest non-trivial potential

that respects the spherical symmetry (up to a gauge transformation) is the magnetic monopole configuration

$$A_\phi = f(1-\cos\theta) \ , \tag{1.5}$$

which implies that $F_{\theta\phi} = f\sin\theta$. The most general two dimensional spherically symmetric metric is given by

$$ds^2 = h_{ab}dy^a dy^b = -d\tau^2 + R^2(\tau)d\Omega^2 \ . \tag{1.6}$$

Therefore, we have $F_{ab}F^{ab} = 2f^2/R^4$, which means that the action can now be written as

$$S = 4\pi\sigma_0 \int R^2(\tau)d\tau + 8\pi\alpha \int \frac{f^2}{R^2(\tau)}d\tau = 4\pi \int \left(\sigma_0 + \frac{2\alpha f^2}{R^4(\tau)}\right) R^2(\tau)d\tau \ . \tag{1.7}$$

Hence, one can obtains an effective surface tension

$$\sigma(R) = \sigma_0 + \frac{2\alpha f^2}{R^4} = \sigma_0 + \frac{\sigma_1}{R^4} \ , \tag{1.8}$$

with $\sigma_1 = 2\alpha f^2$, where α is a constant. when one calculates the effective potential (as we shall do in the following sections) using the effective surface tension, $\sigma(R)$, one may find a local minimum of the potential (for $\alpha > 0$). This allows for a stable configuration for the false vacuum bubble.

Also, it is important to notice that the famous magnetic monopole solutions in the context of gauge theories are precisely stable bubbles of false vacuum [26].

2. ISRAEL JUNCTION CONDITIONS

General relativistic shells provide a non-trivial gravitational system, whose dynamics can be described by a set of equations with a clear geometrical meaning. In systems

with a high degree of symmetry the number of the equations of motion of the system is also significantly reduced. In particular, for a spherically symmetric $2+1$ dimensional shell the number of independent equations of motion is just one. Moreover, this single equation of motion is identical to that of a particle moving in one dimension under the influence of a potential. Hence, the problem of analyzing domain walls dynamics (in our spherically symmetric models) is reduced to analyzing the one dimensional effective potential. Because the usual starting point in our analysis of domain walls dynamics is the equation of motion itself for each specific problem, let us precede our analysis by providing a general derivation of it as an essential review for studying the dynamics of a generic shell of matter-energy.

Our generic system consists of a domain wall that splits the space-time into two spherically symmetric regions, for each of which Einstein's equations are assumed to be satisfied separately. The geometric property of the system manifests itself in the way that the domain wall is embedded in the two regions. In order to compare the two geometries we use the extrinsic curvature of the domain wall, induced by each of the two regions. The jump between the two extrinsic curvature tensors on the brane yields the equation of motion of the domain wall. This is done using the Gauss-Codacci formalism, which is a method of viewing four-dimensional space-time as being sliced up into three-dimensional hyper-surfaces [27].

The four dimensional Einstein Equations are

$$G_{\mu\nu} = R_{\mu\nu} - \frac{1}{2} g_{\mu\nu} R = 8\pi G T_{\mu\nu} \ , \tag{2.1}$$

where the metric has one negative eigenvalue, $G_{\mu\nu}$ is referred to as the Einstein tensor, $R_{\mu\nu}$ is the Ricci tensor, R is the Ricci scalar and $T_{\mu\nu}$ is the matter energy-momentum tensor. Following the procedure given in [4], we begin by introducing a Gaussian normal coordinate system in the vicinity of the domain wall. Using the same notations as before, let us denote the $2+1$ dimensional hyper-surface covered by the domain wall as Σ and

introduce a coordinate system on Σ. For definiteness, two of the coordinates can be taken to be the angular variables on the domain wall, which are always well defined (up to a rotation). For the third coordinate, one can use the proper-time variable τ. Next, let us consider all the geodesics which are orthogonal to Σ. We consider a neighborhood N about Σ so that any point that belongs to N lies on only one geodesic. The first three coordinates of each point in N are then determined by the coordinates of the intersection of this geodesic with Σ. The fourth coordinate η of each point in N can be taken as the proper distance in the positive direction (defined as the direction from $\mathcal{M}_-$ to $\mathcal{M}_+$) from Σ to that point along the geodesic line that connects them. Thus, the full set of coordinates is given by $x^\mu = (x^i, \eta)$, where $x^i = (\tau, \theta, \phi)$ and $i = 1, 2, 3$.
In this coordinate system the metric obeys the following simplifying relations

$$g^{\eta\eta} = g_{\eta\eta} = 1 \ , g^{\eta i} = g_{\eta i} = 0 \ . \tag{2.2}$$

Next, we define a unit vector field $n^\mu(x)$ which is normal to each of the of the $\eta = \text{const}$ hyper-surface. Notice that n^μ is chosen so that the positive direction is pointing from the interior space-time to the exterior. In the Gaussian normal coordinate system, this vector field is given by

$$n^\mu(x) = n_\mu(x) = (0, 0, 0, 1) \ . \tag{2.3}$$

The next step is to describe the extrinsic curvature of the domain wall. The extrinsic curvature is a three dimensional tensor, corresponding to each $\eta = \text{const}$ hyper-surface, whose components are defined by

$$K_{ij} = n_{i;j} \ , \tag{2.4}$$

where the semicolon represents the four-dimensional covariant derivative, but with the indices are restricted to the values $1, 2, 3$ (in fact, the general form of the extrinsic

curvature tensor is given by $K_{ij} = n_{i;j} - \xi n_i a_j$, where $a^i = n^k n^i_{;k}$ is defined as the acceleration vector and $\xi = n_i n^i$. However, when the normal vector field is taken to lie on a geodesic, as in Gaussian normal coordinates $a^i = 0$). The extrinsic curvature measures the fractional shrinkage and deformation of a figure lying in the space-like hyper-surface Σ that takes place when each point in the figure is carried forward a unit interval of proper time "normal" to the hyper-surface out into the enveloping space-time [27].

By choosing the Gaussian normal coordinates system, we now benefit from the simple form that this tensor takes

$$K_{ij} = -\Gamma^{\eta}_{ij} = \tfrac{1}{2}\partial_{\eta} g_{ij} \ . \tag{2.5}$$

It is also clear from the latter that the extrinsic curvature is a symmetric tensor.

Now, the four dimensional tensors $R_{\mu\nu\kappa\xi}$, $R_{\mu\nu}$ and R can be expressed at any point in terms of the corresponding three dimensional tensors and the extrinsic curvature of the hyper surface passing through the given point. One should note that the Gauss-Codacci formalism does not require the use of Gaussian normal coordinates. However, this formalism can be derived in a considerably simpler way by choosing this coordinate system. Noting that the only nonzero components of the affine connection are given by

$$\Gamma^k_{ij} = {}^{(3)}\Gamma^k_{ij} \ , \quad \Gamma^{\eta}_{ij} = -K_{ij} \ , \quad \Gamma^i_{\eta j} = K^i_j \ , \tag{2.6}$$

where the superscript (3) denotes three dimensional geometric quantities. Then, Einstein's equations become

$$G^{\eta}_{\eta} = -\frac{1}{2}\,{}^{(3)}R + \frac{1}{2}\left[(\mathrm{Tr}K)^2 - \mathrm{Tr}(K^2)\right] = 8\pi G T^{\eta}_{\eta} \ , \tag{2.7}$$

$$G^{\eta}_{i} = K^m_{i\ |m} - (\mathrm{Tr}K)_{|i} = 8\pi G T^{\eta}_{i} \ , \tag{2.8}$$

$$\begin{aligned} G^i_j &= {}^{(3)}G^i_j - \partial_\eta \left(K^i_j - \delta^i_j \mathrm{Tr}K\right) - (\mathrm{Tr}K)K^i_j + \tfrac{1}{2}\delta^i_j \left[\mathrm{Tr}(K^2) + (\mathrm{Tr}K)^2\right] = \\ &= 8\pi G T^i_j \ , \end{aligned} \tag{2.9}$$

where a subscript vertical bar denotes the three-dimensional covariant derivative.
In the thin wall approximation, $T_{\mu\nu}$ has a δ-function singularity on the domain wall. Thus, one can define the surface energy-momentum tensor $S_{\mu\nu}$ by writing

$$T_{\mu\nu} = S_{\mu\nu}\delta(\eta) + \text{regular terms} \ . \tag{2.10}$$

It is worth noting that when the matter content on the domain wall is described by a perfect fluid, the energy-momentum tensor on the shell's surface takes the form $S^{\mu\nu} = (\sigma + p)U^\mu U^\nu + p h^{\mu\nu}$, where $h^{\mu\nu} = g^{\mu\nu} - n^\mu n^\nu$ is the projector onto the surface of the shell and U^μ is the four-velocity of the wall.
Inserting Eq. (2.10) into the field equations (2.7 - 2.9), shows that Eqs. (2.7) and (2.8) are satisfied automatically provided that they are satisfied for $\eta \neq 0$ and that g_{ij} is continuous at $\eta = 0$ (so that K_{ij} will not acquire a δ function singularity). The remaining Eq. (2.9) leads to Israel's junction conditions [3]:

$$\gamma^i_j = -8\pi G(S^i_j - \frac{1}{2}\delta^i_j \mathrm{Tr}S) \ , \tag{2.11}$$

where $S^i_j = S^{ik}h_{kj}$ and

$$\gamma_{ij} = \lim_{\epsilon\to 0}[K_{ij}(\eta = +\epsilon) - K_{ij}(\eta = -\epsilon)] \ . \tag{2.12}$$

The spherical symmetry of the system ensures us that the off-diagonal components of the extrinsic curvature tensor vanish and that its angular components are related by $K_{\phi\phi} = \sin^2\theta K_{\theta\theta}$. Hence, the junction conditions are completely determined by the $\theta\theta$ and $\tau\tau$ components of Eq. (2.11).

Next, one needs to express the metric coefficients in terms of the Gaussian normal coordinate system so that the extrinsic curvature is given by Eq. (2.5). Because this is a purely technical step and since we ultimately wish to obtain the equation of motion in terms of the standard metric notation, we shall skip this derivation here. The details of this calculation can be found in [4].

Now, by choosing an equation of state to describe the matter content on the shell, one is able to obtain the energy density on the brane and thus calculate the right hand side of (2.11). Let us write the equation of state for the matter on the bubble surface as $p(R) = \omega\sigma(R)$ (i.e. a perfect fluid), where p is the two dimensional isotropic pressure, ω is a constant and σ is the surface energy density. Then, energy conservation on the shell $S^i_{0\ |i} = 0$ yields the equation $d\sigma = -2(\sigma(R) + p(R))\frac{dR}{R}$. This, of course, is equivalent to the first law of thermodynamics $du = -pda$ (where $u = m(R) = 4\pi R^2\sigma(R)$ is the total energy content and $a = 4\pi R^2$ is the surface area of the bubble). Solving for $\sigma(R)$ we find that

$$\sigma(R) = \sigma_0 R^{-2(1+\omega)} \ , \tag{2.13}$$

where σ_0 is a constant.

Now, we are in a position to write the equation of motion explicitly in terms of the metric coefficients and the energy density on the brane. Taking the $\theta\theta$ component of (2.11) and keeping in mind that due to the spherical symmetry $S^\theta_\theta = S^\phi_\phi$, one notes that, in fact, only the energy density (i.e. S^τ_τ, coming from $\mathrm{Tr}S$), remains in the equation. Then, plugging all the above into (2.11) yields the equation of motion for a general energy-matter shell

$$\beta_- - \beta_+ = 4\pi G\sigma(R)R \ , \tag{2.14}$$

where $\beta_\pm$ are defined as

$$\beta_+ = \epsilon_+(A_+(R) + \dot{R}^2)^{1/2} \quad \text{and} \quad \beta_- = \epsilon_-(A_-(R) + \dot{R}^2)^{1/2} \ , \tag{2.15}$$

where an over-dot denotes a derivation with respect to τ, $A_\pm(R) = -g_{tt}^\pm$ and the signs of the coefficients $\epsilon_\pm$ are to be determined by the geometric analysis of the problem: $\epsilon_\pm = \text{sgn}(n^\mu \partial_\mu r)|_{\mathcal{M}_\pm}$ determine if the radial coordinate r is decreasing ($\epsilon_\pm = -1$) or increasing ($\epsilon_\pm = +1$) along the normal coordinate to the brane, n^μ. Eq. (2.14) is equivalent to the equation of motion of a particle moving in one dimension under the influence of an effective potential of the form $\dot{R}^2 + V_{eff}(R) = 0$ [4].
The proper-time component of Eq. (2.11) yields just the proper-time derivative of Eq. (2.14). Thus, (2.14) determines all the properties of the solution to the general problem of our system. One should notice that for geometries that do not contain wormholes the signs of both β_+ and β_- must be positive.

3. VACUUM DECAY AND CHILD UNIVERSES: A SHORT DISCUSSION

The phase transition which leads to the creation of domain walls involves a phase separation process, where the domain wall is the boundary between the two vacua. This is similar to first order phase transitions effect in thermodynamics. However, following the discussion which appears in [28], it is the purpose of this section to explain that the classical geometrical description is appropriate to provide a comprehensive description of the dynamics of domain walls and also to elaborate on the conditions required for child universes creation.
The above formalism (i.e. Israel junction conditions) has been widely used to describe the formation of child universes. It provides a convenient practical way to implement a more comprehensive description in which the vacuum decay is represented by the decay of a scalar field. If the scalar field has two equilibrium states which have a different energy density and quantum effects are considered, the higher energy density state can

become unstable due to the possibility of tunneling under the potential barrier. This may become transparent already in the semiclassical approximation with a single scalar field with non derivative interactions being considered. The decay process of a volume V of the higher energy density false vacuum into the lower energy density true vacuum has a probability (per unit time per unit volume) which is given by

$$\frac{\Gamma}{V} = Ae^{-B/\hbar}\left[1 + \mathcal{O}(\hbar)\right] \ , \tag{3.1}$$

where the positive exponent constant B [18] and the coefficient A [19] can be computed by standard techniques. This analysis is particularly relevant when it is coupled to gravity. It was recognized by Coleman and De Luccia [20], who studied the effect of gravitation upon the decay of false vacuum, that a study of vacuum decay that would not include gravitational effects would be incomplete.

However, the vacuum bubbles we have described above are true vacuum bubbles, that is, the phase transition is from false vacuum to true vacuum. Nonetheless, the opposite transition is also possible (i.e. a false vacuum bubble can arise in a bulk of true vacuum). This kind of bubbles is particularly interesting in the cosmological context since they can undergo an exponential growth, which recalls the exponential expansion of the early universe during the inflationary era. For example, a detailed analysis of the false vacuum bubble creation by cosmological first order phase transition can be found in [22].

Although all these processes involve the decay of a scalar field, by using the thin shell formalism [4, 29] the problem of bubble nucleation can be analyzed at the classical level by concentrating merely on a general relativistic description. Considering the analysis developed in [4], it is seen that the formalism described in section 2 is perfectly suited to analyze the formation of a vacuum bubble. Moreover, an immediate interpretation of the properties of the model is made possible by the intuitive geometrical meaning of the quantities which appear in the junction condition (i.e. Eq. (2.14)).

In more detail, the model studied in [4] studies the dynamics of a vacuum bubble in

terms of the dynamics of a general relativistic shell separating a region of a de Sitter space-time (i.e. $A_- = 1 - \chi^2 r^2$) from a region of a Schwarzschild space-time (i.e. $A_+ = 1 - 2GM/r$). Because this model corresponds to a standard (or pure, i.e. which does not involve additional matter terms) domain wall, the energy-matter content of the shell is represented by a uniform, positive and constant energy-density σ_0, which is equal to the opposite of the (equal) radial and tangential pressures. Thus, we have $S^{ij} = -\sigma_0 h^{ij}$, where h_{ij} is the induced metric on the shell. Therefore, one is able to define the "mass content" of the bubble as $m(R) = 4\pi\sigma_0 R^2$. This also naturally arises from the models described above by using a scalar field to describe the vacuum phase transition. The study of the solutions of the junction condition can then be performed by obtaining an equivalent effective formulation of Eq. (2.14) that reduces the problem to the analysis of the motion of a classical particle of unit mass under the influence of a potential. However, this reformulation of the junction condition needs to be completed by the understanding of the behavior of the normal vector to the brane. Hence, the results of the behavior of the radial coordinate $R(\tau)$ have to be complemented with the determination of $\epsilon_\pm$, which can also be obtained in closed form in the general case [30].

As we briefly discussed in the introductory subsection 1.1, this model is governed by three parameters: The cosmological constant of the false vacuum bubble $\Lambda = 3\chi^2$ (which can be connected to the vacuum energy density ρ by the relation $\Lambda = 8\pi G\rho$), the Schwarzschild mass of the asymptotically flat region M and the surface energy density σ.

As was explained in Sec. 1.1, and can also easily seen by squaring twice at Eq. (2.14) for a given case (as will be done in the following sections), two qualitatively different types of solutions of (2.14) are obtained when varying these parameters:

1. The system admits solutions which start from a zero radius and grow up to an arbitrarly large R. These solutions become large enough to describe the formation and evolution of an inflationary universe, but develop from an initial singularity.

2. The system admits two kinds of solutions:

   (a) Bounded solutions, which start evolving from a zero radius and, after reaching a maximum radius of expansion, collapse back to a zero radius;

   (b) Bounce solutions, which collapse from large R values up to a minimum radius and then expand again to infinity.

   In these two situations, where a classical transition from a bounded to a bounce solution is forbidden by the existence of a potential barrier, the bounded solutions cannot become big enough to describe the evolution of a universe like ours, while the bounce solutions, cannot evolve in the small radius region (i.e. they are not suited to describe the early evolution of a universe like ours).

It thus seems that the only choice to have a bubble evolution that is suitable for the description of the observed universe is to accept the initial singularity, at least at the classical level. This result is not a failure of the present model, but is connected with general results of singularity theorems in general relativity [31] - [35] (see also [36] and [37] for standard textbook discussions) as it was recognized in [38]. Hence, classical models are still very useful to investigate the essential features of child universes creation process.

As we have discussed in Sec. 1.1, child universes, emerging from a false vacuum bubble, are characterized by an energy density which is larger than that of the surrounding space. Therefore, the bubble encloses a region of lower pressure which makes it impossible for the bubble to expand onto the parent universe (when $M < M_{cr}$ and the bubble starts with a small enough radius). However, when a wormhole is formed the child universe can grow by making its own space on the other side of the wormhole throat. In this case, the late time evolution of the child universe is classically hidden from an observer living in the parent universe by the presence of an event horizon. It is important to remark that it is the wormhole structure of space-time that allows for the creation of the

child universe. The same force that would prevent the expansion to the parent universe side of the wormhole, acts in the opposite direction and, in fact, favors the expansion on the other side of the wormhole. In this region the normal vector to the brane, which is directed from the child universe $\mathcal{M}_-$ toward the parent space $\mathcal{M}_+$, points in the direction of decreasing radius. Mathematically, this is reflected by a negative value for ϵ_+ in equation (2.14). If this condition is met for values of the parameters for which solutions of type 1 above can be realized, then child universes are formed.
To summarize, two requirements have to be met for child universes to be realized as false vacuum bubbles when using the thin-wall approximation:

requirement 1: There must be a process by which a very small bubble can become big enough, so that both the early and late time evolution of our universe can be described. This means that the solution to the junction condition is of type 1.

requirement 2: At late times, the evolution must guarantee that $\epsilon_+ = -1$, so that the child universe is, effectively, classically disconnected from the parent universe. This requirement indicates the presence of a wormhole and that the bubble may expand by creating its own space on the other side of the wormhole.

The above requirements can be applied also to generalizations of the model, which was first analyzed in [4], and also to those generalizations involving semiclassical quantum effects.

4. NEUTRAL SHELL STABILIZATION BY GRAVITATIONAL EFFECTS FROM ELECTRIC FIELDS

Before moving on to analyze the creation of child universes out of an almost empty space, we wish to study the more elementary subject which explores, by using the classical formalism we have described above (i.e. Israel junction conditions), a novel possibility to stabilize a domain wall.

However, first we wish to clarify our choice of parameters space which will be used for the different scenarios in sections 4 and 5. In this work we chose to concentrate on analytical solutions. In order to obtain analytical solutions, we have confined ourselves to a comparatively small region of parameters which have a physical meaning while still keeping the solution analytical. As was explained before, the phase space of the problems which appear in this part of the work is determined by the choice of the inner and outer metrics, as well as the choice for the energy density on the brane. A work theme that makes sense then, is to choose the matter content on the brane and then choose different types of metrics in order to obtain a more general solution. For example, the choice $\omega = -1/2$ leads to $\sigma(R) = \sigma_0/R$. Putting this into the equation of motion (i.e. Eq. (2.14)) yields $\beta_- - \beta_+ = \text{const.}$ which implies that a fairly simple analytical solution may be obtainable. Then, the choice of the inner and outer metrics will determine the shape of the potential. Of course, there are no general solutions to Einstein's equations and therefore no single general solution is obtainable for each choice of ω. In other words, this way of search for (more) general analytical solutions is repeating itself in order to reach a wider family of solutions to the analysis of two dimensional branes. The final results and conclusions of this process are presented in the rest of this part of the work.

In this section we wish to explore a different way, than those mentioned in Sec. 1.2, for achieving stabilization of a two dimensional extended object using the gravitational effects from a massive charged source on an *uncharged* spherical shell. Hence, the stabilization in the case presented here is induced purely from gravitational effects. Following [39], we shall show that obtaining a static and stable domain wall configuration is indeed possible, even without introducing additional mass terms. The major result of our analysis is that the mere presence of a global electric field (that is, an electric field which is present on both regions of the global space-time manifold) can serve as a stabilizing mechanism for a vacuum bubble. Here, the source of this electric field is a massive point charge, located at the center of the vacuum bubble.

4.1. Analysis of the Electro-Magnetic Properties

Since we have a massive and stationary point charge located at the center of the bubble, the general metrics for both regions of our set-up are Reissner-Nordstrom metrics. As the shell does not carry any charge, the charge parameter that appears in both metrics should be equal, leading to

$$\begin{aligned} ds_-^2 &= -\left(1-\tfrac{2Gm}{r}+\tfrac{GQ^2}{r^2}\right)dt^2+\left(1-\tfrac{2Gm}{r}+\tfrac{GQ^2}{r^2}\right)^{-1}dr^2+r^2d\Omega^2,\ r<R\ , \\ ds_+^2 &= -\left(1-\tfrac{2GM}{r}+\tfrac{GQ^2}{r^2}\right)dt^2+\left(1-\tfrac{2GM}{r}+\tfrac{GQ^2}{r^2}\right)^{-1}dr^2+r^2d\Omega^2,\ r>R\ , \end{aligned} \tag{4.1}$$

where m is the mass of the electric field source, with charge Q, and M is the mass-energy of the system as seen by an external observer. The only non-zero component of the electromagnetic tensor will be $F_{0r}=-F_{r0}$. Therefore, Maxwell's equations reduce to the single equation

$$\nabla_r F^{0r}=\frac{1}{\sqrt{-g}}\partial_r\left(\sqrt{-g}g^{00}g^{rr}F_{0r}\right)=0\ , \tag{4.2}$$

for $r\neq 0$. Thus, from classical electrodynamics, we have (for each region) $(\sqrt{g}g^{00}g^{rr})^i F^i_{0r}\propto Q$, where i indexes the different regions. From the latter we find that the electric field is continuous across the shell

$$F_{0r}=\frac{Q}{r^2},\ \forall\ r\ . \tag{4.3}$$

Finally, we find the energy density of the electric field to be

$$T^0_{\ 0}=-\frac{Q^2}{2r^4},\ \forall\ r\ . \tag{4.4}$$

4.2. Dynamical Analysis

Now we turn to derive the effective potential which governs the bubble dynamics and look for at-least one local minimum point which fulfills the condition $V_{eff}(R_{min}) = 0$. For consistency, let us write again the bubble's equation of motion

$$\epsilon_- \sqrt{A_-(R) + \dot{R}^2} - \epsilon_+ \sqrt{A_+(R) + \dot{R}^2} = \frac{Gm(R)}{R} = \kappa(R) \ , \tag{4.5}$$

where the $\pm$ subscripts indicate the exterior and the interior regions of the shell, respectively, $A_\pm(R) = -g_{tt}^\pm$, $m(R) = 4\pi R^2 \sigma(R)$ describes the energy-matter content which is located on the surface of the bubble and the coefficients $\epsilon_\pm = \mathrm{sgn}(n^\mu \partial_\mu r)|_{\mathcal{M}_\pm}$ determine if the radial coordinate r is decreasing or increasing along the normal coordinate to the brane, n^μ.

Let us choose, as we have done in Sec. 2, the equation of state for the matter on the bubble surface to describe a perfect fluid $p(R) = \omega\sigma(R)$, where $p(R)$ is the two dimensional isotropic pressure, ω is a constant and $\sigma(R)$ is the surface energy density. Then, energy conservation on the shell yields

$$\sigma(R) = \sigma_0 R^{-2(1+\omega)} \ , \tag{4.6}$$

where σ_0 is a constant. For example, $\omega = -1$ represents a constant surface tension (i.e. a standard domain wall) and $\omega = -1/2$ represents a matter that can be interpreted as a gas of strings living on the surface of the bubble [40, 41] (a gas of strings in n spatial dimensions satisfies the equation of state $p = -\sigma/n$.). Putting Eq. (4.6) into the equation of motion (4.5) we get

$$\kappa(R) = 4\pi G \sigma_0 R^{-(1+2\omega)} = \kappa_0 R^{-(1+2\omega)} \ , \tag{4.7}$$

where $\kappa_0 = 4\pi G\sigma_0$. Squaring twice Eq. (4.5) yields the effective one dimensional equation

$$\dot{R}^2 + 1 - \frac{\kappa_0^2 R^{-2(2\omega+1)}}{4} - \frac{G(M+m)}{R} + \frac{GQ^2}{R^2} - \frac{G^2(M-m)^2}{\kappa_0^2} R^{4\omega} = 0 \ , \tag{4.8}$$

which defines the effective potential to be

$$V(R) = 1 - \frac{\kappa_0^2 R^{-2(2\omega+1)}}{4} - \frac{G(M+m)}{R} + \frac{GQ^2}{R^2} - \frac{G^2(M-m)^2}{\kappa_0^2} R^{4\omega} \ . \tag{4.9}$$

Let us now concentrate on two specific cases that have a physical meaning: $\omega = -1/2$ and $\omega = 0$. The first case describes a gas of strings which is located on the surface of the bubble, while the second choice corresponds to dust localized on the wall. For these two values of the equation of state parameter the effective potential is tractable and can be solved in closed form.

Let us show now that in both cases the potential can have a local minimum which satisfies $V(R_{min}) = 0$, after some fine tuning. Let us begin with the stringy gas bubble.

4.2.1. String Gas Bubble

The effective potential for this kind of bubble is ($\omega = -1/2$)

$$V_{S.G}(R) = 1 - \frac{\kappa_0^2}{4} - \frac{G(M+m)}{R} + \frac{GQ^2}{R^2} - \frac{G^2(M-m)^2}{\kappa_0^2 R^2} \ . \tag{4.10}$$

Solving the equation $V_{S.G}(R) = 0$, we are lead to a polynomial equation of rank 2. By imposing the demands that the discriminant will equal zero and that $\kappa_0^2 < 4$, we ensure that we will have a global minimum which satisfies $V_{S.G}(R_{min}) = 0$.

The discriminant of the effective potential function is given by

$$\Delta = G^2(M+m)^2 + (\kappa_0^2 - 4)\left(GQ^2 - G^2\frac{(M-m)^2}{\kappa_0^2}\right) \tag{4.11}$$

and by demanding $\Delta = 0$ we arrive at the condition:

$$Q^2 = \frac{G(M+m)^2}{4-\kappa_0^2} + \frac{G(M-m)^2}{\kappa_0^2} \ . \tag{4.12}$$

The radius of curvature of the stable bubble is thus given by

$$R_{min} = 2G\frac{M+m}{4-\kappa_0^2} \ , \tag{4.13}$$

with R_{min} being positive under the imposed conditions.

Now we turn to ask if R_{min} is located behind any horizons. In principle, there might be two different horizons in each region. But, if Q^2 is bigger than GM^2 there will be no horizons in the system (remembering that $M \geq m$, since we do not consider negative surface tension). Comparing Eq. 4.12 to GM^2 is equivalent to comparing the function $f_1(x)$ and the quantity g_1, where:

$$f_1(x) = x^2 + x(\kappa_0^2 - 2) + 1 \ , \tag{4.14}$$

$$g_1 = \frac{\kappa_0^2}{4}(4-\kappa_0^2) \ , \tag{4.15}$$

with $x = m/M$ being the ratio between the masses (which is constrained to $0 < x < 1$). So the condition $Q^2 < GM^2$ is now $f_1(x) < g_1$. The minimum value of $f_1(x)$ is located at $x_{min} = (2-\kappa_0^2)/2$, when $\kappa_0^2 < 2$, and at $x = 0$ when $\kappa_0^2 > 2$. Looking at the minimum value of f_1 we find that it satisfies $f_1(x_{min}) = g_1$. This means that $f_1(x)$ will always be greater than g_1 (i.e $Q^2 > GM^2$) except for the case when the ratio between the masses is fine tuned to equal precisely x_{min} and the surface tension is small enough (i.e $\kappa_0^2 < 2$).

This limiting case means that there would be two degenerate horizons (i.e an extremal black-hole-like object). When $x \neq x_{min}$, we have a naked singularity at $r = 0$, since this corresponds to $Q^2 > GM^2$. When $m = (1 - \kappa_0^2/2)M$ (i.e $x = x_{min}$), the bubble would sit exactly on the degenerate horizon (i.e $R_{min} = GM$) and therefore it would be a light-like brane. However, we consider here only a time-like motion for the brane and this particular case is merely a limiting situation.

The above result is actually an example of the more general relation between the effective potential and the metric coefficients which states that $A_{\pm}(R) - V_{eff}(R) \geq 0$. Thus, when the effective potential is definite positive, as in the cases studied here, the geometries $\mathcal{M}_{\pm}$ can not contain any horizons. A proof for this relation is given in Ref. [42].

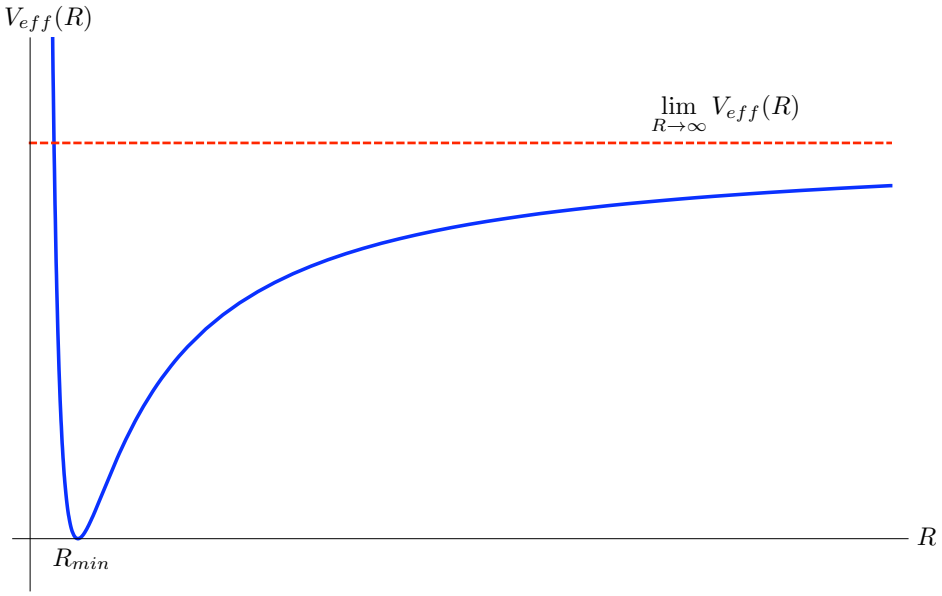

FIG. 1: The general characteristics of the effective potential $V_{eff}(R)$ (continuous line). This graph corresponds to both cases analyzed here: $\omega = -1/2$ and $\omega = 0$, which show similar characteristics of the effective potential. The dashed line corresponds to the limit of $V_{eff}(R)$ at $R \to \infty$: $1 - \kappa_0^2/4$ in the $\omega = -1/2$ case and $1 - (G(M-m)/\kappa_0)^2$ in the $\omega = 0$ case.

4.2.2. Dust Shell

For the case of $\omega = 0$, the effective potential is

$$V_{DUST}(R) = 1 - \frac{\kappa_0^2}{4R^2} - \frac{G(M+m)}{R} + \frac{GQ^2}{R^2} - \frac{G^2(M-m)^2}{\kappa_0^2} \ . \tag{4.16}$$

In the same manner of section 4.2.1, by solving the equation $V_{DUST}(R) = 0$ we encounter again a simple quadratic equation. The conditions for having a stable solution now are (note the different units of κ_0 in this case) $G^2(M-m)^2 < \kappa_0^2 < 4GQ^2$ and

$$\Delta = G^2(M+m)^2 + (\kappa_0^2 - 4GQ^2)\left(1 - \frac{G^2(M-m)^2}{\kappa_0^2}\right) = 0 \ . \tag{4.17}$$

The latter can, again, be written as a constraint on the charge:

$$Q^2 = \frac{\kappa_0^2}{4G}\frac{4G^2Mm + \kappa_0^2}{\kappa_0^2 - G^2(M-m)^2} \ . \tag{4.18}$$

The radius of curvature for the stable bubble is now given by

$$R_{min} = \frac{1}{2}\frac{G(M+m)\kappa_0^2}{\kappa_0^2 - G^2(M-m)^2} \ , \tag{4.19}$$

which is, again, positive under the imposed conditions.
Looking for the location of R_{min} relative to the horizons, we continue in analogy to the prior case, where now

$$f_2(x) \ = \ G^3M^4(1-x)^2 + GM^2\kappa_0^2 x \ , \tag{4.20}$$

$$g_2 \ = \ \kappa_0^2\left(GM^2 - \frac{\kappa_0^2}{4G}\right) \ . \tag{4.21}$$

$f_2(x)$ has one minimum at $x_{min} = 1 - \frac{\kappa_0^2}{2(GM)^2}$, when $\kappa_0^2 < 2(GM)^2$, and at $x = 0$ when $\kappa_0^2 > 2(GM)^2$. It can be easily verified that $f_2(x_{min}) = g_2$. The conclusions are the same as before: there will be no horizons unless $\kappa_0^2 < 2(GM)^2$ and $x = x_{min}$, where the latter means that the two horizons are degenerate and located at $R = GM$, exactly where the bubble would sit. Again, this demonstrates the more general relation $A_\pm(R) - V(R) \geq 0$ [42].

4.2.3. Dynamical Solutions

Here we would like to address the question: what happens to the two types of bubbles we have considered earlier, if the conditions for time independence are not satisfied? Obviously, one option is that no dynamics is possible (when $\Delta < 0$). The other option is that the effective potential will be negative in some region, which will allow a kinetic energy for the shell. Here we have two cases: a finite or an infinite region where $V < 0$. The first case (finite region) corresponds to bounded solutions, or a 'breathing' bubble [43], where the bubble starts off at some radius, expands to a maximum radius value and then shrinks back to the initial radius. On the other hand, the second case corresponds to a bubble which begins with a finite radius and then expands to an infinite size.

The question is whether the bubble blows up onto the surrounding space-time or perhaps there is a possibility for wormholes to exist in this case and allow for a child universe solution (as we discussed before, when wormholes are present the bubble can make its way and expand to infinity by creating its own space completely disconnected from the original space-time).

In order to determine if wormholes might be present in the solution we need to calculate the extrinsic curvature tensor induced on the shell. This was done, of course, in Eq. (4.5). For spherically symmetric metrics the relevant component of the extrinsic curvature is $K_{\theta\theta} \propto \partial g_{\theta\theta}/\partial n$ so that the coefficients $\epsilon_\pm$ determine the behavior of the radial coordinate in the direction orthogonal to the trajectory of the bubble, hence allowing us to determine

the existence of wormholes. Calculating the signs of these coefficients for the two types of bubbles we are considering, we find that for the string gas bubble

$$\mathrm{sgn}(\epsilon_+) = \mathrm{sgn}\left(\frac{2G(M-m)}{R} - \kappa_0^2\right) , \tag{4.22}$$

$$\mathrm{sgn}(\epsilon_-) = +1 , \tag{4.23}$$

and therefore the extrinsic curvature induced on the shell from the exterior changes sign at $R = \frac{2G(M-m)}{\kappa_0^2}$. This change of sign is a generic characteristic for the presence of wormholes since when ϵ_+ is negative the normal coordinate to the brane, which points from the bubble interior to its exterior, is pointing along a direction for which the radial coordinate is actually decreasing rather than, as in the more familiar possibility of non wormhole geometry, increasing. Thus, we conclude that there is a possibility for the bubble to expand to infinity disconnected from the original space-time (i.e a child universe solution).

For the dust shell case, the trajectory constants signs read

$$\mathrm{sgn}(\epsilon_+) = \mathrm{sgn}\left(\frac{2G(M-m)}{R} - \frac{\kappa_0^2}{R^2}\right) , \tag{4.24}$$

$$\mathrm{sgn}(\epsilon_-) = +1 , \tag{4.25}$$

so in the limit $R \to \infty$ we see that ϵ_+ is positive, indicating that the normal to the brane does not point to a direction in which the radial coordinate decreases. Hence, there is no child universe formation.

4.3. Conclusions

To conclude, the electric charge causes a gravitational repulsive effect which balances the natural tendency of two dimensional extended objects to collapse and thus yields a

static and stable shell configuration, even though the latter carries zero charge and does not interact directly with electric fields.

We notice that in the limiting case where the charge parameter of the interior and exterior solutions is zero our results coincide with those presented by Kijowski, Magli and Malafarina [44], where they reviewed the dynamics of spherical time-like shells by matching two different Schwarzschild space-times and also analyzing the canonical formulation of such systems.

In a future research we will study the semi-classical quantization of the bounded excitations of the string gas shell. From the structure of the effective potential , which contains a flat region as $r \to \infty$ (independent of the mass), we see that there is the possibility of "ionization" which could be responsible for a dynamical creation of a universe, since for bigger radii the solutions will approach those studied in reference [45], which represent child universe creation.

In contrast, for the case of a dust shell, the ionization does not produce a child universe, but instead it is simply an "expansion" where the dust shell achieves the critical 'escape velocity' necessary to expand to infinity in the existing space, i.e without creating a new space of its own (a child universe).

5. UNIVERSES OUT OF ALMOST EMPTY SPACE

As we have seen, in order for a classical creation of a child universe to occur (i.e tunneling is not taken into consideration in the process), there exists a mass threshold where M must be greater than the critical value M_{cr}. It is thus interesting, if not required, to ask if this condition is a necessary one. In a previous letter by Guendelman [46], it was shown that in the limits where the volume energy density, Λ, and/or the surface energy density, σ (where the bubble carries a constant surface tension), become very large the mass threshold actually disappears. Therefore, when the child universe is characterized by a very high volume/surface energy density the critical mass above

which the creation process can happen becomes very small. Even if we were interested in the more elaborated tunneling process, it turns out that the upper bound for M, close to which a limited amount of tunneling is required, becomes smaller and smaller. This seems to indicate that the presence of a critical mass is not a necessary feature in the child universe creation process.

The objective of this section is to show that child universes, intended in the broader sense of regions of space-time disconnecting from an ambient space, are relevant also outside the framework of inflationary cosmology. A particular realization of a child universe involving string-gas like matter is studied, to show that it can be created from almost empty space (i.e. with an arbitrarily small M).

5.1. A First Example

A technically straightforward model for child universe creation can be, in fact, obtained even in a framework which is simplified compared to one of the models discussed above. Following [45], in order to demonstrate the principle of the idea of universes out of an almost empty space, let us choose the interior of the bubble to be a Minkowski space-time and the exterior to be a Schwarzschild space-time. Therefore, we eliminate one of the generic parameters of the typical child universe model by setting $\Lambda = 0$. Then, the equation of motion of the wall reads

$$\epsilon_- \sqrt{1+\dot{R}^2} - \epsilon_+ \sqrt{1 - \frac{2GM}{R} + \dot{R}^2} = \frac{Gm(R)}{R} = \kappa(R) \ . \tag{5.1}$$

Again, the function $m(R) = 4\pi R^2 \sigma(R)$ represents the matter content on the surface of the bubble after imposing spherical symmetry conditions on the stress tensor and relating the pressure p and the energy density σ on the bubble surface with an equation of state of the form $p = \omega\sigma$.

Our choice for the equation of state will be $\omega = -1/2$, which implies that the domain

wall is made of strings gas. This gives, from conservation of energy on the domain wall (see Eq. (2.13)), $\sigma = \sigma_0/R$, where σ_0 is a constant, and therefore we get $m(R) = 4\pi\sigma_0 R = \kappa_0 R/G$, where $\kappa_0 = 4\pi G\sigma_0$. Now we are able to identify the effective potential for this case and solve eq. (5.1)

$$\dot{R}^2 + V(R) = 0 \ , \quad V(R) = 1 - \frac{1}{4\kappa_0^2}\left(\frac{2GM}{R} + \kappa_0^2\right)^2 \ , \tag{5.2}$$

where the signs of $\epsilon_\pm$ are given by $\epsilon_- = +1$ and $\epsilon_+ = \mathrm{sgn}(2GM/R - \kappa_0^2)$. One notes that the effective potential $V(R)$ satisfies the following conditions

$$\begin{aligned} \lim_{R\to 0^+} V(R) &= -\infty \ , \\ \lim_{R\to\infty} V(R) &= 1 - \frac{\kappa_0^2}{4} \ , \\ \frac{dV(R)}{R} &> 0 \ . \end{aligned} \tag{5.3}$$

From this we conclude that

1. For $\kappa_0 \geqslant 2$ the potential will be definite negative. Thus, there can be unbounded trajectories when $\kappa_0 \geqslant 2$.

2. The first conclusion is independent of M. Hence, for $\kappa_0 \geqslant 2$, there are unbounded trajectories for any $M > 0$.

3. For any unbounded trajectory ϵ_+ changes sign, being positive for small enough R and negative for large enough R. One should also notice that ϵ_+ changes sign behind the horizon, in this case. When $\kappa_0 \geqslant 2$, at $R = 2GM$ the sign of ϵ_+ is already negative.

The structure of the global space-time, associated with these properties for all unbounded solutions (see Fig. 2), shows that the creation of a child universe will be realized for any positive value of M provided that the density of the string gas is large enough. This is a first example for a child universe which is created out of an almost empty space.

This generalized child universe formation does not necessarily relate to early universe cosmology, but has nonetheless similar properties. In particular, for an outside observer a black hole is formed and the large string density shell that the observer can see looking into the far past eventually disappears behind an event horizon. In this technically simple and transparent example the black hole mass M can be arbitrary (thermodynamics could favor small values of M, but in view of the complexity of the thermodynamics of gravitational systems we use this argument only as a suggestive indication).

One should note that more general equations of state for the shell can be considered without spoiling this result. For instance, models of vacuum decay suggest the presence of a uniform surface tension σ_0. Adding this term we then have $m(R) = \kappa_0 R/G + 4\pi\sigma_0 R^2$ and a sufficient condition not to change the conclusions discussed above is $\kappa_0 + 4\pi G\sigma_0 R \geq 2$. This is certainly satisfied for all values of R if the condition $\kappa_0 \geq 2$ holds. This allows for child universe creation out of an almost empty space in the simple space-time structure we described above (note the important point that the qualitative behavior of ϵ_+ is also unaffected by the presence of σ_0). The condition $\kappa_0 \geq 2$ remains unaltered also if, in the spirit of false vacuum decay, we add a uniform energy density Λ inside the child universe, as we explicitly prove in the next section. Other equations of state can be considered as well, either instead of the one chosen here, or in combination with it, to obtain models with composite matter similar to the one we just mentioned.

We therefore see that this model allows for unbounded child universe creation. However, the model described above is, of course, rather simplified and hence generalizations are desirable, if not required.

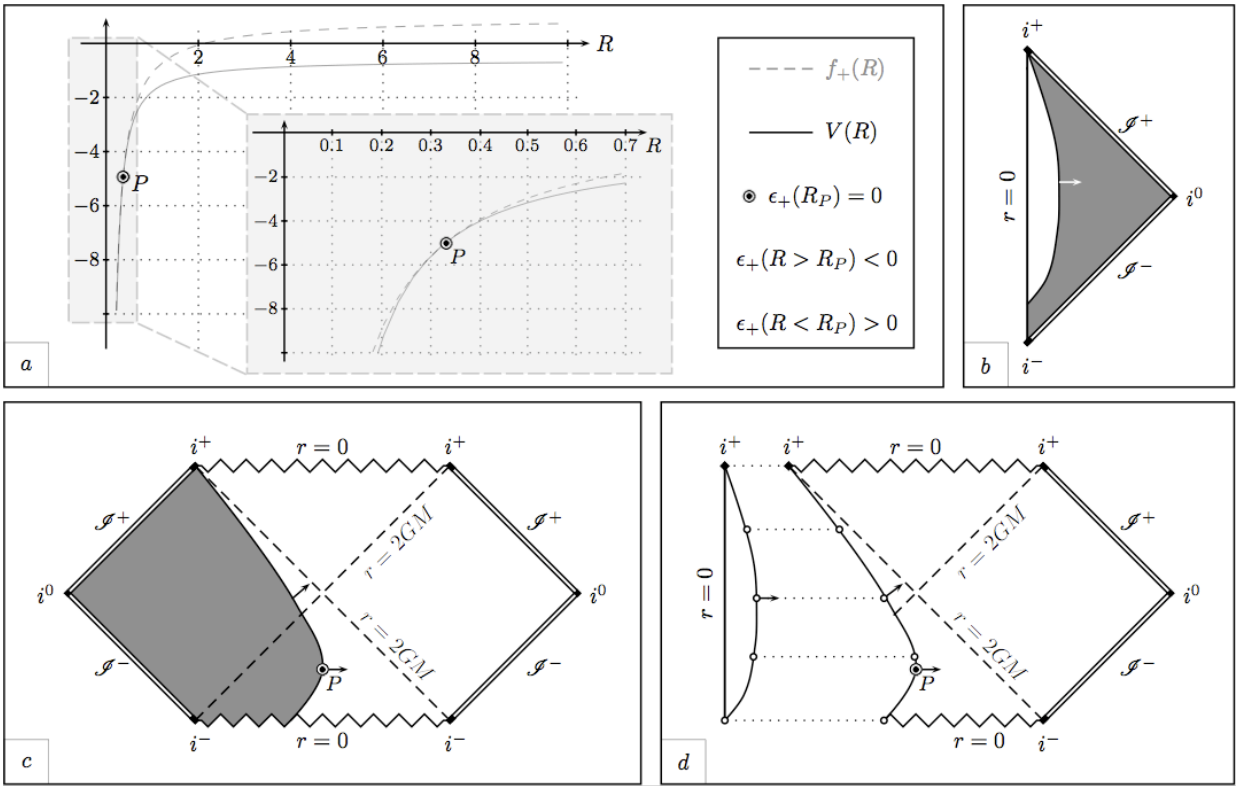

FIG. 2: Construction of the global space-time structure with the classical formation of a child universe for an unbounded solution of the Minkowski-Schwarzschild junction by a sphere of string gas (the boundaries at infinity are labeled according to the conventions in [36]). In panel "a" we plot the effective potential (solid curve) together with the horizon curve $A_+(R) = 1 - 2GM/R$ (dashed gray curve). The effective classical dynamics are given by the motion of the representative point along the R axis, which corresponds to a motion with zero energy in the potential $V(R)$ (cf. eq. (5.2)). Correspondingly the shell starts from zero radius, expanding towards infinity. In the two spacetimes, this motion corresponds to the solid curves in panels "b" and "c". From looking at panel "a", it is clear that the shell will cross the white hole horizon, since it will expand up to arbitrarily large values of the radius R. To determine if the part of spacetime participating in the junction will be the one on the left or on the right of the shell trajectory, we have to look at the normal (also shown in the picture). In Minkowski spacetime (see panel "b") the sign of ϵ_- is always positive, i.e. the normal always points in the direction of increasing radii. Moreover, our convention is that the positive direction of the normal is going from $\mathcal{M}_-$ to $\mathcal{M}_+$ so that the *un*shaded region is, in fact, $\mathcal{M}_-$. An analogous procedure has to be performed in the Schwarzschild spacetime (panel "c"). Again $\mathcal{M}_-$ is the *un*shaded region. In this case, however, a new feature appears, since the sign ϵ_- changes at P, and the normal that before P was pointing in the direction of decreasing radii, after P will point in the direction of increasing radii. This change between the relative orientation of the normal and the increasing radii direction happens when the horizon curve $A(R)$ is tangent to the potential curve $V(R)$ (see the zoomed snapshot in panel "a"). All these properties give rise to the global spacetime structure in panel "d": the fact that the asymptotically flat part of Schwarzschild spacetime includes the central point of the diagram, which in turn is due to the fact that outside the horizon $\epsilon_+ = -1$, certainly shows that a child universe is formed in the process. Courtesy of Stefano Ansoldi.

5.2. The False Vacuum Case

The following couple of sections serve as a proof for the possibility to obtain a child universe solution from an almost empty space for more general space-times. The method for the analysis of the effective potential is essentially the same in both sections. However, since the analysis of the effective potential is becoming more complicated, both sections are included in order for one to be able to rely on the previous proofs to comfortably (as much as possible) track the stages and logic steps of the proofs. In fact, the situation described in Sec. 5.3 will merely generalize its preceding models.

As a second example, it is possible to extend the model and add a cosmological constant to the interior of the bubble (i.e $\Lambda \neq 0$). We wish to show that the same conclusion as above can be achieved for a false vacuum bubble with a string gas on its surface.

Our set up is made with a bubble enclosing on a false vacuum region, where the interior metric is given by

$$ds_-^2 = -(1-\chi^2 r^2)dt^2 + (1-\chi^2 r^2)^{-1}dr^2 + r^2 d\Omega^2 \ , \tag{5.4}$$

while the exterior region metric is given by the Schwarzschild metric

$$ds_+^2 = -(1-\frac{2GM}{r})dt^2 + (1-\frac{2GM}{r})^{-1}dr^2 + r^2 d\Omega^2 \ . \tag{5.5}$$

The effective potential in this case is given by

$$V(R;\kappa_0,\chi,M) = 1 - \frac{\kappa_0^2}{4} - \frac{\chi^4 R^4}{4\kappa_0^2} - \frac{\chi^2 R^2}{2} + \frac{GM\chi^2}{\kappa_0^2}R - \frac{GM}{R} - \frac{(GM)^2}{\kappa_0^2 R^2} \ , \tag{5.6}$$

where, again, $\kappa_0 =$ constant. By making the following substitutions

$$\kappa_0 = 2D, \quad R = \frac{2Dy}{\chi}, \quad M = \frac{8D^3 C}{G\chi} \ , \tag{5.7}$$

(note that when $\chi \geq 0$, $\kappa_0 \geq 0$ and $M \geq 0$, then $C \geq 0$ and $D \geq 0$. Moreover, if $\kappa_0 \geq 2$ then $D \geq 1$) the potential can be written as

$$\begin{aligned} V(R;\kappa_0,\chi,M) &= \bar{V}(y;C,D) = \\ &= 1 - D^2\left(1 + \frac{4C}{y} + \frac{4C^2}{y^2} + y^4 + 2y^2 - 4Cy\right) \ . \end{aligned} \tag{5.8}$$

We wish to analytically obtain the conditions for which $\bar{V}(y;C,D)$ will be definite negative for any $M \geq 0$. To that end, we write the effective potential as a sum of two polynomials

$$\bar{V}(y;C,D) = W(y;C,D) + P(y;C,D) \ , \tag{5.9}$$

where

$$\begin{aligned} W(y;C,D) &= -D^2\left(\tfrac{4C^2}{y^2} + y^4 - 4Cy\right) \\ P(y;C,D) &= 1 - D^2\left(1 + \tfrac{4C}{y} + 2y^2\right) \ . \end{aligned} \tag{5.10}$$

A graph showing the qualitative behavior of $\bar{V}$, W and P is depicted in Fig. 3.
Now, let us analyze these two functions and obtain the conditions which will impose a definite negative potential. Starting with $W(y;C,D)$, we write it as $W(y;C,D) = W_1(y;C,D) + W_2(y;C,D)$ where

$$\begin{aligned} W_1(y;C,D) &= -\tfrac{4C^2D^2}{y^2} \\ W_2(y;C,D) &= 4D^2Cy - D^2y^4 \ . \end{aligned} \tag{5.11}$$

An illustrative graph showing the qualitative characteristics (for the same values used to plot Fig. 3) of $W_1(y;C,D)$ and $W_2(y;C,D)$ is given in Fig. 4.

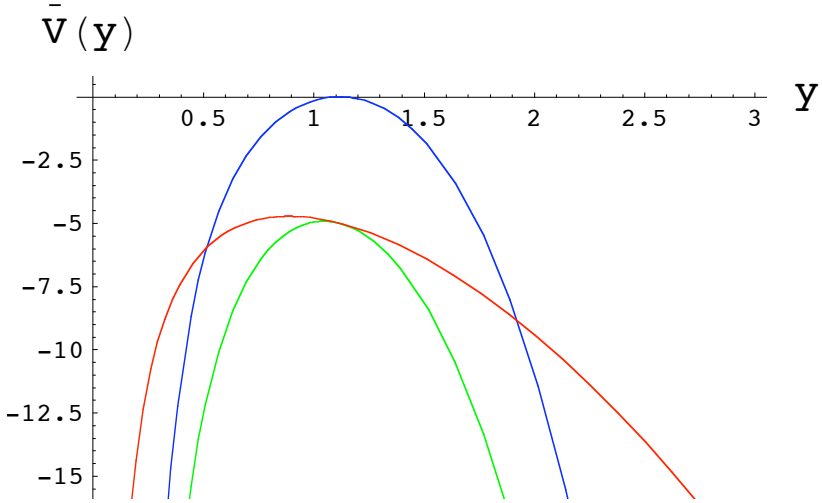

FIG. 3: An Illustrative graph representing $\bar{V}$ and its two components as a function of y, where the range of the parameters values is $D = 1$ and $C > 0$. The blue line is W, the red line is P and the green line is $\bar{V}$.

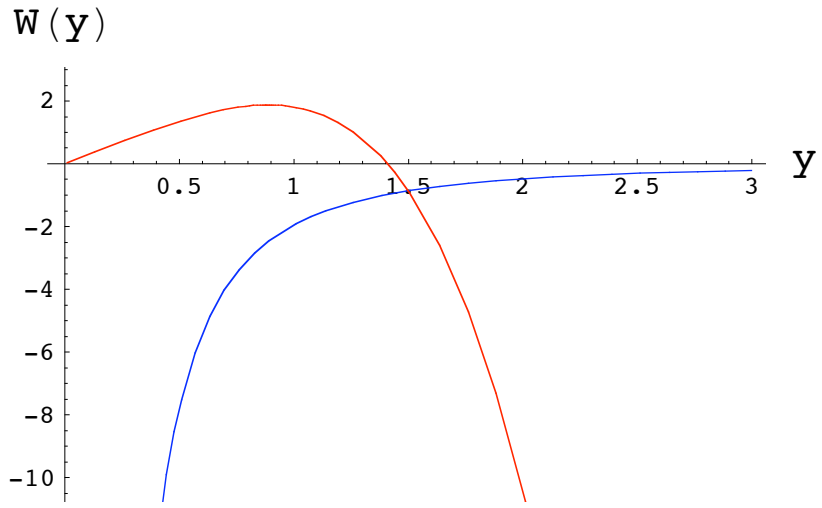

FIG. 4: An illustrative graph representing W_1 and W_2 as functions of y, for the same values of parameters as in Fig. 3. W_1 is represented by the blue line, while W_2 is represented by the red line.

W_1 is a definite negative function which is ascending for all y. W_2 is easily found to have one real maximum point y_2 which satisfies $W_2(y_2) \geqslant 0$. Thus, we can conclude that $W(y; C, D)$ has one real maximum point. The derivative of $W(y; C, D)$ is

$$\frac{\partial}{\partial_y} W(y; C, D) = 4D^2 \left(\frac{2C^2}{y^3} + C - y^3 \right) \ . \tag{5.12}$$

Equating the latter to zero yields the equation

$$y^3(y^3 - C) = 2C^2 \ , \tag{5.13}$$

whose real solution is $y_0 = (2C)^{1/3}$. Putting this into $W(y; C, D)$ shows that

$$W(y_0; C, D) = -D^2(2^{4/3} + 2^{4/3} - 2^{7/3})C^{4/3} = 0 \ . \tag{5.14}$$

Therefore, the maximum value of $W(y; C, D)$ is zero for any value of D and for all $C \geqslant 0$. Now, if the maximum value of $P(y; C, D)$ will be less than zero, we will be able to conclude that $\bar{V}$ is definite negative.
The derivative of P is

$$\frac{\partial P(y; C, D)}{\partial y} = -D^2 \left(4y - \frac{4C}{y^2} \right) \ . \tag{5.15}$$

Equating to zero we get

$$y = \frac{C}{y^2} \ , \tag{5.16}$$

which is, essentially, the same equation we obtained when looking for the maxima of $W_2(y; C, D)$. Thus, we have one real solution which is $y_1 = C^{1/3}$. Putting this into $P(y; C, D)$ we get

$$P(y_1; C, D) = 1 - D^2(1 + 6C^{2/3}) \ . \tag{5.17}$$

Demanding that $P(y = C^{1/3}; C, D) < 0$ yields the condition $D^2(1+6C^{2/3}) > 1$. Isolating $C^{2/3}$ shows that we must have

$$C^{2/3} > \frac{1}{6}\left(\frac{1}{D^2} - 1\right) \ . \tag{5.18}$$

Since we have already restricted our phase space to $C \geqslant 0$, this condition will always be fulfilled for $D \geqslant 1$ (which is equivalent to $\kappa_0 \geqslant 2$). Therefore, $\bar{V}$ will be definite negative under the conditions $C \geqslant 0$ and $D \geqslant 1$.

Lastly, we discuss the possibility for creating a child universe. As we discussed before, the coefficients $\epsilon_\pm$ determine the behavior of the radial coordinate in the direction orthogonal to the trajectory of the bubble, hence allowing us to determine the existence of wormholes.

For our metric

$$\begin{aligned} \epsilon_+ &= \mathrm{sgn}[-\chi^2 R^2 + \tfrac{2GM}{R} - \kappa_0^2] \ , \\ \epsilon_- &= \mathrm{sgn}[-\chi^2 R^2 + \tfrac{2GM}{R} + \kappa_0^2] \ . \end{aligned} \tag{5.19}$$

Since at small R values ϵ_+ is positive. at large R values we demand that ϵ_+ will change sign to allow for the bubble to expand to infinity disconnected from the original spacetime. The dominating term at large R values is $-\mathrm{sgn}[\chi^2 R^2]$ which implies that the second requirement for a child universe (as stated in Sec. 3) creation is indeed satisfied.

5.3. A More General Case

We now examine a more general case of a bubble with a hedgehog de-Sitter space in the interior and a Schwarzschild de-Sitter space in the exterior.

The hedgehog configuration is a spherically symmetric configuration where the isospin index of an isovector scalar field is identified (up to a constant) with the radial unit vector of space. In a nonlinear σ model, the scalar field part of the Lagrangian is given by

$$\mathcal{L}_f = \tfrac{1}{2}\partial_\mu\vec{\phi}\partial^\mu\vec{\phi} + \lambda(\vec{\phi}\cdot\vec{\phi} - f^2)^2 \ . \tag{5.20}$$

Concentrating on the limiting case $\lambda \to \infty$, we get

$$\mathcal{L}_f = \tfrac{1}{2}\partial_\mu\vec{\phi}\partial^\mu\vec{\phi} \ , \tag{5.21}$$

where $\vec{\phi}$ constrained to $\vec{\phi}\cdot\vec{\phi} = f^2$. Thus, $\vec{\phi}$ is parallel to the radial direction $\vec{\phi} = \pm f\hat{r}$, with $\hat{r} = (\sin\theta\cos\varphi, \sin\theta\sin\varphi, \cos\theta)$ [8]. This leads to a metric which is a configuration of a global magnetic monopole, with f being the strength of the magnetic monopole. Both of these forms for $\vec{\phi}$ lead to the same energy-momentum tensor $T_{\mu\nu}$ and also solve the scalar field equations of motion when the metric is of a spherically symmetric form. The energy-momentum tensor produced by (5.21) is given by

$$T_{\mu\nu} = \partial_\mu\vec{\phi}\partial_\nu\vec{\phi} - g_{\mu\nu}\left(\tfrac{1}{2}\partial_\rho\vec{\phi}\partial^\kappa\vec{\phi}\right) \ , \tag{5.22}$$

which yields, for $\vec{\phi} = \pm f\hat{r}$,

$$T^0_0 = T^r_r = -\frac{f^2}{r^2} \ , T^\varphi_\varphi = T^\theta_\theta = 0 \ . \tag{5.23}$$

All other components of T^μ_ν vanish. For a metric of the form $ds^2 = -sdt^2 + sdr^2 + r^2d\Omega^2$, where s is a space-time constant, $8\pi G T^\mu_\nu = G^\mu_\nu$ gives the only nonzero terms

$$T^0_0 = T^r_r = \frac{s-1}{8\pi G r^2} \ . \tag{5.24}$$

Hence, we have $s = 1 - 8\pi G f^2$. Therefore, for $8\pi G f^2 < 1$ (i.e. $s > 0$), the metric corresponds to a static geometry, while for $8\pi G f^2 > 1$ (i.e. $s < 0$) we get an anisotropic cosmology. This is because the time coordinate becomes a space-like coordinate while r becomes a time-like one and the term $r^2 d\Omega^2$ represents an expanding two-sphere with a singularity at $r = 0$. The positivity of energy (T_{00} for $s > 0$ and T_{rr} for $s < 0$) is assured provided $s < 1$.

Returning back to our case of study, the metric coefficients are now

$$\begin{aligned} A_- &= s - \chi_-^2 r^2 \ , \\ A_+ &= 1 - \tfrac{2GM}{r} - \chi_+^2 \ , \end{aligned} \tag{5.25}$$

where s should satisfy the condition $0 \leq s \leq 1$ to ensure a static geometry and positive energy. The effective potential is given by

$$\begin{aligned} V(R;\kappa_0,\chi_-,\chi_+,s,M) = \tfrac{s+1}{2} - \tfrac{\kappa_0^2}{4} - \tfrac{(s-1)^2}{4\kappa_0^2} - GM\left(1 - \tfrac{1-s}{\kappa_0^2}\right)\tfrac{1}{R} - \tfrac{(GM)^2}{\kappa_0^2 R^2} + \\ + \tfrac{GM\chi^2}{\kappa_0^2}R - \tfrac{\chi_-^2+\chi_+^2}{2}R^2 + \tfrac{s-1}{\kappa_0^2}\chi^2 2R^2 - \tfrac{\chi^4 R^4}{4\kappa_0^2} \ , \end{aligned} \tag{5.26}$$

where $\chi^2 = \chi_-^2 - \chi_+^2$.

The characteristics of the potential can be analyzed with the same method as before: Writing the effective potential as the sum $V(R;\kappa_0,\chi_-,\chi_+,s,M) = W + P$ where

$$\begin{aligned} W &= -\tfrac{(GM)^2}{\kappa_0^2 R^2} + \tfrac{GM\chi^2}{\kappa_0^2}R - \tfrac{\chi^4 R^4}{4\kappa_0^2} \ , \\ P &= \tfrac{s+1}{2} - \tfrac{\kappa_0^2}{4} - \tfrac{(s-1)^2}{4\kappa_0^2} - GM\left(1 - \tfrac{1-s}{\kappa_0^2}\right)\tfrac{1}{R} - \left(\tfrac{\chi_-^2}{2}\left(1 + \tfrac{1-s}{\kappa_0^2}\right) + \tfrac{\chi_+^2}{2}\left(1 - \tfrac{1-s}{\kappa_0^2}\right)\right)R^2 \ . \end{aligned} \tag{5.27}$$

By making the same substitutions as in Eq. (5.7) we arrive again at Eq. (5.10) for W. Therefore, the maximum value of $W(y;C,D)$ is zero for any value of D and for all $C \geqslant 0$. Now, if the maximum value of $P(y;C,D)$ will be less than zero, we will be able to conclude that $\bar{V}$ is definite negative.

$P(y;C,D)$ has one extremum point at

$$R_0 = \left(\frac{GM\left(1-\frac{1-s}{\kappa_0^2}\right)}{2\left(\frac{\chi_-^2}{2}\left(1+\frac{1-s}{\kappa_0^2}\right)+\frac{\chi_+^2}{2}\left(1-\frac{1-s}{\kappa_0^2}\right)\right)} \right)^{1/3} , \tag{5.28}$$

so that

$$\begin{aligned} P(R_0) &= \tfrac{s+1}{2} - \tfrac{\kappa_0^2}{4} - \tfrac{(s-1)^2}{4\kappa_0^2} - \\ &- \left(GM\left(1-\tfrac{1-s}{\kappa_0^2}\right)\right)^{2/3}\left(2\left(\tfrac{\chi_-^2}{2}\left(1+\tfrac{1-s}{\kappa_0^2}\right)+\tfrac{\chi_+^2}{2}\left(1-\tfrac{1-s}{\kappa_0^2}\right)\right)\right)^{1/3} - \\ &- \left(GM\left(1-\tfrac{1-s}{\kappa_0^2}\right)\right)^{2/3}\tfrac{1}{2^{2/3}}\left(\tfrac{\chi_-^2}{2}\left(1+\tfrac{1-s}{\kappa_0^2}\right)+\tfrac{\chi_+^2}{2}\left(1-\tfrac{1-s}{\kappa_0^2}\right)\right)^{1/3} . \end{aligned} \tag{5.29}$$

Defining the parameters

$$\begin{aligned} A &= \kappa_0^2 + 1 - s \\ B &= \kappa_0^2 - 1 + s \end{aligned} \tag{5.30}$$

where $A \geq B$, A is always non negative and B is non negative for $\kappa_0^2 \geq 1-s$, $P(R_0)$ can be written as

$$P(R_0) = 1 - \tfrac{A^2}{4\kappa_0^2} - \left(\tfrac{GM}{2\kappa_0^2}B\right)^{2/3}\left(\tfrac{\chi_-^2}{2\kappa_0^2}A + \tfrac{\chi_+^2}{2\kappa_0^2}B\right)^{1/3} . \tag{5.31}$$

Demanding that $P(R_0)$ will not be greater than zero yields the condition

$$1 - \tfrac{A^2}{4\kappa_0^2} \leq \left(\tfrac{GM}{2\kappa_0^2}B\right)^{2/3}\left(\tfrac{\chi_-^2}{2\kappa_0^2}A + \tfrac{\chi_+^2}{2\kappa_0^2}B\right)^{1/3} . \tag{5.32}$$

Of course, for this equation to have a meaning we must demand that B will not be negative, which gives the condition $\kappa^2 \geq 1-s$. Because we wish to have a child universe

solution with an arbitrarily small M, we now demand that $1-\frac{A^2}{4\kappa_0^2} \leq 0$, which is equivalent to

$$\kappa_0^4 - 2\kappa_0^2(1+s) + (1-s)^2 \geq 0 \ . \tag{5.33}$$

The zeros of the polynomial with κ_0^2 being the argument are at $1+s\pm 2\sqrt{s}$. It is easy to check that both zeros are always positive. Thus, the general solution is $1+s+2\sqrt{s} \leq \kappa_0^2$ and $\kappa_0^2 \leq 1+s-2\sqrt{s}$. Now, the condition for the non negativeness of B comes in handy and leaves us with the sole condition $1+s+2\sqrt{s} \leq \kappa_0^2$. When there is no hedgehog and $s=1$, this solution converges to the usual solution $\kappa_0 \geq 2$.

Turning to discuss the possibility for creating a child universe, we obtain

$$\begin{aligned} \epsilon_+ &= \mathrm{sgn}[s-1-(\chi_-^2-\chi_+^2)R^2 + \tfrac{2GM}{R} - \kappa_0^2] \ , \\ \epsilon_- &= \mathrm{sgn}[s-1-(\chi_-^2-\chi_+^2)R^2 + \tfrac{2GM}{R} + \kappa_0^2] \ . \end{aligned} \tag{5.34}$$

Since at small R values ϵ_+ is positive. at large R values we demand that ϵ_+ will change sign to allow for the bubble to expand to infinity disconnected from the original space-time. The dominating term at large R values is $-\mathrm{sgn}[(\chi_-^2-\chi_+^2)R^2]$ which implies that we the condition for a child universe creation is $\chi_-^2 > \chi_+^2$. This, of course, is valid for false vacuum bubbles.

5.4. Conclusions

In this section, as well as in the preview Sec. 3, we have discussed the formation of a child universe, reviewing in an historical perspective the relevance and distinctive features of the process. We have also described a refinement of one of the simplest realizations of a region of space-time disconnecting from an ambient one, namely the one in which the interior region is described by Minkowski space-time and the exterior one by Schwarzschild space-time. In the models we have reviewed, the consideration of

a string gas for the matter composing the thin shells that separates the two domains, supports the interesting idea that child universe creation can take place out of almost empty space. We have also proceeded to make natural generalizations of this model and have seen that they preserve this suggestive result.

To summarize, the main picture that emerges from this discussion is as follows. Firstly, although we certainly have in mind applications to early universe cosmology, we have used the term 'child universe' in a more generic sense, as a region of space-time that eventually disconnect from a pre-existing *parent* one. We have also seen that this process can take place starting from almost empty space under the generic condition of κ_0 being large enough. Therefore, when the string content on the shell exceeds a critical value, the creation of a child universe can happen at an arbitrary small value of M, i.e. the critical mass threshold is completely absent.

These results strongly support the idea that, in general, child universe creation is more likely to happen when the energy density of the child universe becomes bigger and bigger. In field theory realizations of child universe creation, the energy density of the space-time is related to the vacuum expectation value of a scalar field: The higher its energy density, the more excited the state (false vacuum). In this sense, child universes with a higher energy density are more excited than child universes with a lower energy density and it appears that the creation of more excited child universes is more likely. Further developments of these ideas and a more detailed account of their possible applications are subject to our current research and will be reported in the future.

Part III

Axion-Photon Conversion in Two Spatial Dimensions

6. AXIONS: AN INTRODUCTION

The Peccei-Quinn (PQ) mechanism [47, 48] is the most compelling solution of the strong CP problem, namely the question why this discrete symmetry is not violated by the non-trivial vacuum structure of QCD. Central to the PQ mechanism is the axion [49–52], the Goldstone boson of a new spontaneously broken symmetry $\mathrm{U(1)_{PQ}}$, with properties closely related to those of the neutral pion. The axion mass m_a is given by $m_a f_a \sim m_\pi f_\pi$, where $m_\pi = 135$ MeV and $f_\pi = 92$ MeV are the pion mass and decay constant, respectively, and f_a is the PQ symmetry breaking scale. The axion couplings with matter and radiation scale as $1/f_\mathrm{a}$. Experimental and astrophysical constraints imply that $f_a \gtrsim 10^9$ GeV, corresponding to $m_a \lesssim 10$ meV [53]. Thus, axions are expected to be very light, very weakly interacting and very long lived. The peculiar properties of axions allow them to be produced in the early universe as coherent field oscillations and therefore to provide all or part of the cold dark matter [54, 55].

Nonetheless, it might still be possible to find these "invisible axions" in terrestrial experiments. The generic $a\gamma\gamma$ vertex allows for axion-photon conversion in external electric or magnetic fields in analogy to the Primakoff effect for neutral pions. The smallness of the axion mass allows this conversion to take place coherently over macroscopic distances, compensating for the smallness of the interaction strength [56]. It is especially promising to use the sun as a source for axions. A strong magnet directed toward the sun and follows it allows one to search for keV-range X-rays produced by an axion-photon conversion, a process best visualized as a particle oscillation phenomenon [57] (in analogy

to neutrino flavor oscillations).

The aim of this introductory section is to provide the reader with a summarized review of axions theory. This calls for an introduction of the strong CP problem and, of course, the PQ mechanism as a possible solution, since these lead to the prediction of the axion as a consequence of the PQ symmetry breaking. Before, however, going through these subjects, let us begin this review by discussing the subject of chiral anomalies, concentrating mainly on the QCD anomalies.

6.1. The Chiral Anomaly in QCD

In (quantum) physics an anomaly is the failure of a symmetry which exists at the theory's classical level to exist as a symmetry of any regularization of the full quantum theory. In this section we wish to analyze the chiral anomaly which arises in the theory of strong interactions, Quantum Chromo-Dynamics (QCD).

The QCD Lagrangian has approximate axial symmetries, under which the right and left handed parts of the light quarks are rotated in opposite directions. In the limit of vanishing fermion masses (as m_u, $m_d \ll \Lambda_{\mathrm{QCD}}$ this approximation makes sense, at least for these quarks) the chiral transformation

$$\psi(x) \to \mathrm{e}^{\frac{i}{2}\alpha\gamma_5}\psi(x) \ , \tag{6.1}$$

which corresponds to the following Noether current (often called the axial vector current)

$$j^{\mu 5}(x) = \bar{\psi}(x)\gamma^\mu\gamma^5\psi(x) \ , \tag{6.2}$$

is an exact symmetry (one can easily compute $\partial_\mu j^{\mu 5} = 2im\bar{\psi}\gamma^5\psi$ assuming that ψ satisfies Dirac's equation. Hence $j^{\mu 5}$ is conserved for $m = 0$). Because the transformation $\psi(x) \to \mathrm{e}^{i\alpha/2}\psi(x)$, with the corresponding Noether vector current $j^\mu(x) = \bar{\psi}(x)\gamma^\mu\psi(x)$,

is also a symmetry of the Lagrangian, one would expect the strong interactions with N flavors to be approximately $U(N)_V \times U(N)_A$ invariant.

However, this symmetry is true in the classical picture of massless QED and QCD. In gauge theories, the conservation of the axial vector current is actually incompatible with gauge invariance and radiative corrections add a nonzero term to the divergence of $j^{\mu 5}$, as we now wish to show.

For simplicity, let us begin with massless four dimensional QED. It is known that the fermion fields satisfy the following equations of motion

$$\not{\partial}\psi = -ie\not{A}\psi \ , \quad \partial_\mu \bar{\psi}\gamma^\mu = ie\bar{\psi}\not{A} \ . \tag{6.3}$$

Of course, at first sight, these equations may lead us again to conclude the $j^{\mu 5}$ is conserved. However, the axial vector current is a composite operator of fermion fields. It is known that products of local operators are often singular. Therefore, following the discussion in [58], let us define $j^{\mu 5}$ by placing the fields at two different points separated by distance η and then carefully take the limit as $\eta \to 0$

$$j^{\mu 5} = \text{symm} \lim_{\eta \to 0} \left[\bar{\psi}(x + \tfrac{\eta}{2}) \gamma^\mu \gamma^5 \exp\left(-ie \int_{x-\eta/2}^{x+\eta/2} A(z) dz \right) \psi(x - \tfrac{\eta}{2}) \right] \ . \tag{6.4}$$

One should notice that for $j^{\mu 5}$ to transform properly under Lorentz transformations, the limit has to be taken symmetrically

$$\text{symm} \lim_{\eta \to 0} \frac{\eta^\mu}{\eta^2} = 0 \ , \quad \text{symm} \lim_{\eta \to 0} \frac{\eta^\mu \eta^\nu}{\eta^2} = \frac{1}{d} g^{\mu\nu} \ , \tag{6.5}$$

with $d = 4$ in our case. Now, taking the divergence of Eq. (6.4) and keeping terms up to order η, we arrive at

$$\partial_\mu j^{\mu 5} = \text{symm} \lim_{\eta \to 0} \left[\bar{\psi}(x + \tfrac{\eta}{2}) \left(-ie\gamma^\mu \eta^\nu (\partial_\mu A^\nu - \partial_\nu A^\mu) \right) \gamma^5 \psi(x - \tfrac{\eta}{2}) \right] \ . \tag{6.6}$$

To find the anomaly in closed form, one must calculate the singular terms (which arise in a nonzero background gauge field) in the operator product of the two fermion fields in the limit $\eta \to 0$. The leading term in this calculation is vanishing and thus it is required to consider higher order terms in the expansion of the product of two operators. The second order term is already nonzero and gives

$$\langle \bar{\psi}(x+\tfrac{\eta}{2})\gamma^\mu\gamma^5\psi(x-\tfrac{\eta}{2})\rangle \sim 2e\epsilon^{\alpha\beta\mu\gamma}F_{\alpha\beta}(x)\left(\frac{i\eta_\gamma}{8\pi^2\eta^2}\right) \ , \tag{6.7}$$

where $F_{\alpha\beta}$ is the electromagnetic field tensor and α and β are Lorentz indices. Plugging this result into Eq. (6.6) we obtain

$$\partial_\mu j^{\mu 5} = \text{symm}\lim_{\eta\to 0}\left[\frac{e}{4\pi^2}\epsilon^{\alpha\beta\mu\gamma}F_{\alpha\beta}\frac{i\eta_\gamma}{\eta^2}(-ie\eta^\nu F_{\mu\nu})\right] \ . \tag{6.8}$$

Now, we take the symmetric limit which yields

$$\partial_\mu j^{\mu 5} = \frac{e^2}{16\pi^2}\epsilon^{\alpha\beta\mu\nu}F_{\alpha\beta}F_{\mu\nu} = \frac{e^2}{8\pi^2}\tilde{F}^{\mu\nu}F_{\mu\nu} \ , \tag{6.9}$$

where $\tilde{F}^{\mu\nu} = \frac{1}{2}\epsilon^{\alpha\beta\mu\nu}F_{\alpha\beta}$ is the dual electromagnetic field tensor. This equation demonstrates the anomalous non-conservation of $j^{\mu 5}$ and is known as the Adler-Bell-Jackiw anomaly [59].

Turning to QCD, let us again put an emphasis on the fact that we are ignoring all but the lightest quarks (i.e. u and d) for the sake of the discussion to follow. Then, the fermionic part of the QCD Lagrangian is

$$\mathcal{L} = \bar{u}i\not{D}u + \bar{d}i\not{D}d - m_u\bar{u}u - m_d\bar{d}d \ , \tag{6.10}$$

where $D_\mu = \partial_\mu - igA^a_\mu t^a$ is the gauge covariant derivative, with g being the coupling constant, A^a_μ are the eight gluon gauge fields and t^a are the group generators. The

mass terms are very small and thus may be neglected. With this approximation, the Lagrangian has isospin symmetry which mixes between the two quarks fields. However, this classical Lagrangian has no coupling between left and right handed quarks it does obey the separate unitary transformations

$$\begin{pmatrix} u \\ d \end{pmatrix}_L \to U_L \begin{pmatrix} u \\ d \end{pmatrix}_L \ , \quad \begin{pmatrix} u \\ d \end{pmatrix}_R \to U_R \begin{pmatrix} u \\ d \end{pmatrix}_R \ . \tag{6.11}$$

Separating the $SU(2)$ and $U(1)$ parts of these transformations, we see that $\mathcal{L}$ is invariant under $SU(2)_L \times SU(2)_R \times U(1)_L \times U(1)_R$ symmetry group. Denoting the quark doublet by Q, with the chiral components

$$Q_L = \left(\frac{1-\gamma^5}{2}\right)\begin{pmatrix} u \\ d \end{pmatrix} \ , \quad Q_R = \left(\frac{1+\gamma^5}{2}\right)\begin{pmatrix} u \\ d \end{pmatrix} \ , \tag{6.12}$$

one can write the currents associated with this symmetry group as

$$\begin{aligned} j_L^\mu &= \bar{Q}_L \gamma^\mu Q_L \ , \quad j_R^\mu = \bar{Q}_R \gamma^\mu Q_R \ , \\ j_L^{\mu a} &= \bar{Q}_L \gamma^\mu \tau^a Q_L \ , \quad j_R^{\mu a} = \bar{Q}_R \gamma^\mu \tau^a Q_R \ , \end{aligned} \tag{6.13}$$

where the $\tau^a = \sigma^a/2$ are the generators of the $SU(2)$ group, with $a, b, c...$ being the Lie symmetry group indices here and throughout this section. Now it is simple to take the differences of these currents to find the axial vector currents

$$j^{\mu 5} = \bar{Q}\gamma^\mu \gamma^5 Q \ , \quad j^{\mu 5 a} = \bar{Q}\gamma^\mu \gamma^5 \tau^a Q \ , \tag{6.14}$$

where $j^{\mu 5 a}$ are the axial isotriplet currents and $j^{\mu 5}$ is the isospin singlet axial current. Next, to discover whether or not these currents are anomalous, one needs to modify the chiral conservation laws due to the coupling of the quark currents to the gluon fields.

Then, one discovers that the anomaly equation should be the Abelian result, supplemented by an appropriate group theory factor, or the anomaly coefficient. Moreover, since the axial current is gauge invariant, the anomaly must be gauge invariant as well and hence contain the full non-Abelian field strength.

For the general case, this totally symmetric coefficient is given by $\mathcal{A}_{abc} = \mathrm{Tr}[t^a\{t^b, t^c\}]$ and is a trace over the group matrices in the representation R. So that in general, the divergence of an axial vector current is given by

$$\partial_\mu j_a^\mu = \frac{\mathcal{A}_{abc}}{64\pi^2} g^2 \epsilon^{\alpha\beta\mu\nu} M^b_{\alpha\beta} M^c_{\mu\nu} \ , \tag{6.15}$$

where $M^c_{\mu\nu}$ is the field strength corresponding to the general symmetry and g is the associated gauge coupling strength. Therefore, unless $\mathcal{A}_{abc}$ vanishes the current j_a^μ is not conserved.

In our model, we can find the anomaly coefficient for the Adler-Bell-Jackiw anomaly from the triangle diagrams (illustrated in Fig. 5). Then, for the axial isospin currents

$$\partial_\mu j^{\mu 5a} = \frac{g^2}{32\pi^2} \epsilon^{\alpha\beta\mu\nu} G^c_{\alpha\beta} G^d_{\mu\nu} \cdot \mathrm{Tr}[\tau^a t^c t^d] \ , \tag{6.16}$$

where $G^c_{\mu\nu}$ is the gluon field strength, τ^a is the isospin matrix, t^c is a color matrix and the trace is taken over colors and flavors. Since the trace of a single τ^a vanishes we have $\mathrm{Tr}[\tau^a t^c t^d] = 0$ and the axial isospin currents are unaffected by the Adler-Bell-Jackiw anomaly of QCD.

However, for the isospin singlet axial current, τ^a is replaced by the matrix 1 on flavors and hence one finds that

$$\partial_\mu j^{\mu 5} = \frac{g^2 N}{32\pi^2} \epsilon^{\alpha\beta\mu\nu} G^c_{\alpha\beta} G^c_{\mu\nu} \ , \tag{6.17}$$

with $N = 2$ in the current model we are examining. Therefore, this current is indeed not conserved in QCD.

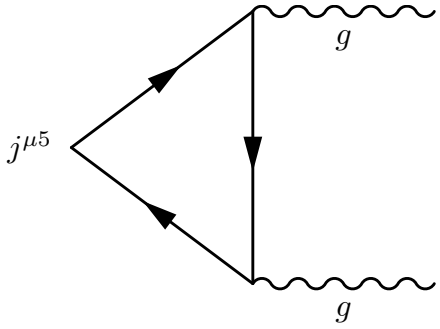

FIG. 5: The triangle diagram associated with the four dimensional anomaly.

Let us conclude this section by mentioning that the axial isospin currents, although anomaly free from QCD interactions, do suffer from an anomaly associated with the coupling of quarks to electromagnetism. This anomaly is responsible to the matrix element of the decay $\pi^0 \to 2\gamma$.

6.2. The Strong CP Problem and QCD vacuum topology

In the massless quark limit, the chiral anomaly of QCD we have derived in the previous section affects the action in the following way

$$\delta W = \alpha \int d^4x \partial_\mu j^{\mu 5} = \alpha \frac{g^2 N}{32\pi^2} \int d^4x \epsilon^{\alpha\beta\mu\nu} G^c_{\alpha\beta} G^c_{\mu\nu} \ . \tag{6.18}$$

An interesting puzzle that arrises from this anomaly term, is that the pseudoscalar density is in fact a total derivative

$$\tilde{G}^{c\mu\nu} G^c_{\mu\nu} = \partial_\mu K^\mu \ , \text{ with } \ K^\mu = \epsilon^{\mu\alpha\beta\gamma} A_{c\alpha} (G_{c\beta\gamma} - \tfrac{g}{3} f_{cab} A_{a\beta} A_{b\gamma}) \ . \tag{6.19}$$

Thence, δW is a surface integral

$$\delta W = \alpha \frac{g^2 N}{32\pi^2} \int d^4x \partial_\mu K^\mu = \alpha \frac{g^2 N}{32\pi^2} \int d\sigma_\mu K^\mu \ . \tag{6.20}$$

If one uses the naive boundary conditions with $A_c^\mu = 0$ at spatial infinity, the last integral vanishes. However, 't Hooft showed [60, 61] that the correct boundary condition is that A_c^μ should be a pure gauge field at spatial infinity. In other words, A_c^μ should be 0 or a gauge transformation of 0. With these boundary conditions, the surface integral does not vanish and $U(1)_A$ is not a symmetry of QCD.

Let us follow the discussion in [51] to show this point and its consequences. If one chooses the temporal gauge $A_c^0 = 0$ and considers $SU(2)$ QCD for simplicity, one is left to consider only spatial gauge fields A_c^i. The gauge transformation of these fields is given by

$$\tfrac{1}{2}\tau^c A_c^i = A^i \to \Omega A^i \Omega^{-1} + \frac{i}{g}\nabla^i \Omega \Omega^{-1} \ , \tag{6.21}$$

where Ω is the gauge transformation matrix. This equation implies that vacuum configurations either vanish or have the form $\frac{i}{g}\nabla^i\Omega\Omega^{-1}$. A topological distinction between various possible vacuum states (which are classically associated with pure gauge transformations) is introduced by demanding that at spatial infinity the gauge fields should vanish. Hence, when $r \to \infty$, the gauge transformations in Eq. (6.21) are restricted to those that obey $\lim_{r\to\infty} \Omega \to 1$. These transformations define a mapping of the three dimensional space with points at infinity identified into the group space.

Remembering that we have restricted ourselves to an $SU(2)$ subgroup of QCD, this mapping is a $S^3 \to S^3$ mapping, since the manifold of $SU(2)$ is also homomorphic to the three dimensional sphere S^3. It is known that these mappings fall into distinct (homotopy) classes that cannot be continuously distorted into each other and are classified by an integer n. For the $SU(2)$ QCD case we are concentrating here, the matrices Ω can be written as

$$\Omega_n = \mathrm{e}^{i2\pi n} \ , \quad \text{for } r \to \infty \text{ and where } n = 0, \pm 1, \pm 2, \dots \ , \tag{6.22}$$

where the index n indicates to which homotopy class they belong. Hence, the gauge fields A^i (and thus the associated vacua) can also be classified by the integer n

$$A^i_n = \frac{i}{g}\Omega_n \nabla^i \Omega_n^{-1} \ . \tag{6.23}$$

The so called winding number n can be expressed by an integral over the gauge fields A^i_n [62]

$$n = \frac{ig^3}{24\pi^2}\int d^3r \ \mathrm{Tr}[\epsilon_{ijk}A^i_n A^j_n A^k_n] \ . \tag{6.24}$$

The latter can be understood since the term $\epsilon_{ijk}A^iA^jA^k$ is essentialy the Jacobian of the transformation from from S^3 to the hypersphere in group space, with n measuring the number of windings of S^3 on the group space.
Let us see now how this gives a further way to classify the vacuum configurations. The expression for n is closely related to K^μ, where in the gauge we have chosen, only $K^0 \neq 0$ and one finds for pure gauge fields

$$K^0 = -\frac{g}{3}\epsilon_{ijk}\epsilon_{abc}A^i_a A^j_b A^k_c = \frac{4}{3}ig\epsilon_{ijk}\mathrm{Tr}[A^iA^jA^k] \ . \tag{6.25}$$

Hence, we see now that the space-time integral of $\tilde{G}G$ is now determined by the change of the charge $\frac{g^2}{32\pi^2}\int d^3xK^0 = N_{cs}$ (indeed, in the vacuum we have $N_{cs} = n$. However this relation does not hold in the general case) between initial and final surfaces [63]

$$\begin{aligned} &\tfrac{g^2}{32\pi^2}\int d\sigma_\mu K^\mu\big|^{t=t_f\to\infty}_{t=t_i\to-\infty} = \tfrac{g^2}{32\pi^2}\int d^3xK^0(x,t_f) - \tfrac{g^2}{32\pi^2}\int d^3xK^0(x,t_i) = \\ &= \tfrac{g^2}{32\pi^2}\int d^4x\tilde{G}^{c\mu\nu}G^c_{\mu\nu} = N_{cs}(t_f) - N_{cs}(t_i) \ , \end{aligned} \tag{6.26}$$

where the quantity N_{cs} is called the Chern-Simons number of the gauge field configuration.

Then, even though the pseudoscalar density is a total derivative it can indeed have a physical implication, because the change in N_{cs} does not need to vanish in vacuum to vacuum transitions. The reason for this is that the QCD vacuum is topologically non-trivial. The existence of this charge implies that the QCD ground state is not unique. In fact, it consists of a combination of degenerate states which are distinguished by their N_{cs} eigenvalue.

To see that, let us first notice that representations of Ω_n are constructed by $\Omega_n = (\Omega_1)^n$. Then, one can change the gauge field A^i_n to A^i_{n+1}. Even though one can regard a vacuum state associated with each of the gauge field classes A^i_n, the true vacuum state of QCD cannot be anyone of these $|n\rangle$ (where $N_{cs}|n\rangle = n|n\rangle$) vacua since they are not gauge invariant ($\Omega_1|n\rangle = |n+1\rangle$). So one can conclude that the true vacuum is, in fact, a *superposition* of these so called n-vacua and is called the θ vacuum

$$|\theta\rangle = \sum_n \mathrm{e}^{-in\theta}|n\rangle \ , \tag{6.27}$$

where now $\Omega_1|\theta\rangle = \sum_n \mathrm{e}^{-in\theta}|n+1\rangle = \mathrm{e}^{i\theta}|\theta\rangle$.

Now, one can write the vacuum to vacuum transition amplitude

$${}_+\langle\theta|\theta\rangle_- = \sum_{m,n} \mathrm{e}^{im\theta}\mathrm{e}^{-in\theta}\ {}_+\langle m|n\rangle_- = \sum_\nu \mathrm{e}^{i\nu\theta}\sum_n\ {}_+\langle n+\nu|n\rangle_- \ , \tag{6.28}$$

where $\nu = n_+ - n_-$, the $+$ and $-$ subscripts refer to later and earlier times, respectively. Hence, the vacuum amplitude is a sum over vacuum transition amplitudes, in which ν is the net change in the winding number between later and earlier times (see Eq. (6.26)). The phase factor $\mathrm{e}^{i\nu\theta}$ in Eq. (6.28) can be interpreted as an effective *additional* term in the QCD Lagrangian. The transition amplitudes ${}_+\langle n+\nu|n\rangle_-$ are given by a path integral in which the space-time integral of $\tilde{G}G$ is fixed by Eq. (6.26). Then, using the usual path integral representation for the vacuum to vacuum amplitude, one finds that [51]

$$ {}_+\langle\theta|\theta\rangle_- = \sum_\nu \int \delta A \mathrm{e}^{iS_{eff}[A]} \delta \left(\nu - \frac{g^2}{32\pi^2} \int d^4x \ \tilde{G}^{c\mu\nu} G^c_{\mu\nu} \right) \ , \tag{6.29} $$

where

$$ S_{eff}[A] = S_{\mathrm{QCD}}[A] + \theta \frac{g^2}{32\pi^2} \int d^4x \ \tilde{G}^{c\mu\nu} G^c_{\mu\nu} \ , \tag{6.30} $$

and A is the non-abelian gauge field. Therefore, the complicated nature of the QCD vacuum effectively adds a term to the QCD Lagrangian, the famous θ term

$$ \mathcal{L}_\theta = \theta \frac{g^2}{32\pi^2} \tilde{G}^{c\mu\nu} G^c_{\mu\nu} \ . \tag{6.31} $$

However, if one includes the weak interactions in the theory, then the quark mass matrix M is in general complex

$$ \mathcal{L}_{mass} = \bar{q}_{iR} M_{ij} q_{jL} + \mathrm{h.c.} \tag{6.32} $$

When one transforms this to a physical basis, one performs a chiral transformation in order to diagonalize this mass matrix. By doing so, θ changes by the term Arg Det$M$. Hence, in the full theory the coefficient of the pseudoscalar density term $\tilde{G}G$ is in fact

$$ \bar{\theta} = \theta + \mathrm{Arg\ Det} M \ . \tag{6.33} $$

Then, the additional term in the Lagrangian is in fact

$$ \mathcal{L}_{\bar{\theta}} = \bar{\theta} \frac{g^2}{32\pi^2} \tilde{G}^{c\mu\nu} G^c_{\mu\nu} \ . \tag{6.34} $$

This term violates P and T but conserves the C invariance. Therefore, this term violates the CP symmetry, unless $\bar{\theta}$ is very small. Experiments show that this is indeed the case and CP violation is not observed in strong interactions. The value of $\bar{\theta}$ can be determined from the neutron electric dipole moment (nEDM) d_n, which is induced by the additional term $\mathcal{L}_{\bar{\theta}}$. The nEDM can be estimated by [63]

$$d_n \simeq \bar{\theta} \frac{e\, m_u m_d}{(m_u + m_d) m_n^2} \,, \tag{6.35}$$

where m_n is the mass of the neutron. The experimental bound of d_n is $|d_n| \leq 3 \times 10^{-26}\ e$ cm [64] leads to the constraint $\bar{\theta} \lesssim 10^{-9}$. This remarkably small magnitude of $\bar{\theta}$ means, in practice, that low energy QCD is approximately CP conserving. Such a low value of $\bar{\theta}$ is allowed. However, it implies that either both of the contributions to $\bar{\theta}$ in (6.33) are very small or that these contributions cancel each other, resulting in a fine-tuning of the parameters. Thus, the strong CP problem really asks why is the $\bar{\theta}$ angle, coming from both strong and weak interactions, is so small, rather than questioning the smallness of merely θ. In other words, we ask why do the strong interactions seem to not violate CP - when CP violation is not forbidden by the theory.

6.3. The $U(1)_{PQ}$ Symmetry and Axions

There are, in principle, three possible solutions to the strong CP problem. The first involves unconventional dynamics (for example, that the boundary conditions that give rise to the θ vacuum are an artifact, or that the θ vanishes from the form of the vacuum energy). The second considers spontaneously broken CP to justify setting $\theta = 0$ already at the Lagrangian level.

However, the most attractive and widely excepted, and also perhaps natural, way to solve the strong CP problem is to introduce an additional global chiral $U(1)$ symmetry, which has become known as the $U(1)_{PQ}$ symmetry, as this chiral symmetry effectively

rotates the θ-vacua away. This symmetry is necessarily spontaneously broken and its introduction into the Lagrangian effectively replaces the the static CP violating angle $\bar{\theta}$ with a dynamical, CP conserving, field: The axion.

6.3.1. The Peccei-Quinn Mechanism

As a starting point to the dynamical θ solution, let us introduce the original idea by Peccei and Quinn. As we have seen, the non-trivial vacuum to vacuum transition amplitude in QCD gives rise to an effective term in the Lagrangian

$$\mathcal{L}_{eff} = \mathcal{L} + \theta \frac{g^2}{32\pi^2} \tilde{G}^{c\mu\nu} G^c_{\mu\nu} \ . \tag{6.36}$$

If $\mathcal{L}$ describes a non abelian gauge theory of the strong interactions this effective term gives rise to strong CP violation, as we saw in the previous section. Then, Peccei and Quinn claimed that $\mathcal{L}$ must posses a chiral $U(1)$ invariance, such that changes in θ are equivalent to changes in the definitions of the various fields in $\mathcal{L}$ and have no physical implications. Any such theory is then equivalent to a $\theta = 0$ theory and this has no strong CP violation. The famous and novel contribution made by Peccei and Quinn to previous theories (which shown that the argument for obtaining a CP violation free theory holds for theories in which $\mathcal{L}$ represents a non abelian gauge field coupled to massless fermions only) was that this argument "remains true when some fermion masses are included in $\mathcal{L}$, or even when all strongly interacting fermions become massive, provided that at least one fermion gets its entire mass from a Yukawa coupling to a scalar field, such that the full $\mathcal{L}$ can posses at least a single $U(1)$ invariance" [48].
Here, following [48], we consider $\mathcal{L}$ to describe a simplified model with one flavor of fermion coupled to a single complex color singlet scalar field with Yukawa coupling strength f

$$\mathcal{L} = -\tfrac{1}{4}G^c_{\mu\nu}G^{c\,\mu\nu} + \bar{\psi}i\not{D}\psi + \bar{\psi}\left[f\phi\left(\tfrac{1+\gamma^5}{2}\right) + f^*\phi^*\left(\tfrac{1-\gamma^5}{2}\right)\right]\psi$$
$$-|\partial_\mu\phi|^2 - \mu^2|\phi|^2 - h|\phi|^4 \ , \tag{6.37}$$

with $\mu^2 < 0$ and h being the parameters which determine the renormalizable self interaction term. In this theory where there is an anomalous term in the effective Lagrangian, a chiral transformation (i.e. Eq. (6.1)) redefines the θ parameter (see Eq. (6.18), which implies that $\theta \to \theta - \alpha$). If all fermions are massive such a rotation will also change the fermion mass term $f\langle\phi\rangle$. Thus, one can define inequivalent theories with the same mass terms for different θ values. However, equivalent theory classes related by the transformation (6.1) exist as well. Moreover, only one such class of theories , where $\theta \to 0$ when all the fermion masses have been made real by an appropriate chiral transformation, will give a CP invariant theory.

The effective potential for the scalar fields in the theory is θ dependent an does not have the same symmetry as the scalar self interaction term in $\mathcal{L}$. Hence, the minimum of the potential corresponds to a particular choice of phases for the various scalar vacuum expectation values (VEVs). These phases appear in the fermion mass terms and are such that when the fermion masses are made real, then $\theta = 0$.

To show that these theories are CP invariant one defines $\kappa = \mathrm{Arg}[\mathrm{e}^{i\theta}f\langle\phi\rangle]$ and demand that this term will be zero

$$\kappa = \mathrm{Arg}[\mathrm{e}^{i\theta}f\langle\phi\rangle] = 0 \ . \tag{6.38}$$

The latter is equivalent to the demand we expressed before, i.e. that the fermion mass $f\langle\phi\rangle$ will be real when the fields are defined so that $\theta = 0$.

Peccei and Quinn were able to prove that Eq. (6.38) is indeed satisfied. However, we shall supply the reader with only a short summary of their proof and then move on to explain its consequences and implications.

By examining the generating functional of the scalar Green's functions, one finds that the scalar VEV is defined by

$$\langle\phi\rangle = \lambda \mathrm{e}^{i\beta} \ , \tag{6.39}$$

where λ and β are real constants. Then, one can make the change of variables $\phi = \mathrm{e}^{i\beta}(\lambda + \rho + i\alpha/2)$, where ρ and α are real scalar fields. By integrating out vector and fermion fields and obtaining an expression for the generating functional of the scalar Green's functions in terms of non-local polynomials of the scalar fields, one is able to write the constraints $\langle\rho\rangle = \langle\alpha\rangle = 0$. These constraints require that $\kappa = 0,\ \pi$, which are stationary points of the scalar potential. To find which of these points is the true minimum point, it is required to examine the potential itself. Peccei and Quinn did so to leading order for small f and h and found that the true vacuum occurs for $\kappa = 0$: In this approximation the scalar potential is given by

$$V_\theta(\phi) = U(\phi) + K\,|f\phi|\cos\kappa \ , \tag{6.40}$$

where

$$U(\phi) = -\mu^2\phi^*\phi - h(\phi^*\phi)^2 \ , \tag{6.41}$$

$$K = \frac{\int (dA_\mu)_1 \int d\psi \int d\bar{\psi} \int d^4x \bar{\psi}(x)\frac{1}{2}(1+\gamma^5)\psi(x)\ \exp[\int d^4x'(-\frac{1}{4}FF + \bar{\psi}i\not{D}\psi)]}{\int (dA_\mu)_0 \int d\psi \int d\bar{\psi}\ \exp[\int d^4x(-\frac{1}{4}FF + i\bar{\psi}i\not{D}\psi)]} \ , \tag{6.42}$$

and K is a real and positive constant. The subscript q of $(dA_\mu)_q$ defines the θ vacuum on which the paths are summed (terms with $|q| \geq 2$ contribute only in the order f^2 and therefore are not considered in this approximation).

From the form of the scalar potential V_θ it is seen that it does not posses the $U(1)$ symmetry which was required in the original Lagrangian (i.e. without the additional effective θ term) and thus in $U(\phi)$. Therefore, "for some range of the parameters $\kappa = 0$ is the true minimum of the scalar potential and thus the resultant theory is CP conserving" [48]. In their paper, Peccei and Quinn did consider the inclusion of weak and electromagnetic interactions. However, we shall save this for later as we just wish to present the principal of the PQ mechanism here. Hence, this concludes our short summary of the proof given by Peccei and Quinn.

A few important points should be noticed here. Although Peccei and Quinn were able to find a successful solution to the strong CP problem by the dynamical relaxation of θ, they considered a crude approximation for the scalar potential (in their own words). This is seen by the fact that the parameters f and h may indeed be small in some physical situations, the combination $f\lambda$ should not be so small as it is, in fact, the fermion mass scale. Moreover, they did not consider one of the consequences of their model in what concerns the existence of a Goldstone boson (since a global chiral symmetry was broken). In the following, we shall discuss the interpretation of Weinberg [49] and Wilczek [50] to the chiral symmetry breaking. This model, sometimes referred to as the PQWW model, introduces a new Higgs doublet and gives rise to the so called standard axion.

6.3.2. The PQWW Axion

Soon after the appearance of the PQ mechanism as a solution to the strong CP problem, it was realized separately by Weinberg [49] and Wilczek [50] that this mechanism involves a pseudoscalar Goldestone boson, the axion field.

The PQWW axion is the common phase field in the two Higgs doublet fields in the standard $SU(3)_c \times SU(2)_L \times U(1)_Y$ electroweak theory. With only one Higgs doublet, three phases of this doublet are absorbed to the longitudinal components of the $W^\pm$ and Z gauge bosons and the remaining Higgs boson has a potential term. Therefore, one needs

at least two Higgs doublets. Thus, this model is an extension of the Standard Model (SM). However, this condition is not sufficient. A further condition for the existence of the axion field is the absence of a potential term (except, of course, for the *effective* potential arising from the $a\tilde{G}G$ interaction). This can be achieved by introducing a spontaneously broken global symmetry, the PQ symmetry. The PQ symmetry must be axial in order for it to be broken via the fermion anomaly where the axion couples to the anomaly by the term $a\tilde{G}G$. This coupling is a result of the triangle diagram which effectively arises in the theory in much the same way as the π^0 field couples to two photons. In short, one has to introduce the axion field a and impose the $U(1)_{PQ}$ symmetry where a appears as the Goldstone boson of this spontaneously broken symmetry, so that a does not have a potential [65].

For two Higgs doublets, the most general renormalizable Higgs potential which posses a reflection symmetry between the Higgs fields is given by

$$\begin{aligned} &V(\phi_1,\ \phi_2) = -\mu_1^2(\phi_1^\dagger\phi_1) - \mu_2^2(\phi_2^\dagger\phi_2) + \\ &+ \textstyle\sum_{i,j} a_{ij}\phi_i^\dagger\phi_i\phi_j^\dagger\phi_j + \sum_{i,j} b_{ij}\phi_i^\dagger\tilde{\phi}_i\tilde{\phi}_j^\dagger\phi_j + \sum_{i\neq j}(c_{ij}\phi_i^\dagger\tilde{\phi}_j\tilde{\phi}_i^\dagger\phi_j + \text{H.C.})\ , \end{aligned} \tag{6.43}$$

where $a_{i,j}$ and $b_{i,j}$ are real and symmetric, $c_{i,j} = c_{j,i}^*$ is Hermitian, $\tilde{\phi} = i\sigma_2\phi^*$ and the two Higgs fields have hypercharge $Y(\phi_1) = \frac{1}{2}$ and $Y(\phi_2) = -\frac{1}{2}$. This potential has a $U(1)_Y$ symmetry which is not useful for an independent global symmetry. Hence, Peccei and Quinn [47, 48] imposed the condition $c_{i,j} = 0$ to allow for an additional global $U(1)_{PQ}$ symmetry, under which the Higgs doublets transform as

$$\phi_1 \to \mathrm{e}^{i\alpha\Gamma_1}\phi_1\ ,\quad \phi_2 \to \mathrm{e}^{i\alpha\Gamma_2}\phi_2\ , \tag{6.44}$$

where Γ_1 and Γ_2 are the PQ charges of ϕ_1 and ϕ_2 and the phase α is now the available phase for the axion. When the term $(\mu_\epsilon^2\phi_1^\dagger\tilde{\phi}_2 + \text{H.C.})$ is introduced, the $U(1)_{PQ}$ symmetry is broken and μ_ϵ^2 will satisfy the condition for the dynamical relaxation of θ.

One also has to add Yukawa couplings in order for the $U(1)_{PQ}$ symmetry to be preserved.

$$\mathcal{L}_Y = -f_{ij}^{u*}\bar{Q}_{Lj}\phi_2 u_{Ri} - f_{ij}^{u}\phi_2^{\dagger}\bar{u}_{Ri}Q_{Lj} - f_{ij}^{d*}\bar{Q}_{Lj}\phi_1 d_{Ri} - f_{ij}^{d}\phi_1^{\dagger}\bar{d}_{Ri}Q_{Lj} \ , \tag{6.45}$$

where $i,\ j$ are summed over flavors. Therefore, the $Q_{EM} = -\frac{1}{3}$ quarks get their masses form the VEV of ϕ_1 and the $Q_{EM} = \frac{2}{3}$ quarks get their masses form the VEV of ϕ_2. Now, the $U(1)_{PQ}$ transformations for the fermions are

$$\begin{aligned} &u_L \to \mathrm{e}^{\frac{i}{2}\alpha\Gamma_2}u_L \ , \ u_R \to \mathrm{e}^{-\frac{i}{2}\alpha\Gamma_2}u_R \ , \\ &d_L \to \mathrm{e}^{\frac{i}{2}\alpha\Gamma_1}d_L \ , \ d_R \to \mathrm{e}^{-\frac{i}{2}\alpha\Gamma_1}d_R \ . \end{aligned} \tag{6.46}$$

These Yukawa interactions yield the coupling between the axion and the quarks. The coupling between leptons and the axion, although easily obtained in a similar way to the above, will not be considered in this discussion.

Next, one needs to identify the axion components in the phases of the Higgs fields. Noting that the axion is the Goldstone boson of the spontaneously broken $U(1)_{PQ}$ symmetry, we write ϕ_1^0 and ϕ_0^2 as

$$\phi_1^0 = \frac{v_1 + \rho_1}{\sqrt{2}}\mathrm{e}^{iP_1/v_1} \ , \quad \phi_2^0 = \frac{v_2 + \rho_2}{\sqrt{2}}\mathrm{e}^{iP_1/v_2} \ , \tag{6.47}$$

where the VEV of the Higgs components are $\langle\phi_1^0\rangle = \frac{v_1}{\sqrt{2}}$ and $\langle\phi_2^0\rangle = \frac{v_2}{\sqrt{2}}$ and ρ_1 and ρ_2 are the real Higgs fields. Now we are able to see that one linear combination of P_1 and P_2 is absorbed in the Z gauge boson by the Higgs mechanism, while the other combination is the Goldstone boson of the broken symmetry - the axion

$$\begin{aligned} h &= -P_1\sin\gamma + P_2\cos\gamma \ , \\ a &= P_1\cos\gamma + P_2\sin\gamma \ , \end{aligned} \tag{6.48}$$

where the angle γ is given by

$$\cos\gamma = \frac{v_1\Gamma_1}{\sqrt{v_1^2\Gamma_1^2 + v_2^2\Gamma_2^2}} \ , \quad \sin\gamma = \frac{v_2\Gamma_2}{\sqrt{v_1^2\Gamma_1^2 + v_2^2\Gamma_2^2}} \ . \tag{6.49}$$

From the condition that the Goldstone boson h is absorbed into the Z boson and a similar argument for the axion component one can determine that

$$h = \frac{-v_1 P_1 + v_2 P_2}{\sqrt{v_1^2 + v_2^2}} \ . \tag{6.50}$$

By comparing the latter with Eq. (6.48), one obtains $\tan\gamma = v_1/v_2$. Thus, we can determine the ratio Γ_1/Γ_2

$$\Gamma_1 : \Gamma_2 = v_2/v_1 : v_1/v_2 = x : 1/x \ , \tag{6.51}$$

with $x = v_2/v_1$. Then

$$a = \frac{v_2 a P_1 + v_1 P_2}{v_F} \ , \tag{6.52}$$

where $v_F = \sqrt{v_1^2 + v_2^2} \simeq 250$ GeV is the electroweak scale. Lastly, we notice that the three remaining field degrees of this broken symmetry are identified as π^0 and η mesons.

6.3.3. Inclusion of The Weak and Electromagnetic Interactions

Let us shortly summarize what we have found so far. By introducing a global chiral $U(1)$ symmetry, the $U(1)_{PQ}$ symmetry, one sees that in the Lagrangian of the theory in hand the effective θ term is dynamically eliminated. This symmetry must be spontaneously broken and it effectively replaces the static CP violating angle by a dynamical CP conserving field. This field is the Goldstone boson of the broken $U(1)_{PQ}$ symmetry, i.e. the axion. Hence, the axion field transforms under $U(1)_{PQ}$ as

$$a(x) \to a(x) + \alpha f_a \ , \tag{6.53}$$

where f_a is the order parameter associated with the breaking of $U(1)_{PQ}$. For the PQWW axion $f_a = v_F$, where v_F is the electroweak breaking scale.
The SM Lagrangian can be written in a $U(1)_{PQ}$ invariant way by adding the effective axion coupling term

$$\mathcal{L} = \mathcal{L}_{SM} + \bar{\theta}\frac{g_s^2}{32\pi^2}\tilde{G}^{c\mu\nu}G^c_{\mu\nu} - \frac{1}{2}\partial_\mu a \partial^\mu a + \mathcal{L}_{int}(\tfrac{\partial^\mu a}{f_a}, \psi) + \xi\frac{a}{f_a}\frac{g_s^2}{32\pi^2}\tilde{G}^{c\mu\nu}G^c_{\mu\nu} \ , \tag{6.54}$$

where g_s is the coupling strength of the strong interactions and ξ is the anomaly coefficient. The last term on the right hand side of the latter gives rise to the $U(1)_{PQ}$ chiral anomaly

$$\partial_\mu j^\mu_{PQ} = \xi\frac{g_s^2}{32\pi^2}\tilde{G}^{c\mu\nu}G^c_{\mu\nu} \ . \tag{6.55}$$

This term also serves as an effective potential for the axion field. With this term, not all values of $\langle a \rangle$ are allowed in the vacuum: Inclusion of the anomaly term induces a VEV of the axion field at $\langle a \rangle = -\bar{\theta} f_a/\xi$, where the $\bar{\theta}$ term cancels out and thus the theory is CP invariant. The minimum of the CP violating density $G\tilde{G}$ is periodic in the relevant θ parameter of the theory (i.e. the effective vacuum angle $\bar{\theta} + \langle a \rangle \xi/f_a$). For example, in the instanton approximation $\langle G\tilde{G} \rangle$ is proportional to $\cos(\bar{\theta} + \langle a \rangle \xi/f_a)$. This makes the VEV of $\langle G\tilde{G} \rangle$ to vanish precisely when the axion is at its VEV. Of course, writing the Lagrangian in terms of the physical axion field, i.e. the excitation with the VEV removed, $a_{phys} = a - \langle a \rangle$ rules out the CP violating term.
The axion is nominally massless as a Goldston boson, however, it acquires a mass as a result of the chiral anomaly via expansion of its effective potential

$$m_a^2 = \left\langle \frac{\partial^2 V_a}{\partial a^2} \right\rangle = -\frac{\xi}{f_a} \frac{g_s^2}{32\pi^2} \frac{\partial}{\partial a} \left\langle G^{c\mu\nu} \tilde{G}^c_{\mu\nu} \right\rangle \Big|_{\langle a \rangle = -\bar{\theta} f_a/\xi} . \tag{6.56}$$

6.3.4. The Mass of the Axion

Our next goal is to derive the mass of the axion. This was first done explicitly by Bardeen et. al. [66]. However, we shall trace the logic of [67] and use an effective Lagrangian derivation of the axion mass m_a.

The $U(1)_{PQ}$ current, given by

$$j^\mu_{PQ} = -v_F \partial^\mu a + x \sum_i \bar{u}_{Ri} \gamma^\mu u_{Ri} + \frac{1}{x} \sum_i \bar{d}_{Ri} \gamma^\mu d_{Ri} , \tag{6.57}$$

reveals the anomaly coefficient ξ (see Eq. (6.54)) [51]

$$\xi = \frac{N}{2} \left(x + \frac{1}{x} \right) . \tag{6.58}$$

To obtain the axion mass it is useful to consider, again, a model with only the lightest quarks (i.e. u and d). For this model, one may introduce a 2×2 matrix of Goldstone fields

$$\Sigma = \exp\left(i \frac{\vec{\tau} \cdot \vec{\pi} + \eta}{f_\pi} \right) , \tag{6.59}$$

where f_π is the pion decay constant. This matrix corresponds to the meson sector of the two light quark theory. Then, this appears in the Lagrangian as

$$\tilde{\mathcal{L}} = \mathcal{L}_{chiral} + \mathcal{L}_{mass} , \tag{6.60}$$

where

$$\mathcal{L}_{chiral} = \frac{f_\pi^2}{4}\ \mathrm{Tr}(\partial_\mu \Sigma \partial^\mu \Sigma^\dagger)\ , \tag{6.61}$$

and

$$\mathcal{L}_{mass} = \frac{1}{2}(f_\pi m_\pi^0)\ \mathrm{Tr}(\Sigma A M + (\Sigma A M)^\dagger)\ , \tag{6.62}$$

with

$$A = \begin{pmatrix} \mathrm{e}^{-iax/v_F} & 0 \\ 0 & \mathrm{e}^{-ia/xv_F} \end{pmatrix}\ ,\quad M = \begin{pmatrix} \frac{m_u}{m_u+m_d} & 0 \\ 0 & \frac{m_d}{m_u+m_d} \end{pmatrix}\ . \tag{6.63}$$

However, a further term is required in order to have a CP free Lagrangian and give the axion its mass. This term takes into account the anomalies in both $U(1)_A$ and $U(1)_{PQ}$ and considers the contributions of heavy quarks to the PQ anomaly

$$\mathcal{L}_{anomaly} = -\frac{(m_\eta^0)^2}{2}\left(\eta + a\frac{f_\pi}{v_F}\frac{(N/2-1)(x+1/x)}{2}\right)^2\ , \tag{6.64}$$

where $(m_\eta^0)^2 \simeq m_\eta^2 \gg m_\pi^2$. The coefficient in front of the axion field in $\mathcal{L}_{anomaly}$ reflects the relative strength of the couplings of a and η to $G\tilde{G}$ as a result of the anomalies in $U(1)_{PQ}$ and $U(1)_A$. Naively, the ratio of these couplings is just $f_\pi/2v_F\xi$. However, the reason that $N/2-1$ appears in the above, rather than just $N/2$, is that $\mathcal{L}_{mass}$ already includes the light quark interactions of axions, so only the contribution of heavy quarks to the PQ anomaly should be taken into account in $\mathcal{L}_{anomaly}$.

By diagonalizing the quadratic terms in both $\mathcal{L}_{mass}$ and $\mathcal{L}_{anomaly}$, one obtains the axion mass and the axion-pion and axion-eta mixing parameters for the PQ model. Defining, for convenience,

$$\bar{m}_a = m_\pi \frac{f_\pi}{v_F}\frac{\sqrt{m_u m_d}}{m_u+m_d} \simeq 25\ \mathrm{keV}\ , \tag{6.65}$$

we find that

$$m_a = \lambda_m \bar{m}_a \ , \quad \xi_{a\pi} = \lambda_3 \tfrac{f_\pi}{v_F} \ , \quad \xi_{a\eta} = \lambda_0 \tfrac{f_\pi}{v_F} \ , \tag{6.66}$$

where

$$\begin{aligned} \lambda_m &= \tfrac{N}{2}\left(x + \tfrac{1}{x}\right) \ , \\ \lambda_3 &= \tfrac{1}{2}\left[\left(x - \tfrac{1}{x}\right)\tfrac{N}{2}\left(x + \tfrac{1}{x}\right)\tfrac{m_d - m_u}{m_d + m_u}\right] \ , \\ \lambda_0 &= \tfrac{1}{2}\left(1 - \tfrac{N}{2}\right)\left(x + \tfrac{1}{x}\right) \ . \end{aligned} \tag{6.67}$$

It is important to notice that in addition to the three parameters in Eq. (6.67), all axion models are also characterized by axion couplings to two photons. In fact, this interaction is most important when considering terrestrial axion search experiments. These use this interaction to convert an axion in an external magnetic field to a photon, which is detectable in a lab. This interaction can be described in the Lagrangian by the term

$$\mathcal{L}_{a\gamma\gamma} = \frac{\alpha}{4\pi} K_{a\gamma\gamma} \frac{a_{phys}}{f_a} \tilde{F}^{\mu\nu} F_{\mu\nu} \ , \tag{6.68}$$

where we need to find the coupling strength $K_{a\gamma\gamma}$ for this model. Again, from the anomaly of the PQ current in this effective Lagrangian one may find [51]

$$\xi_{a\gamma\gamma} = \frac{4}{3}\frac{N}{2}\left(x + \frac{1}{x}\right) \ . \tag{6.69}$$

Again, one needs to separate the light quarks contribution to the anomaly and add back the $a\gamma\gamma$ contribution from the the coupling of π^0 and η to two photons via the axion-pion and axion-eta mixing ($\lambda_3 + \frac{5}{3}\lambda_0$). Thus, $\xi^{eff}_{a\gamma\gamma} = \frac{4}{3}\frac{N}{2}\left(x + 1/x\right) - \frac{4}{3}x - \frac{1}{3}\frac{1}{x}$ and

$$K_{a\gamma\gamma} = \frac{N}{2}\left(x + \frac{1}{x}\right)\frac{m_u}{m_u + m_d} \ . \tag{6.70}$$

6.4. Invisible Axion Models

The main phenomenological drawback of the PQWW axion is that its physics is coupled at the electroweak symmetry breaking scale. This model, with $f_a = v_F$, was rather quickly ruled out by experiment, where this axion was tested in decay modes of K, in reactor experiments, beam dump experiments and astrophysics. All these lead to the belief that this model's phenomenology is incorrect with reasonable value of the ratio of the two Higgs' doublets, x. However, axion models with $f_a \gg v_f$ are still feasible. Kim [68] was the first to introduce a model where the PQ scale is separated from the electroweak scale. To that end, the axion field should not reside in the phase of neutral Higgs doublets (which transform nontrivially under $SU(2) \times U(1)$), but rather in the phase of an $SU(2) \times U(1)$ singlet complex scalar field which carries a PQ charge (denoted below as σ). This gives rise to the so called invisible axion models, a branch of models which suggest that the axion is a very light, very weakly interacting and very long lived particle. The introduction of this scalar field is the common feature for the invisible axion models, although different models can have different phenomenological implications.

After understanding where to "house" the axion, the next task is to have $U(1)_{PQ} - SU(3)_C - SU(3)_C$ anomaly. For this anomaly to be present some quarks must carry nontrivial PQ charges. In the standard model with one Higgs doublet, the light quarks cannot carry PQ charges, sine then the quarks cannot obtain phenomenologically acceptable masses. Therefore we need more fields to have the desired anomaly, in addition to the scalar field σ.

In principal, two important such models have been proposed. The first, suggested by Kim [68] and Shifman, Vainshtein and Zakharov [69], introduces the scalar field σ with $f_a = \langle\sigma\rangle \gg v_F$ and a super-heavy quark Q with $M_Q \sim f_a$ as the only fields carrying a PQ charge. This model is usually referred to as the KSVZ axion. The second model, suggested by Dine, Fiscler and Srednicki [70] and Zhitnisky [71], introduces (along with σ) an additional Higgs doublet so that both light quarks and Higgs doublets carry non-

vanishing PQ charges. This model is usually called the DFSZ model. Let us illustrate now shortly how these models work.

6.4.1. The KSVZ Axion

To realize the PQ symmetry Q should not have a bare mass. Assuming, for simplicity, that Q is a color triplet, the Yukawa coupling and Higgs potential are given by

$$\begin{aligned} &\mathcal{L}_Y = -f\bar{Q}_L\sigma Q_R - f^*\bar{Q}_R\sigma^* Q_L \ , \\ &V(\sigma,\phi) = -\mu_\phi^2\phi^\dagger\phi - \mu_\sigma^2\sigma^*\sigma + \lambda_\phi\left(\phi^\dagger\phi\right)^2 + \lambda_\sigma\left(\sigma^*\sigma\right)^2 + \lambda_{\phi\sigma}\phi^\dagger\phi\sigma^*\sigma \ , \end{aligned} \tag{6.71}$$

where ϕ is the Higgs doublet of the SM. The transformation rules are

$$\begin{aligned} &a \to a + \alpha f_a \ , \\ &\sigma \to \mathrm{e}^{iQ_\sigma\alpha}\sigma \ , \\ &Q_L \to \mathrm{e}^{\frac{i}{2}\gamma_5 Q_\sigma\alpha} Q_L \ , \\ &Q_R \to \mathrm{e}^{-\frac{i}{2}\gamma_5 Q_\sigma\alpha} Q_R \ , \end{aligned} \tag{6.72}$$

where Q_σ is the PQ charge of σ. Then, the axion can be identified as the phase of σ

$$\sigma = \frac{1}{\sqrt{2}}(v+\rho)\mathrm{e}^{i\frac{a}{v}} \ , \tag{6.73}$$

which leads to $f_a = Q_\sigma v/\sqrt{2} \gg v_F$ and the PQ scale is determined by the VEV of σ. Of course, with the normalization $Q_\sigma = 1$ we get $f_a = \langle\sigma\rangle$, as stated at the beginning of this section.

It is also useful to obtain the axion mass for this model using the effective Lagrangian, as we did in Sec. 6.3.4. By construction, the KSVZ axion does not interact with leptons and it only interact with light quarks through the strong and electromagnetic anomalies [51]

$$\mathcal{L}_{axion}^{KSVZ} = \frac{a}{f_a}\left(\frac{g_s^2}{32\pi^2}\tilde{G}^{c\mu\nu}G_{c\mu\nu} + 3e_Q^2\frac{\alpha}{4\pi}\tilde{F}^{\mu\nu}F_{\mu\nu}\right) \ , \tag{6.74}$$

where e_Q is the electromagnetic charge of Q. The interactions of the axion with the light quark sector come from the effective anomaly mass term (as the Higgs field does not carry a PQ charge in this model)

$$\mathcal{L}_{anomaly} = -\frac{(m_\eta^0)^2}{2}\left(\eta + \frac{f_\pi}{2f_a}a\right)^2 \ . \tag{6.75}$$

As before, one needs to add the quadratic term coming from light quarks

$$\mathcal{L}_{mass} = -\frac{(m_\pi^0)^2}{2}\left(\frac{m_u}{m_u+m_d}(\pi^0+\eta)^2 + \frac{m_d}{m_u+m_d}(\eta-\pi^0)^2\right) \ . \tag{6.76}$$

Diagonalizing $\mathcal{L}_{anomaly}$ and $\mathcal{L}_{mass}$ we find that

$$m_a = \lambda_m\frac{v_F}{f_a}\bar{m}_a \ , \quad \xi_{a\pi} = \lambda_3\frac{f_\pi}{f_a} \ , \quad \xi_{a\eta} = \lambda_0\frac{f_\pi}{f_a} \ , \tag{6.77}$$

where, for the KSVZ model, one has

$$\lambda_m = 1 \ , \quad \lambda_3 = -\frac{m_d-m_u}{2(m_u+m_d)} \ , \quad \lambda_0 = -\frac{1}{2} \ . \tag{6.78}$$

Expressing the mass of the axion in terms of the light quark masses, the pion mass and the pion decay constant we have [72]

$$m_a = \frac{v_F}{f_a}\bar{m}_a = \frac{m_\pi f_\pi}{f_a}\frac{\sqrt{m_u m_d}}{m_u+m_d} \simeq \frac{0.60 \text{ meV}}{f_a/10^{10} \text{ GeV}} \ . \tag{6.79}$$

We are left with the calculation of $K_{a\gamma\gamma}$. To that end, one should add to the contribution of the super-heavy quark in the electromagnetic anomaly $3e_Q^2$ the contribution from the mixing of the axion with pion and eta mesons. Hence,

$$K_{a\gamma\gamma} = 3e_Q^2 - \frac{4m_d + m_u}{3(m_u + m_d)} \ . \tag{6.80}$$

6.4.2. The DFSZ Axion

In this model, the desired $A\tilde{G}G$ coupling is realized from the light quarks. The scalar field σ is coupled to the Higgs doublets which then couple to the light quarks (σ is not coupled directly to the light quarks because it is an $SU(2) \times U(1)$ singlet). We shall not repeat the analogous calculations for the DFSZ axion here, but we shall just state the final results.

Let us define, for convenience, [51]

$$X_1 = \frac{2v_2^2}{v_F^2} \ , \quad X_2 = \frac{2v_1^2}{v_F^2} \ , \tag{6.81}$$

where v_1 and v_2 are, as usual, the VEVs of the two Higgs doublets. Next, let us rescale $f_a \to f_a/N$. Then, the axion mass is given by the same equation as in the KSVZ model Eq. (6.79) with $\lambda_m = 1$. With this rescaling one can also find

$$\lambda_3 = \frac{1}{2}\left(\frac{X_1 - X_2}{N} - \frac{m_d - m_u}{2(m_u + m_d)}\right) \ , \quad \lambda_0 = \frac{1 - N/2}{N} \ , \tag{6.82}$$

and

$$K_{a\gamma\gamma} = \frac{4}{3} - \frac{4m_d + m_u}{3(m_u + m_d)} \ . \tag{6.83}$$

As a last note, although the axions in the models we have just reviewed (i.e. the KSVZ and DFSZ models) are referred to as "invisible", they are, however, predicted to convert to and from photons in the presence of strong magnetic fields through the effective

anomaly terms in the Lagrangian. This property is used to detect axions in terrestrial experiments, where, basically, an axion beam is passing through a large (as possible) magnet with magnetic field perpendicular to the axions' momentum. Then, the axions are predicted to convert to photons with a specific energy. The experimentalists are looking to find these specific photons and isolate them from the background in order to determine wether or not they were originated from the scattering of an axion in the magnetic field. We will discuss this in more detail in the following sections.

6.4.3. The Primakoff Effect and Bounds on the Invisible Axion

Bounds on the mass of the axion can be obtained from astrophysics. Axion emission, through Compton production (i.e. $e\gamma \to ea$) and the Primakoff effect, lead the energy loss in stars [73].

The Primakoff effect was first proposed in 1951 by Henry Primakoff to study the $\pi^0 - \gamma$ coupling. The two-photon coupling of pions or other pseudo-scalars allows for the conversion $a \leftrightarrow \gamma$ in an external electric or magnetic field by virtue of the amplitude shown in Fig. 6a. The Primakoff effect turns out to be important for non relativistic conditions, where $T \ll m_e$ (T being the temperature and m_e is the electron mass) so that both electrons and nuclei may be treated as heavy relative to typical energies of the ambient photons. The Primakoff effect gives rise to conversions of axions to photons and vice versa in strong electromagnetic fields. Hence, axions could be produced in the Sun's core when X-ray photons scatter off electrons and protons in the presence of strong electric fields and thus are converted to axions. These axions may be converted back into photons by passing the axion flux through a strong magnetic field in a terrestrial laboratory.

For example, Sikivie [56] proposed to search for galactic axions by means of a Primakoff-like method. The $a \to \gamma$ conversion of non-relativistic axions in the μeV mass range produces photons in the microwave (GHz) range. Thus, placing a microwave cavity in a

strong magnetic field may excite cavity modes by the axion field. The electromagnetic modes of the cavity and the free axion field modes can be viewed as oscillations coupled by an interaction term of the form $\mathcal{L} = -\frac{1}{4} g_{a\gamma} F_{\mu\nu} \tilde{F}_{\mu\nu} a = g_{a\gamma} \vec{E} \cdot \vec{B} a$, where $\vec{E}$ corresponds to an electromagnetic cavity mode and $\vec{B}$ is the external static field. The Axion Dark Matter eXperiment (ADMX) is an ongoing experimental search for axions in the milky way's dark matter halo, which is using Sikivie's idea to conduct its research. It is located at the University of Washington's Center for Experimental Nuclear Physics and Astrophysics (CENPA).

In the very same paper, Sikivie proposed to apply the same idea to the solar axion flux since in a strong magnetic field axions are expected to convert to X-ray photons ("the axion helioscope"). For example, the CERN Axion Solar Telescope (CAST) experiment is currently underway to detect solar axions by converting them back to X-rays in a strong magnetic dipole field (≈ 9 T) mounted in the laboratory.

Another type of experiment using conversions of photons to axions and vice versa, which will be mentioned in the following sections, is the so called "light shining through the wall" experiment. In this type of experiments, a beam of light is passed through an intense magnetic field in an attempt to observe the conversion of photons into axions by placing an opaque plate (which can be made of an antiferromagnet, such as aluminum for example) in the middle of the magnetic field region. This plate will block the passage of photons while allowing the passage of the low interacting axions. This, supposedly purely axionic, beam is then expected to convert back into (detectable) photons on the other side of the plate. An example for this type of experiment is the Optical Search for QED vacuum magnetic birefringence, Axions and photon Regeneration (OSQAR) experiment at CERN.

The Primakoff effect, which in the frame of this work refers to the conversion of axions to photons and vice-versa in strong electromagnetic fields, serves as the basis for the calculations carried out in sections 8 and 9, where different possible experiments which use axion-photon conversion are presented. This effect can lead to experiments which

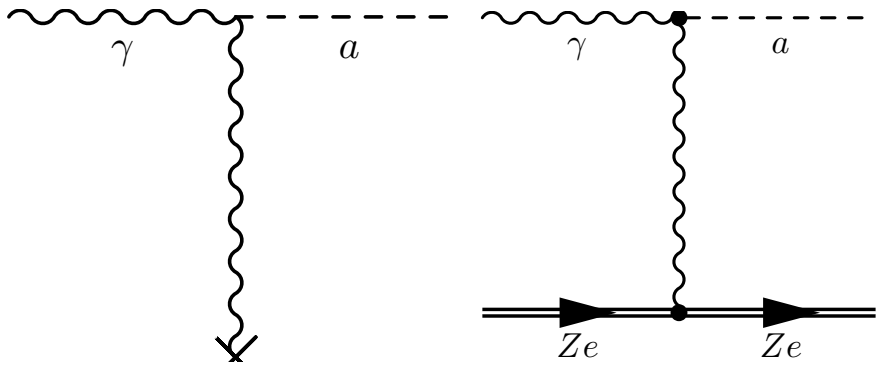

(a)Axion production in an external electromagnetic field.

(b)Axion production in the sun.

FIG. 6: The Feynman diagrams for the Primakoff effect.

address the questions of the existence of the invisible axion.

The energy loss in stars is inversely proportional to f_a^2 and therefore proportional to m_a^2. Hence, axions must be light enough in order to not affect stellar evolution. Another bound on the mass of the axion can be found from the energy-loss limit from SN 1987A, as axion emission in the core collapse affects the neutrino signal [74]. This suggests that QCD axions have $f_a \gtrsim 10^9$ GeV or $m_a \lesssim$ 10–20 meV. Moreover, if axions also interact with electrons, axions nearly saturating the SN 1987A limit could explain the apparent anomalous energy loss of white dwarfs [75–78].

Cosmology gives an ever lower bound on the mass of the axion. When the universe went through the PQ phase transition at temperature $T \sim f_a \gg \Lambda_{QCD}$, the QCD anomaly was not yet relevant. Therefore, in the early universe $\langle a_{phys} \rangle$ is arbitrary. But, as the universe cooled down to a temperature of the order $T \sim \Lambda_{QCD}$, the axion acquired a mass which leads to $\langle a_{phys} \rangle \to 0$. The PQ mechanism is not an instantaneous process and thus $\langle a_{phys} \rangle$ oscillates to its final value. These coherent axion oscillations contribute to the energy density of the universe and axions act as cold dark matter. The energy density of the axion oscillations is proportional to f_a. Hence, bounds on the energy density of the cold dark matter in the universe leads to a bound on f_a and thus on m_a.

To summarize, axions are produced in the early universe by the misalignment mechanism [54, 55]. If the PQ symmetry is restored by reheating after inflation, axion strings and domain walls form and decay, providing an additional source of axions. These relic axions provide the cold dark matter for $m_a \sim 10$ μeV, with a large uncertainty in either direction, and actually m_a could be as large as 200 μeV [55].

7. AXION-PHOTON DUALITY SYMMETRY

In a series of recent publications by Guendelman [79, 80] it was shown that an axion-photon system displays a continuous axion-photon duality symmetry when an external magnetic field is present and when the axion mass is neglected. This allows one to analyze the behavior of axions and photons in external magnetic fields in terms of an axion-photon complex field. For example, the deflection of light from magnetars has been recently studied using these techniques [81]. It is important to note here that the same duality symmetry exists also when considering massive photons, under the condition $m_\gamma = m_a$, that is, the photon and the axion masses are equal. These conditions can be achieved when conducting experiments where the axion-photon conversion region is filled with a suitable refractive gas. In the next part of the thesis we will show that the coupling of axion-photon complex particles to a localized magnetic flux generated by a solenoid renders scattering solutions with a cross section which could conceivably be measured.

To see this, let us write the Lagrangian describing the relevant light pseudoscalar coupling to the photon,

$$\mathcal{L} = -\tfrac{1}{4}F^{\mu\nu}F_{\mu\nu} + \tfrac{1}{2}\partial_\mu a \partial^\mu a - \tfrac{1}{2}m_a^2 a^2 - -\tfrac{g}{8}a\epsilon^{\mu\nu\alpha\beta}F_{\mu\nu}F_{\alpha\beta}\ . \tag{7.1}$$

Following [82], we focus on the case where an electromagnetic field with propagation along the x and y directions and a strong magnetic field pointing in the z-direction are

present. The magnetic field may have an arbitrary space dependence in x and y, but it is assumed to be time independent.

For small electromagnetic perturbations around the static magnetic background (i.e, the axion and the electromagnetic wave), we consider only small quadratic terms in the Lagrangian for the axion and the electromagnetic fields. By choosing a static magnetic field pointing in the z direction and having an arbitrary x and y dependence and specializing to x and y dependent electromagnetic field perturbations and axion fields, the interaction between the background magnetic field and the axion and photon fields reduces to

$$\mathcal{L}_I = -\beta a E_z \ , \tag{7.2}$$

where $\beta(x, y) = gB(x, y)$. Choosing the temporal gauge for the electromagnetic field and considering only the z-polarization for the electromagnetic waves (since only this polarization couples to the axion) we get the following 2+1 dimensional effective Lagrangian

$$\mathcal{L}_2 = \frac{1}{2}\partial_\mu A \partial^\mu A + \frac{1}{2}\partial_\mu a \partial^\mu a - \frac{1}{2}m_a^2 a^2 + a\beta\partial_t A \ , \tag{7.3}$$

where A is the z-polarization of the photon, so that $E_z = -\partial_t A$.

Without assuming any particular x and y dependence for β, but insisting that it will be static, we see that neglecting the axion mass m_a (the validity of this assumption will be discussed at the end of this work), we discover a continuous axion photon duality symmetry. This is due to a rotational $O(2)$ symmetry in the axion-photon field space, allowed by the axion and photon kinetic terms and by expressing the interaction term, $\mathcal{L}_I$, in an $O(2)$ symmetric way by dropping a total time derivative from it:

$$\mathcal{L}_I = \frac{1}{2}\beta(a\partial_t A - A\partial_t a) \ . \tag{7.4}$$

Defining now the axion-photon complex field, Ψ, as

$$\Psi = \frac{1}{\sqrt{2}}(a + iA) \tag{7.5}$$

and plugging this into the Lagrangian results in

$$\mathcal{L} = \partial_\mu \Psi^* \partial^\mu \Psi - \frac{i}{2}\beta(\Psi^* \partial_t \Psi - \Psi \partial_t \Psi^*) \ , \tag{7.6}$$

where Ψ^* is the charge conjugation of Ψ. From this we obtain the equation of motion for Ψ

$$\partial_\mu \partial^\mu \Psi + i\beta \partial_t \Psi = 0 \ . \tag{7.7}$$

We therefore have the magnetic field, or $\beta/2$ (the $U(1)$ charge), coupled to a charge density. Introducing the charge conjugation [82] , that is

$$\Psi \to \Psi^* \ , \tag{7.8}$$

shows that the free part of the action is indeed invariant under (7.8). When acting on the free vacuum the A and a fields give rise to a photon and an axion respectively, but in terms of the particles and antiparticles (defined in terms of Ψ), we see that a photon is an antisymmetric combination of particle and antiparticle and an axion a symmetric combination, since

$$a = \frac{1}{\sqrt{2}}(\Psi^* + \Psi) \ \text{ and } \ A = \frac{1}{i\sqrt{2}}(\Psi - \Psi^*) \ . \tag{7.9}$$

Hence, the axion is even under charge conjugation, while the photon is odd. These two eigenstates of charge conjugation will propagate without mixing as long as no external

magnetic field in the perpendicular direction to the eigenstates (i.e axion and photon) spatial dependence is applied. The interaction with the external magnetic field is not invariant under (7.8). In fact, under (7.8) we can see that

$$S_I \to -S_I \ , \tag{7.10}$$

where $S_I = \int \mathcal{L}_I dxdydt$. Therefore, these symmetric and antisymmetric combinations, corresponding to axion and photon, will not be preserved in the presence of B in the analog QED language, since the "analog external electric potential" breaks the symmetry between particle and antiparticle and therefore will not keep in time the symmetric or antisymmetric combinations. In fact, if the corresponding external electric potential is taken to be a repulsive potential for particles, it will be an attractive potential for antiparticles, so the symmetry breaking is maximal.

Even at the classical level these two components suffer opposite forces, thus under the influence of an inhomogeneous magnetic field both a photon or an axion will be decomposed through scattering into their particle and antiparticle components, each of which is scattered in a different direction, since the corresponding electric force is related to the gradient of the effective electric potential, i.e., the gradient of the magnetic field, times the $U(1)$ charge which is opposite for particles and antiparticles. If we look at the scattering amplitudes for particles and antiparticles, we see that they have opposite signs. Calling S the scattering amplitude for a particle, the amplitude for an antiparticle is then $-S$. Therefore, an axion [i.e. the symmetric combination of particle antiparticle $(1,1)$] goes under scattering to $(1,1) + (S,-S)$. So the amplitude for axion going into photon $(1,-1)$ is S. Hence, we conclude that the amplitude for axion-photon conversion is equal to the particle scattering amplitude.

For this effect to have meaning, we have to work at least in a 2+1 formalism [80]. The 1+1 reduction [79], [82] which allows motion only in a single spatial direction, is unable to produce such separation, since in order to separate particle and antiparticle

components we need at least two dimensions to obtain a final state with particles and antiparticles propagating in slightly different directions.

This is in a way similar to the Stern-Gerlach experiment in atomic physics [83], where different spin orientations suffer a different deflection force proportional to the gradient of the magnetic field in the direction of the spin. Here, instead of spin we have that the photon is a combination of two states with different $U(1)$ charge and each of these components will suffer opposite force under the influence of the external inhomogeneous magnetic field. Notice also that since particle and antiparticles are distinguishable, there are no interference effect between the two processes.

Therefore an original beam of photons will be decomposed through scattering into two different elementary particle and antiparticle components (and also, of course, the photons that were not scattered). These two beams are observable, since they both have photon components, so the observable consequence of the axion-photon coupling will be the splitting of a photon, or axion, beam by a magnetic field of the configuration considered here, whereas in the normal Primakoff effect analysis there is no explicit recognition of a splitting. This effect is, moreover, of first order in the axion-photon coupling (g), unlike the "light shining through a wall" phenomena which depend on the coupling constant squared (g^2).

Perhaps this is the place to mention that the splitting of axion and photon in an inhomogeneous magnetic field can be understood in terms of different indices of refraction of modes of the axion and photon system, which here we associate to particle - anti particle representation [81].

8. PHOTON PRODUCTION FROM THE SCATTERING OF AXIONS OUT OF A SOLENOIDAL MAGNETIC FIELD

Here, following [84], we calculate the total cross section for the production of photons from the scattering of axions by a strong inhomogeneous magnetic field in the form of

a 2D δ-function, a cylindrical step function and a 2D Gaussian distribution, which can be approximately produced by a solenoidal current. These theoretical results are then used to estimate the axion-photon conversion probability which could be expected in a reasonable experimental situation. Comparison between the 2D conversion probabilities for QCD inspired axions and those derived by applying the celebrated 1D calculation of the (inverse) coherent Primakoff effect is made using an averaging prescription procedure of the 1D case. We also consider scattering at a resonance $E_{axion} \sim m_{axion}$, which corresponds to the scattering from a δ-function and gives the most enhanced results. The goal which guidelines this study, is to obtain the expected conversion probabilities in different possible terrestrial experiments, using a magnetic field with a cylindrical symmetry. There are some practical difficulties in using a solenoid for solar axions search as we mention later, in Sec. 11. However, as a first attempt for obtaining some phenomenological results of the 2D particle anti-particle formalism in 2D we ignore these difficulties for now and treat this research as a study case from which one can learn and gain a further insight on this novel axion-photon conversion formalism in 2D.

To apply the results of the previous section to a specific system with magnetic field, one writes separately the time and space dependence of the axion-photon field as $\Psi(\vec{r}, t) = \mathrm{e}^{-i\omega t}\psi(\vec{r})$. This will be done in all the following cases in order to analyze the Ψ fields interaction with the external magnetic field and obtain the axion-photon conversion probability.

8.1. First Approximation: A Magnetic Field of an Infinitely Thin Solenoid

As a first model, let us consider an inhomogeneous magnetic field of the form $B = \Phi\delta^2(x, y)$, where Φ is the magnetic field flux. This kind of a potential can not, of course, be realized in the lab, however, we will show that the results for this, presumably purely theoretical, calculation have physical significance in the resonance case, where the scattering becomes isotropic.

Separating the time and space dependence of Ψ and considering the δ function potential reduces Eq. (7.7) to

$$[-\vec{\nabla}^2 + g\Phi E\delta^2(x,y)]\psi(\vec{r}) = E^2\psi(\vec{r}) \ . \tag{8.1}$$

In terms of momentum space wave functions, $\phi(\vec{k}) = \int \mathrm{e}^{i\vec{k}\cdot\vec{r}}\psi(\vec{r})d^2r$, the latter equation is now

$$\vec{k}^2\phi(\vec{k}) + g\Phi E\psi(0) = E^2\phi(\vec{k}) \ , \tag{8.2}$$

from which the solution

$$\phi(\vec{k}) = (2\pi)^2\delta^2(\vec{k} - \vec{k}_0) - \frac{g\Phi E\psi(0)}{k^2 - E^2} \ , \tag{8.3}$$

with $k_0^2 = E^2$, is obtained. The constant $g\Phi E\psi(0)$ is determined from Eq. (8.3) by integration over momentum space

$$\psi(0) = 1 - g\Phi E I_2(-E^2 - i\epsilon)\psi(0) \ , \tag{8.4}$$

where

$$I_2(-E^2 - i\epsilon) = \int \frac{d^2k}{(2\pi)^2}\frac{1}{k^2 - E^2 - i\epsilon} = \frac{1}{4\pi}\log(\frac{\Lambda^2}{z}) \ , \tag{8.5}$$

with and $z = -E^2 - i\epsilon$ and Λ is a cutoff constant that was introduced to regulate the integral $I_2(z)$ by limiting k. It is straightforward to calculate $g\Phi E\psi(0)$ from Eq. (8.4)

$$g\Phi E\psi(0) = \left[\frac{1}{g\Phi E} + \frac{\log(\Lambda^2/z)}{4\pi}\right]^{-1} = \left[\frac{1}{g\Phi E} + \frac{\log(\Lambda/E)}{2\pi} + \frac{i}{2}\right]^{-1} \ . \tag{8.6}$$

To obtain the scattering amplitudes, we write the wave functions in position space

$$\psi(\vec{r}) = \mathrm{e}^{i\vec{k}\cdot\vec{r}} - g\Phi E\psi(0)G_k(r) \ , \tag{8.7}$$

where $G_k(r)$ is Green's function in two dimensions

$$(-\nabla^2 - k^2)G_k(r) = \delta(\vec{r}) \ , \tag{8.8}$$

$$G_k(r) = \frac{i}{4}H_0^{(1)}(kr) \overset{r\to\infty}{\longrightarrow} \frac{1}{2\sqrt{2\pi kr}}\mathrm{e}^{i(kr+\pi/4)} \ . \tag{8.9}$$

By identifying the scattering amplitude from the asymptotic behavior of the scattering wave function

$$\psi(\vec{r}) \to \mathrm{e}^{i\vec{k}\cdot\vec{r}} + \frac{1}{\sqrt{r}}f(\theta)\mathrm{e}^{i(kr+\pi/4)} \ , \tag{8.10}$$

we get for the *constant* scattering amplitude

$$f(\theta) = -\frac{1}{\sqrt{2\pi E}}\frac{g\Phi E}{2}\psi(0) \ , \tag{8.11}$$

since $k^2 = E^2$. Since there is no dependence on the scattering angle in $f(\theta)$ the scattering from a δ function is completely isotropic. The total cross-section in 2 dimensions is given by $\sigma_{tot} = \int_0^{2\pi} |f(\theta)|^2 d\theta$. Hence, by expanding $f(\theta)$ to first order in g we find that

$$\sigma_{tot}^{\delta} = \frac{g^2\Phi^2 E}{4} \ . \tag{8.12}$$

Our primary motivation comes from the QCD inspired axions, with mass up to the $\sim$1 eV range. To estimate the magnitude of the total cross-section, we take the value of

the coupling constant g from a recent result from the CAST collaboration. CAST is searching for axions produced in the sun and travelling to earth by trying to detect photons from the conversion of axions inside a constant magnetic field, following the coherent inverse Primakoff effect. Along with the Japanese axion helioscope Sumico [85], CAST has set an upper limit on the magnitude of the axion-photon coupling constant of $g \lesssim 2.2 \times 10^{-10}$ GeV^{-1} for an axion mass of $m_a \lesssim 0.4$ eV [86]. We choose to use $g = 10^{-10}$ GeV^{-1} throughout this paper. The dimensionless magnetic flux is, of course, given by $\Phi = \pi B_0 R^2$, where B_0 is the magnetic field strength inside the solenoid and R is the solenoid radius. Lastly, the mean energy of axions arriving at the earth from the sun is estimated to be $E = 4.2 \times 10^3$ eV [87].

In order to get the 3D total cross-section (i.e the scattering cross-section) σ_S we multiply the 2D cross-section σ_{tot} by the length of the solenoid L, taking $L = 10$ cm as an example. Multiplying the scattering cross-section by the flux of axions coming from the sun, $F = 3.67 \times 10^{11}$ /cm$^2 \cdot$ sec [87], we can estimate the number of events per second N.

The quantity we are ultimately looking for is the axion-photon conversion probability. To obtain this, we calculate the ratio between the number of axions arriving at the solenoid to the number of photons produced. The number of axions hitting the solenoid is given by multiplying the flux of axions arriving by the geometrical cross section of the solenoid, given by $\sigma_G = DL$, where D is the solenoid diameter and L is its length. Of course, the δ function does not have any volume, however, when conducting an experiment where the wavelength of the Ψ wave function will be smaller, or even comparable to the length scale of a cylindrical potential the scattering becomes more and more isotropic and we essentially obtain δ function scattering. This issue and the physical realization of δ scattering will be discussed at the end of these section, after presenting the resonant scattering case.

The number of produced photons is found by multiplying the scattering cross section ($\sigma_S = \sigma_{tot} \cdot L$) times the flux. Thus, the probability is given by

$$P_\delta = \sigma_S/\sigma_G = \frac{g^2\Phi^2 E}{4D} = \frac{\pi^2 g^2 B_0^2 R^3 E}{8} \ . \tag{8.13}$$

Notice that the dependence on the magnetic field strength is squared. However, the dependence on the surface magnetic field gradient is "hidden", since it was implied in deriving this relation. A few examples for the cross-section, number of events and probability are given below in TABLE I.

B [Tesla]	D [cm]	σ^δ_{tot} [cm]	N_δ [sec^{-1}]	$P_\delta = \sigma_S/\sigma_G$
10	1	3.08×10^{-15}	0.01	3.08×10^{-15}
10	10	3.08×10^{-11}	112.98	3.08×10^{-12}
6	2	1.77×10^{-14}	0.07	8.87×10^{-15}
6	20	1.77×10^{-10}	650.78	8.87×10^{-12}

TABLE I: Total cross-section, number of events and axion-photon conversion probablity for different choices of the magnetic field strength (B) and the solenoid diameter (D) and for $g = 10^{-10}$ GeV^{-1}. We have used rationalized natural units to convert the magnetic field units from Tesla to eV^2, where the conversion is 1 T = 195 eV^2 (please see appendix A in [88] for more details).

8.2. Finite Sized Solenoidal Generated Potentials

8.2.1. Gaussian Distributed Magnetic Field

We wish to obtain eventually measurable quantities which can be incorporated in a laboratory experiment, thus we have to consider a more realistic function to describe the magnetic field generated by the solenoid. As a first model, we choose to describe the inhomogeneous magnetic field by a Gaussian distribution around the solenoid's axis.

$$\vec{B}(r) = B_0 \mathrm{e}^{\frac{-r^2}{R^2}} \hat{z} \ . \tag{8.14}$$

The Gaussian function is normalized so that the total magnetic flux equals to $B\pi R^2$, the flux through a cylinder with radius R and constant magnetic field B.
Introducing again Green's function in the x , y plane, we write the wave function in position space

$$\psi(\vec{r}) = \psi_{free}(\vec{r}) + \int G(\vec{r} - \vec{\rho}) gEB(\rho) \psi(\vec{\rho}) d^2\rho \ , \tag{8.15}$$

where $\psi_{free} = \mathrm{e}^{i\vec{k}\cdot\vec{r}}$ is the solution of the free field equation. To first Born approximation, noting that

$$\mathrm{e}^{i\vec{k}\cdot\vec{\rho}} \mathrm{e}^{ik|\vec{r}-\vec{\rho}|} = \mathrm{e}^{ikr} \mathrm{e}^{i\left(\vec{k} - k\frac{\vec{r}}{r}\right)\cdot\vec{\rho}} \tag{8.16}$$

and using again the asymptotic approximation of Green's function in 2 dimensions (see Eq. 8.9) we arrive at

$$\psi(\vec{r}) = \mathrm{e}^{i\vec{k}\cdot\vec{r}} + \frac{\mathrm{e}^{ikr}}{2\sqrt{2\pi r E}} \int gEB(\vec{\rho}) \mathrm{e}^{i\vec{q}\cdot\vec{\rho}} d^2\rho \ , \tag{8.17}$$

where $\vec{q} = \vec{k} - k\frac{\vec{r}}{r}$ is the momentum transfer in the scattering process. To evaluate the integral, $B(\vec{q}) = \int B(\vec{\rho}) \mathrm{e}^{i\vec{q}\cdot\vec{\rho}} d^2\rho$, we write $\vec{\rho}\cdot\vec{q} = q\rho\cos\phi$ and get

$$B_0 \int_0^\infty \mathrm{e}^{\frac{-\rho^2}{R^2}} \rho d\rho \int_0^{2\pi} d\phi \mathrm{e}^{iq\rho\cos\phi} = 2\pi B_0 \int_0^\infty \mathrm{e}^{\frac{-\rho^2}{R^2}} \mathrm{J}_0(q\rho)\rho d\rho = \pi B_0 R^2 \mathrm{e}^{-\frac{1}{4}(Rq)^2} \ . \tag{8.18}$$

Hence, the wave function becomes

$$\psi(\vec{r}) = \mathrm{e}^{i\vec{k}\cdot\vec{r}} + \frac{\sqrt{\pi} g B_0 R^2 \sqrt{E}}{2\sqrt{2r}} \mathrm{e}^{-\frac{1}{4}(Rq)^2} \mathrm{e}^{i(kr+\pi/4)} \ . \tag{8.19}$$

By defining, as before,

$$\psi(\vec{r}) \to \mathrm{e}^{i\vec{k}\cdot\vec{r}} + \frac{1}{\sqrt{r}} f(\theta)\mathrm{e}^{i(kr+\pi/4)} \ , \tag{8.20}$$

we find for the scattering amplitude

$$f(\theta) = \sqrt{(\pi/8)} g B_0 R^2 E^{1/2} \mathrm{e}^{-\frac{1}{4}(Rq)^2} \ , \tag{8.21}$$

where the explicit dependence of q on the angle is given by

$$q^2 = 2k^2(1-\cos\theta) = 4k^2\sin^2(\theta/2) \ . \tag{8.22}$$

Hence, The total 2D cross-section is given by

$$\int_0^{2\pi} |f(\theta)|^2 d\theta = \frac{\pi}{8}(gB_0)^2 R^4 E \int_0^{2\pi} \mathrm{e}^{-\frac{1}{2}(Rq)^2} d\theta = \frac{\pi^2}{4}(gB_0)^2 R^4 E \mathrm{e}^{-(Rk)^2} I_0((Rk)^2) \ , \tag{8.23}$$

where $I_0(x) = J_0(ix)$ is the modified Bessel function. The argument of this function (i.e $(Rk)^2$) is very large (1 eV $\times$ 1 cm $\approx 10^5$) so we can use the asymptotic from of the modified Bessel function

$$I_n(x) = \frac{\mathrm{e}^x}{\sqrt{2\pi x}} \left(1 + \frac{(1-2n)(1+2n)}{8x} + ...\right) \ . \tag{8.24}$$

Keeping only the first order term gives the result

$$\sigma_{tot}^{Gauss} = \frac{\pi^{3/2}}{\sqrt{32}} g^2 B_0^2 R^3 \ . \tag{8.25}$$

Again, we find the axion-photon conversion probability $P = \sigma_S/\sigma_G$ to be

$$P_{Gauss} = \frac{\pi^{3/2}}{8\sqrt{2}} g^2 B_0^2 R^2 \ . \tag{8.26}$$

The geometrical cross-section is taken as $2RL$, as in the previous section, to keep the correspondence to a cylinder with radius R and constant magnetic field B_0.

This is the place to notice that one can yield the cross section (or, equivalently, the scattering amplitude) for the δ function scattering (Eq. (8.11)) directly from the Gaussian case by taking the limit $Rk \to 0$ of Eq. (8.23) (using $I_0(x) \xrightarrow{x \ll 1} 1$).

Notice that the comparison between the 1D and the 2D calculations is not straight forward since in the 1D case there is no concept of ?small angle scattering? and hence all the scattering is either forward or backward. We will address this issue more thoroughly at the last section of this work.

B [Tesla]	D [cm]	σ_{tot}^{Gauss} [cm]	N_{Gauss} [sec^{-1}]	P_{Gauss}
10	1	1.17×10^{-23}	4.29×10^{-11}	1.17×10^{-23}
10	10	1.17×10^{-20}	4.29×10^{-8}	1.17×10^{-21}
6	2	3.38×10^{-23}	1.24×10^{-10}	1.69×10^{-23}
6	20	3.38×10^{-20}	1.24×10^{-7}	1.69×10^{-21}

TABLE II: Total 2D cross-section, number of events and the axion-photon conversion probablity for different choices of the magnetic field strength (B) and the solenoid diameter (D) for the finite sized solenoid with Gaussian distributed magnetic field case. Again, we use $g = 10^{-10}$ GeV^{-1} and rationalized natural units to convert the magnetic field units from Tesla to eV^2, where the conversion is 1 T = 195 eV^2.

8.2.2. Solenoidal Generated Potential - Square Well Approximation

Now we turn to consider the magnetic field generated by an ideal solenoidal current which is described by a step function realizing a uniform magnetic field pointing in the

$\hat{z}$ direction and constrained to a cylindrical region around the origin

$$\vec{B}(r) = \begin{cases} B_0\hat{z} \ , & r < R \ , \\ 0 \ , & r > R \ . \end{cases} \tag{8.27}$$

Repeating the same manipulation as in equations (8.15) to (8.22) and using the Fourier transformation of the step function

$$B_0 \int_0^R \rho d\rho \int_0^{2\pi} d\phi \mathrm{e}^{iq\rho\cos\phi} = 2\pi B_0 \int_0^R \rho d\rho \mathrm{J}_0(q\rho) = \frac{2\pi R B_0}{q}\mathrm{J}_1(qR) \ , \tag{8.28}$$

we find that the scattering amplitude is now given by

$$f(\theta) = \sqrt{\frac{\pi}{2}}\frac{B_0 R g E^{1/2}}{q}\mathrm{J}_1(qR) \ , \tag{8.29}$$

where the explicit dependence of q on the angle is given by Eq. (8.22).
Before evaluating the integral for the total cross-section, let us write the total cross section for the square well case in terms of the delta function cross-section, calculated in section 8.1

$$\sigma_{tot.}^{well} = \frac{\pi}{32} g^2 B_0^2 D^4 E \left[\int_0^{2\pi} \left|\frac{J_1(qR)}{qR}\right|^2 d\theta\right] = \sigma_{tot.}^{\delta}\frac{2}{\pi}\left[\int_0^{2\pi} \left|\frac{J_1(qR)}{qR}\right|^2 d\theta\right] = \sigma_{tot.}^{\delta}\frac{2}{\pi} I(ER) \ , \tag{8.30}$$

where $I(ER) = \int_0^{2\pi} \left|\frac{J_1(qR)}{qR}\right|^2 d\theta$ is a dimensionless quantity which is a function of the multiplication $E \cdot R$. Using the relation $P = \sigma_{tot}/D$ (where we use the same notations as in section 8.1), the proportionality constant connects also the conversion probabilities for the δ function and square well cases

$$P_{well} = P_\delta \frac{2}{\pi} I = \frac{\pi}{32} g^2 B_0^2 D^3 E I(ER) \ . \tag{8.31}$$

Denoting $ER = kR$ by η, the integral can be analytically solved with the solution

$$I(\eta) = \frac{\pi}{2}\ {}_2F_3(\{\tfrac{1}{2}, \tfrac{2}{3}\}; \{1, 2, 3\}\,; -4\eta^2)\ , \tag{8.32}$$

where ${}_2F_3$ is an hypergeometric function.

To analyze this solution we expand the hypergeometric function ${}_2F_3$ to a series. Then, for small η, $I(\eta)$ is converging toward the constant value $\pi/2$, thus giving the equality $\sigma_{tot.}^{well} = \sigma_{tot.}^{\delta}$. This result is expected since considering only small η values is equivalent to considering isotropic scattering because $\eta \ll 1$ means that $ER \ll 1$. Hence, the wavelength of Ψ is very large compared to the length scale of the potential. Therefore, this approximation corresponds to the δ function limit of the step function, which, in turn, means that we consider isotropic scattering.

This conclusion can also be deduced from the following viewpoint regarding the scattering angle: The integrand of I is becoming extremely oscillatory as its argument (i.e. qR) is bigger and therefore for a reasonable scale of ER ($\approx 10^5$) we have a highly oscillatory integrand which is also decaying very fast as a function of θ (since the momentum transfer q is a function of the scattering angle). Thus, the biggest contribution will come from smaller angles. In fact, demanding that the integrand will be of order one is equivalent to considering scattering angles that satisfy $\theta \lesssim 1/ER \approx 10^{-5}$. Then, using the asymptotic form of the Bessel function for small arguments we have $I \approx \pi/2$ which simply gives the solution $\sigma_{tot.}^{well} = \sigma_{tot.}^{\delta} = \pi^2 g^2 B_0^2 R^4 E/4$. Considering only small angles is equivalent to demanding that the argument of the Bessel function will satisfy the condition $ER \cdot \sin(\theta/2) \ll 1$. Without limiting the range of the scattering angle, this of course means that $\eta = ER \ll 1$, the condition which coincides with the small η expansion of $I(\eta)$.

On the other end, we have the expansion for large η. This reveals the fact that the integral approaches the limit $I \to \frac{8}{3\pi\eta} = \frac{8}{3\pi ER}$ very fast. For example, for $\eta = 10$ we already have $\frac{8}{30\pi}/I(\eta = 10) = 0.997$. A plot of $I(\eta)$ and its limit $\frac{8}{3\pi\eta}$ is shown in Fig. 7.

Putting this limit into Eq. (8.31) gives the result

$$P_{well} = \frac{1}{6} g^2 B_0^2 D^2 = \frac{2}{3} g^2 B_0^2 R^2 \ . \tag{8.33}$$

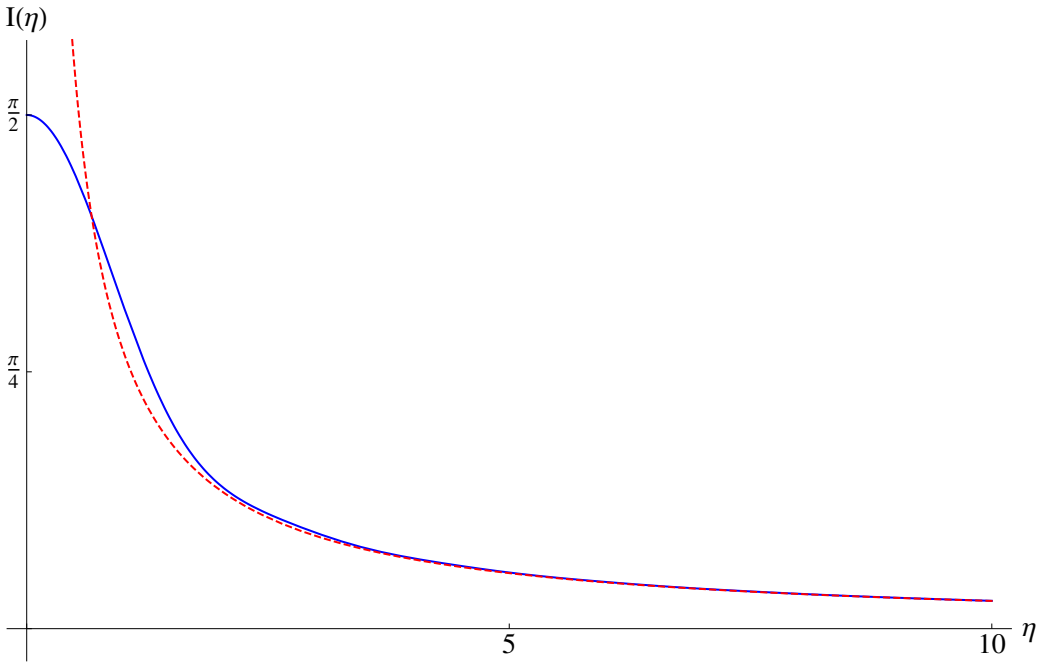

FIG. 7: The solution of the integral $I(\eta)$, defined by Eq. 8.30, is an hypergeometric function $I(\eta) = \frac{\pi}{2}\ {}_2F_3(\{\frac{1}{2}, \frac{2}{3}\}; \{1, 2, 3\}\,; -4\eta^2)$. This figure shows a plot of $I(\eta)$ as a function of the multiplication $ER = \eta$ in the solid line. The dashed line represents the fast approached limit of $I(\eta)$, which is given by $\frac{8}{3\pi\eta}$. At $\eta = 10$ both lines are close enough so that the ratio $\frac{8}{30\pi}/I(\eta = 10)$ already equals 0.997.

Since the generalized hypergeometric function is difficult to analytically work with for large arguments (large η values), we have also calculated the total 2D cross-section numerically to verify our results for the entire spectrum of η. In order to evaluate the integral I we have used the 'MATLAB' program, running the new 'quadgk' function

which is using the Gauss-Kronrod quadrature and is efficient specifically for oscillatory integrands. The results of the the analytical and numerical calculations match to very high precision and both results are practically the same. In fact, when considering solar axions (i.e. $ER = \eta$ is of order 10^8), the numerical calculation gave the result of Eq. (8.33) as well. A few examples for the cross-section, number of events and conversion probability for solar axions are given below in TABLE III.

B [Tesla]	D [cm]	σ_{tot}^{well} [cm]	N_{well} [sec^{-1}]	P_{well}
10	1	1.58×10^{-23}	5.80×10^{-11}	1.58×10^{-23}
10	10	1.58×10^{-20}	5.80×10^{-8}	1.58×10^{-21}
6	2	4.56×10^{-23}	1.67×10^{-10}	2.28×10^{-23}
6	20	4.56×10^{-20}	1.67×10^{-7}	2.28×10^{-21}

TABLE III: Total 2D cross-section, number of events and the axion-photon conversion probablity for different choices of the magnetic field strength (B) and the solenoid diameter (D) for the finite sized ideal solenoid case. We use $g = 10^{-10}$ GeV^{-1} and rationalized natural units to convert the magnetic field units from Tesla to eV^2, where the conversion is 1 T = 195 eV^2

When comparing the cross-sections of the Gaussian distributed magnetic field to the step function, one expects the step function cross-section to be bigger than a cross-section generated by a smooth function, in agreement with similar studies done in the context of nuclear physics models, where it has been shown that a step function potential gives a bigger scattering cross-section than a smooth potential like, for example, the Woods-Saxon Diffuse potential [90]. Our results qualitatively agree with Woods and Saxon, as can be seen by comparing Tables II and III.

8.3. Resonant Scattering For $E \sim m_a$

So far in this study, we have considered the axion field as a massless field in order to get the $U(1)$ symmetry between axions and photons. In fact, this symmetry holds up whenever the axion mass is equal to the (effective) photon mass inside a medium, or when the interaction term is much bigger than the mass term [91]. For example, in axion helioscope experiments photons acquire an effective mass [87] if one fills the conversion region with a suitable refractive gas.

Of course, if we had recalculated our results with massive axions and "massive" photons (of equal mass to that of the axion), our conclusions will have to be modified. The term that has to be taken under consideration is an $1/\sqrt{(E^2-m^2)^{1/2}}$ term which comes from the Green's function and will replace the current $1/\sqrt{E}$ in the scattering amplitude. Thus, in the $m_a \sim m_{photon} \neq 0$ case, the total two dimensional cross-section (for the δ function case) would have the following energy dependence

$$\sigma_{tot} = \frac{\pi g^2 B_0^2 R^4 E^2}{4\sqrt{(E^2-m^2)}} \ , \tag{8.34}$$

and we obtain a resonance when $E = m$, which has, in a sense, a similar behavior to the 1D problem analyzed by Adler et. al. [92] (notice that Adler et. al. consider the conversion between a massive axion and a massless photon), where of course the resonance here appears at $m_{axion} \sim m_{photon}$. In Eq. (8.34) the relation $m_{axion} \sim m_{photon}$ is assumed from the beginning and we see that the additional resonance appears as $E \sim m$. For an axion rest mass below ~ 1 eV, this can have practical consequences, for example, in laser generated axions (e.g in "light shining through the wall" experiments) when one can control the energy of the photon/axion beam.

We can see here that the 1D treatment of this process can not be justified since in the limit of zero momentum (or infinite wavelength) the scattering amplitude and the differential scattering cross-section become isotropic (i.e equal for all angles) and it is

impossible to consider only one direction in the scattering. In fact, in the limit of exactly zero momentum (assuming there is a tunable laser capable of very fine accuracy to obtain E very close to m) the amplitude of a finite potential becomes of the form to Eq. (8.34). This is since taking the limit of zero momentum implies zero momentum transfer (from Eq. 8.22) which means to consider only zero modes in the Fourier transform of the magnetic field. Hence, the cross-section of a finite potential becomes of the form of the modified δ function potential. It is an experimental question whether such a fine tuning is possible with an existing laser, if the axion has a mass of the order of eV. But, in astrophysical environments this can occur occasionally.

Achieving a resonance requires a material which has a zero index of refraction. The real part of the refractive index is given by

$$n_R(\omega) = 1 + K\frac{\omega_0 - \omega}{(\omega_0 - \omega)^2 + \gamma^2}, \tag{8.35}$$

where $K = Ne^2 f$ with N being the number density of atoms, e is the electron charge and f transition oscillator strength, ω_0 is the transition frequency and γ represents dissipative interactions [93]. Equating the latter to zero requires the condition $K^2 > 4\gamma^2$. A negative and zero refractive indices are indeed possible as was experimentally observed by Shelby et al. [94]. Let us hope that one day it will be possible to implement this in an axion detection lab experiment.

A similar problem of a resonant interaction between axions and photons was also studied by Sikivie [56], who has considered a rather similar resonance condition $E = m$ in the case where the external magnetic field is applied to a cavity with a resonance frequency ω. What is special in our case is that at the resonance the corrections to the 1D scattering (i.e going away from a forward direction) become big. In other words, there are two enhancements in this case: one due to the summation on all angles in 2D and the other because of the resonance.

8.4. Summary, Discussion and Conclusions

In this section we have studied the first examples of scattering which is not one dimensional and we have obtained enhanced probabilities. This effect is further increased in the case of resonant scattering that appears when $E = m$ and corresponds to isotropic scattering (as in the δ function scattering). One should notice that allowing for two dimensional scattering is the same as allowing the possibility of axion-photon splitting which does not make sense in 1D scattering. We have studied here merely magnetic fields with a cylindrical structure. Further generalizations should include the scattering from, for example, a quadrupole magnetic field (as we shall do in the following section), which is more complicated than the cylindrical symmetric case we have studied here but, on the other hand, is quite accessible as a possible experimental setup.

In the 1D case the conversion probability is $P_{1D} = g^2B^2l^2/4$, where l is the linear dimension associated with the extent of the magnetic field [89]. Hence, when trying to compare the conversion probability for the cylindrically symmetric geometry found by the method used in this work with the known 1D calculation it is not so obvious what is the correct length scale l that should be taken to calculate P_{1D}. The problem is, of course, that the notion of splitting does not make sense in 1D and that the scattering region is not an area but a line. Hence, the best way to discuss the relation between the two calculations will be to average the 1D probability over the scattering region for each case. In other words, we look at the 2D experiment as the weighted average of an infinite number of 1D experiments.

For the step function case the scattering region is a cylinder with radius R. Writing $l = 2\sqrt{R^2 - y^2}$, where the wave travels in the $\hat{x}$ direction and $\hat{y}$ is the transverse dimension, the average of P_{1D} is

$$P_{1D}^{well\ avg.} = \frac{\int_{-R}^{R} P_{1D}dy}{\int_{-R}^{R} dy} = \frac{1}{2R} \cdot 2\int_0^R \tfrac{1}{4}g^2B_0^2 4(R^2 - y^2)dy = \frac{2}{3}g^2B_0^2R^2 \ , \tag{8.36}$$

a result which coincides with Eq. (8.33).

The general case is more complicated since the scattering region may be infinite and the magnetic field may not be homogenous. However, a 1D analogue to the 2D experiment can be found and the weighted average can be done by choosing the magnetic flux as the averaging measure

$$P_{1D}^{avg} = \frac{\int_{-\infty}^{\infty}\int_{-\infty}^{\infty}\frac{1}{4}g^2|\int_{-\infty}^{\infty}B(x',y)dx'|^2B(x,y)dxdy}{\int_{-\infty}^{\infty}\int_{-\infty}^{\infty}B(x,y)dxdy} \ . \tag{8.37}$$

Then, of course, eq. (8.36) is a special case of the latter.

When considering the Gaussian case ($B(x,y) = B_0 \mathrm{e}^{-\frac{x^2+y^2}{R^2}}$) the averaged 1D probability is

$$P_{1D}^{Gauss.avg.} = \frac{\pi}{\sqrt{3}}\frac{g^2B_0^2R^2}{4} \ . \tag{8.38}$$

The comparison of this result with Eq. (8.26) gives $P^{Gauss}/P^{Gauss.avg.} = 1.085$ and thus the two formulations do not exactly coincide.

However, despite Eq. (8.37) not all 2D experiments can have a 1D analogue. In fact, we have seen in the previous section that when considering resonant scattering, the limit of zero momentum implies that the cross section is isotropic and there is no way to describe such a process with an analogous 1D calculation since there is no way to consider only one scattering dimension.

When considering scattering from a finite sized potential (Gaussian and step function potentials) the enhancement of the conversion probability compared to the 1D case still gives probabilities in the same order of magnitude. This is due to the fact that the wavelength ($1/E$) of the Ψ wave function is much smaller than the length scale of the potential (R), which essentially results in a quasi-1D behavior of the system. If the wavelength will be larger, or even comparable to the length scale of the potential the deviation between the two results gets bigger since in this case the scattering becomes

more and more isotropic and we essentially obtain δ function scattering, as was discussed in the previous subsection.

The wavelength is determined by the momentum of the particles. For the massive case, the momentum approaches zero when the magnitude of the particle?s energy approaches the order of the particle's mass. This situation, where the wavelength of the particles is much larger than any other length scale in the problem, is realized in the resonant scattering case, as discussed in section 8.3. There we have shown explicitly that this limit gives an isotropic scattering for a finite potential and thus, conversion probabilities of the order of the δ function case (shown in table I).

The cross-section in the resonance case was calculated at tree level. This gives a singularity of the cross-section at $E = m$. However, in practice a resonance effect should have a certain width and this, of course, should also be the case for the resonance case found here. We notice also that the resonance behavior comes together with a breakdown of the 1D treatment of axion-photon conversion and also that a finite width can be originated from absorption effects. All these problems will be addressed in a future publication.

9. AXIONS SCATTERING FROM A QUADRUPOLE MAGNETIC FIELD

The question of the scattering of axions from a quadrupole magnetic field has recently been proposed as a new possible method for detecting axions on terrestrial experiments such as the CAST experiment at CERN. Current axion detection experiments use a constant magnetic field, that can be generated by a particle accelerator dipole magnet for example, to trace QCD axions. These experiments use a standard 1D analysis (i.e the inverse Primakoff effect) [56] to evaluate the axion-photon reconversion. Therefore, it is an interesting question wether a magnetic field which is varying over the scattering region, and thus should be analyzed by a 2D formalism, could improve the probability of QCD axion detection in the near future. Here we follow [96] to estimate the cross-

section and conversion probability of solar axions that scatter along a long accelerator like quadrupole magnet, using the novel 2D scattering method which accounts for an axion-photon splitting and presented in the means of an axion-photon duality symmetry.

9.1. The Scattering Amplitude in a 2D Eikonal Approximation

As we did for the cylindrical symmetric case (Sec. 8), we write separately the time and space dependence of the axion-photon field as $\Psi(\vec{r},t) = \mathrm{e}^{-i\omega t}\psi_k(\vec{r})$, which yields

$$(-\omega^2 - \nabla^2 + \omega\beta)\psi_k = 0 \ . \tag{9.1}$$

In order to develop the space dependent term of the axion-photon field, let us consider a high energy, non-relativistic scattering. We assume that the wavelength of the ψ field is short, i.e $kR \gg 1$, where R is the length scale of the scattering region and k is the momentum of the incoming beam, and that $|V_0|/E \ll 1$, where $|V_0| = gB_0$ is the averaged magnitude of the potential over the scattering region and E is the energy of the incoming beam. Under these assumptions we can address the problem by assuming small scattering angles and representing our equation in the integral from of the Lippman-Schwinger equation

$$\psi_k(r) = \mathrm{e}^{i\vec{k}\cdot\vec{r}} + \int d^2r' G_0^{(+)}(r,r')U(r')\psi_k(r') \ , \tag{9.2}$$

where $G_0^{(+)}(r,r')$ is Green's function given by

$$G_0^{(+)} = \frac{1}{2\sqrt{2\pi k|r-r'|}}\mathrm{e}^{i(k|r-r'|+\pi/4)} = \frac{1}{(2\pi)^2}\lim_{\epsilon\to 0}\int d^2k' \frac{\mathrm{e}^{ik'(r-r')}}{k'^2 - k^2 - i\epsilon} \ , \tag{9.3}$$

where $k = \omega$ for a massless field. writing the spatial part ot the wave function $\psi_k(r)$ as

$$\psi_k(r) = \mathrm{e}^{i\vec{k}\cdot\vec{r}}\phi(r) \ , \tag{9.4}$$

and substituting into Eq.(8.15) yields an equation for $\phi(r)$ [97]

$$\begin{aligned}\phi(r) &= 1 + \mathrm{e}^{-i\vec{k}\cdot\vec{r}} \int d^2r' G_0^{(+)}(r,r') U(r') \mathrm{e}^{i\vec{k}\cdot\vec{r'}} \phi(r') = \\ &= 1 + \tfrac{1}{(2\pi)^2} \int d^2r' \int d^2k' \tfrac{\mathrm{e}^{i(\vec{k'}-\vec{k})\cdot(\vec{r}-\vec{r'})}}{k'^2-k^2-i\epsilon} U(r')\phi(r') = 1 + I(r) \ .\end{aligned} \tag{9.5}$$

Choosing $\vec{k} = (k, 0)$ and $\vec{k'} = (k\cos(\theta), k\sin(\theta))$, the momentum transfer vector $\vec{q} = \vec{k'} - \vec{k}$ is just $\vec{q} = (0, k\theta)$ for small angles. Changing integration variables from k' to q in the latter equation gives

$$I(r) = \frac{1}{(2\pi)^2} \int d^2r' \int d^2q \frac{\mathrm{e}^{i\vec{q}\cdot(\vec{r}-\vec{r'})}}{2\vec{k}\cdot\vec{q} + \vec{q}^2 - i\epsilon} U(r')\phi(r') \ , \tag{9.6}$$

and since $|\vec{q}| \ll 1$ we can expand $I(r)$ to a power series in terms of $|\vec{q}|^2$

$$\frac{1}{2\vec{k}\cdot\vec{q} + \vec{q}^2 - i\epsilon} \approx \frac{1}{2\vec{k}\cdot\vec{q} - i\epsilon} - \frac{1}{(2\vec{k}\cdot\vec{q} - i\epsilon)^2} q^2 + \cdots \tag{9.7}$$

As a result of this expansion the transmitted part of the wave function and the scattering amplitude can be written as a series as well

$$\begin{aligned}\phi(r) &= \phi^{(1)} + \phi^{(2)} + \ldots \\ f(k,\theta) &= f^{(1)} + f^{(2)} + \ldots .\end{aligned} \tag{9.8}$$

Now we turn to calculate $I(r)$ to first order, bearing in mind that we chose the incident wave to propagate along the $\hat{x}$ axis, hence giving

$$\begin{aligned}I^{(1)}(r) &= \tfrac{1}{(2\pi)^2} \int d^2r' \int dq_x dq_y \tfrac{\mathrm{e}^{i(q_x(x-x')+q_y(y-y'))}}{2kq_x - i\epsilon} U(r')\phi(r') = \\ &= \tfrac{1}{(2\pi)} \int d^2r' \int dq_x \tfrac{\mathrm{e}^{iq_x(x-x')}}{2kq_x - i\epsilon} \delta(y-y') U(r')\phi(r') = \\ &= \tfrac{i}{2k} \int d^2r' \Theta(x-x')\delta(y-y') U(r')\phi(r') = \tfrac{i}{2k} \int_{-\infty}^{x} dx' U(x',y)\phi(x',y) \ .\end{aligned} \tag{9.9}$$

Using the latter result we can evaluate $\phi(r)$ and the wave function

$$\begin{aligned} \phi(r) = 1 + \tfrac{i}{2k} \int\limits_{-\infty}^{x} dx' U(x',y)\phi(x',y) = \mathrm{e}^{\frac{i}{2k}\int\limits_{-\infty}^{x} dx' U(x',y)} \ , \\ \psi_k(r) \approx \mathrm{e}^{i(\vec{k}\cdot\vec{r} + \frac{1}{2k}\int\limits_{-\infty}^{x} dx' U(x',y))} \ . \end{aligned} \tag{9.10}$$

Since we consider here asymptotic scattering, we need to evaluate Green's function under the approximation $|r| \ll |r'|$ and hence

$$|\vec{r} - \vec{r'}| = \sqrt{\vec{r}^2 - 2\vec{r}\cdot\vec{r}\,' + \vec{r}\,'^2} \approx r\sqrt{1 - 2\frac{\hat{r}}{r}\cdot\vec{r}\,'} \approx r - \vec{r}\,'\cdot\hat{r} \ , \tag{9.11}$$

and then, from Eq. (8.15), the wave function can be written as

$$\psi_k(r) = \mathrm{e}^{i\vec{k}_i\cdot\vec{r}} + \frac{\mathrm{e}^{i(kr+\pi/4)}}{\sqrt{8\pi kr}} \int d^2r' \mathrm{e}^{-i\vec{k}_f\cdot\vec{r}'} U(r')\psi_k(r') \ , \tag{9.12}$$

where $k_i = k\hat{x}$ and $k_f = k\hat{r}$ is defined to be the scattered wave. Identifying the scattering amplitude from the asymptotic behavior of the wave function

$$\psi_k(r) = \mathrm{e}^{i\vec{k}\cdot\vec{r}} + \frac{1}{\sqrt{r}} f(\theta)\mathrm{e}^{i(kr+\pi/4)} \ , \tag{9.13}$$

we get for the scattering amplitude

$$f(k,\theta) = \frac{1}{\sqrt{8\pi k}} \int d^2r' \mathrm{e}^{i(\vec{k}_f - \vec{k}_i)\cdot\vec{r}\,'} U(r') \mathrm{e}^{\frac{i}{2k}\int\limits_{-\infty}^{x'} dx'' U(x'',y')} \ . \tag{9.14}$$

9.2. Comparison of the Eikonal Approximation With Previous Results

In this section we apply the eikonal approximation to two cases, a square well potential and a magnetic field with Gaussian ditribution, which were addressed in [84] and compare the results obtained in [84] by using Born's approximation with the new method presented here.

9.2.1. A Solenoid Magnet

Let us consider a magnetic field generated by an ideal solenoidal current which is described by a step function realizing a uniform magnetic field pointing in the $\hat{z}$ direction and constrained to a cylindrical region around the origin

$$\vec{B}(r) = \begin{cases} B_0\hat{z} \ , & r < R \ , \\ 0 \ , & r > R \ . \end{cases} \tag{9.15}$$

Thus, the potential associated with the square well is $U(x,y) = \omega g B_0 \Theta(x^2+y^2-R^2)$, where B_0 is the strength of the magnetic field, g is the coupling constant, and ω is the energy of the incident wave. Then, we obtain

$$\frac{i}{2k}\int_{-\infty}^{x'} dx'' U(x'',y') = \frac{igB}{2}(x' + \sqrt{R^2-y'^2}) \ . \tag{9.16}$$

Using the current limits on the axion-photon coupling constant (i.e $g \lesssim 10^{-19}$ eV^{-1} [86]), the energy of solar axions (4.2 eV) and current limits on terrestrial magnetic fields (< 16 T in the best permanent magnets, using the Nb3Sn superconductor), the condition $|V|/E \ll 1$ is obviously satisfied. These values for the parameters will be used throughout the rest of this work.

For this potential the 2D scattering amplitude, Eq. (9.14), is

$$f(k,\theta) = \frac{\omega g B_0}{\sqrt{8\pi k}} \int dx' dy' \mathrm{e}^{i(\vec{k}_f - \vec{k}_i)\cdot\vec{r}'} \mathrm{e}^{\frac{igB_0}{2}(x' + \sqrt{R^2-y'^2})} \ , \tag{9.17}$$

where the integration is preformed over the scattering region. Following the procedure from the previous section, we evaluate $\vec{k}_f - \vec{k}_i$ for small scattering angles (i.e $\vec{q} = \vec{k}_f - \vec{k}_i \approx (0, k\theta)$) to get

$$f(k,\theta)=\frac{\omega g B_0}{\sqrt{8\pi k}}\int\limits_{-R}^{R}dx'\mathrm{e}^{\frac{i}{2}gB_0x'}\int\limits_{-\sqrt{R^2-x'^2}}^{\sqrt{R^2-x'^2}}dy'\mathrm{e}^{ik\theta y'+\frac{i}{2}gB_0\sqrt{R^2-y'^2}}\ . \tag{9.18}$$

In order to calculate the total cross section we shall use the optical theorem in 2D. Since the latter equation is continuous in θ, one can take $\theta = 0$. We can further simplify this integral by expanding the exponential to a series in powers of gB_0R. For reasonable values for a terrestrial length scale of the scattering region and the same values mentioned above for the coupling constant g and magnetic field strength B_0 the first order approximations for the exponent can indeed be justified. This expansion would be done at the end of the calculation in order to have a result which is comparable to the Born approximation calculation, hence we might as well do it now. Hence, we obtain

$$\begin{aligned}\sigma_{tot}^{well}=2\sqrt{\tfrac{2\pi}{k}}\mathrm{Im}\{f(k,0)\}\approx\tfrac{1}{2}g^2B^2\int\limits_{-R}^{R}dx'\int\limits_{-\sqrt{R^2-x'^2}}^{\sqrt{R^2-x'^2}}dy'(x'+\sqrt{R^2-y'^2})=\\ =\tfrac{(gB_0)^2R^3}{2}\int_{-1}^{1}d\xi\int_{-\sqrt{1-\xi^2}}^{\sqrt{1-\xi^2}}d\eta\left(\xi+\sqrt{1-\eta^2}\right)=\\ =\tfrac{8}{3}\tfrac{(gB_0)^2R^3}{2}\ .\end{aligned} \tag{9.19}$$

As was explained in Sec. 8, to obtain the conversion probability, we calculate the ratio between the number of axions arriving at the solenoid and the number of photons produced in the conversion process. The number of axions hitting the solenoid is given by multiplying the flux of incoming axions by the geometrical cross section of the solenoid, given by $\sigma_G = 2RL$, where L is the solenoid length. In order to get the 3D total cross-section (i.e the scattering cross-section) σ_S we multiply the 2D cross-section σ_{tot} by the length of the solenoid L. The number of produced photons is found by multiplying the scattering cross section ($\sigma_S = \sigma_{tot} \cdot L$) times the flux. Thus, the conversion probability is given by

$$P_{well} = \sigma_S/\sigma_G = \frac{4}{3}\frac{g^2 B_0^2 R^3}{2R} = \frac{2}{3}g^2 B_0^2 R^2 \ . \tag{9.20}$$

Comparing this result to the result obtained by using the Born approximation in Sec. 8.2.2 for the same setup (Eq. (8.33) there) we get precisely

$$P_{well}^{eikonal}/P_{well}^{Born} = 1 \ . \tag{9.21}$$

Hence, there is a complete correspondence between the eikonal approximation and the Born approximation in this case.

9.2.2. Gaussian Magnetic Field

In this setup the potential has the form

$$U(x,y) = \omega g B_0 \mathrm{e}^{-\frac{x^2+y^2}{R^2}} \ . \tag{9.22}$$

Integrating the potential along the axis of the incident wave yields

$$\frac{i}{2k}\int_{-\infty}^{x'} dx'' U(x'',y') = i\frac{gB_0}{2}\frac{\sqrt{\pi}R}{2}[1+\mathrm{Erf}(\frac{x'}{R})]\mathrm{e}^{-\frac{y'^2}{R^2}}, \tag{9.23}$$

where $\mathrm{Erf(x)} = \frac{2}{\sqrt{\pi}}\int_0^x \mathrm{e}^{t^2} dt$. The scattering amplitude is given by

$$\begin{aligned} f(k,\theta) = \sqrt{\tfrac{\omega}{8\pi}} g B_0 \int_{-\infty}^{\infty} dy' \mathrm{e}^{ik\theta y'} \mathrm{e}^{-\frac{y'^2}{R^2}} \mathrm{e}^{\frac{i}{4}gB_0R\sqrt{\pi}\mathrm{e}^{-\frac{y'^2}{R^2}}} \int_{-\infty}^{\infty} dx' \mathrm{e}^{-\frac{x'^2}{R^2}} \mathrm{e}^{\frac{i}{4}gB_0R\sqrt{\pi}\mathrm{Erf}(\frac{x'}{R})\mathrm{e}^{-\frac{y'^2}{R^2}}} = \\ = \sqrt{\tfrac{\omega}{8\pi}} 4 \int_{-\infty}^{\infty} dy' \mathrm{e}^{ik\theta y'} \mathrm{e}^{\frac{i}{4}gB_0R\sqrt{\pi}\mathrm{e}^{-\frac{y'^2}{R^2}}} \sin(\tfrac{1}{4}gB_0R\sqrt{\pi}\mathrm{e}^{-\frac{y'^2}{R^2}}) \ . \end{aligned} \tag{9.24}$$

In order to calculate the total cross section we use, as usual, the optical theorem in 2D and by using the same reasoning as in Eq. (9.18) to consider only the $\theta = 0$ angle we get

$$\sigma_{tot}^{Gauss} = 4\int_{-\infty}^{\infty} dy' \sin^2(\frac{1}{4}gB_0R\sqrt{\pi}\mathrm{e}^{-\frac{y'^2}{R^2}}) \ . \tag{9.25}$$

To obtain an analytic result and simplify the calculation, we can use the fact that $\exp\{-\frac{y'^2}{R^2}\} \leq 1$ for all y and that reasonable values of the parameters g, B_0 and R allow us to make a first order approximation. Thus, Eq. (9.25) can be written as

$$\sigma_{tot}^{Gauss} \approx \frac{\pi}{4}g^2B_0^2R^2\int_{-\infty}^{\infty} dy'\mathrm{e}^{-\frac{2y'^2}{R^2}} = \frac{\pi^{\frac{3}{2}}}{\sqrt{32}}g^2B_0^2R^3 \ . \tag{9.26}$$

Hence, using the same method we used in the previous setup, the probability will be

$$P_{Gauss} = \frac{\pi^{\frac{3}{2}}}{8\sqrt{2}}g^2B_0^2R^2. \tag{9.27}$$

The comparison to the probability of conversion calculated in Sec. 8.2.1, using the Born approximation, (Eq. (8.26)) gives

$$P_{Gauss}^{eikonal}/P_{Gauss}^{Born} = 1, \tag{9.28}$$

so that there is again a complete correspondence between the eikonal approximation and the Born approximation. Thus, we conclude that the Eikonal approximation is indeed valid and will most probably yield a correct results under our assumptions for a high energy, yet non-relativistic scattering.

9.3. Axions Scattering in a Quadrupole Magnet

After verifying the accuracy of the eikonal approximation for two known problems, we now turn to calculate the scattering of axions from a quadrupole magnetic field.

Placing the quadrupole magnet in the yz plane with the x axis (the direction of the incoming beam) along the symmetry axis of the quadrupole field, the quadrupole magnetic field distribution can be approximated (for a quadrupole magnet with a narrow aperture compared to its length) by [99]

$$\vec{B}(x,y,z) = s\vec{\nabla}(yz) = s(z\hat{y} + y\hat{z}) = \frac{2B_0}{R}(z\hat{y} + y\hat{z}) \ , \tag{9.29}$$

where $s = \frac{2B_0}{R}$ is the quadrupole gradient, B_0 is the value of the magnetic field at the pole tips (i.e at the points $(0, \pm\frac{R}{2}, 0)$ and $(0, 0, \pm\frac{R}{2})$), where we chose a rectangular aperture for simplicity. However, since in our formalism we chose to analyze the case where the magnetic field is pointing in the z direction, only the z component of the external magnetic field will take part in the scattering process and we effectively have an inhomogeneous magnetic field of the form $B_z = \frac{2B_0}{R}y$. However, the y component of the magnetic field will, of course, give the same contribution to the scattering process as the z component with the sole difference that the final photons will be with a y-polarization. Thus, we need to take into account the Ψ particle that has the y-polarization of the vector potential as one of its conjugate fields. This will be done at the end of this section.
Defining, in this case, the potential as:

$$U = \omega g \frac{2B_0}{R} y \ , \tag{9.30}$$

for $-R/2 \leq y \leq R/2$ and $-L/2 \leq x \leq L/2$, we get

$$\frac{i}{2k}\int_{-\infty}^{x'} dx'' U(x'', y') = ig\frac{B_0}{R}y'(x' + L/2) \ . \tag{9.31}$$

Putting this into Eq. (9.14) we have for the scattering amplitude

$$
\begin{aligned}
f(\theta) &= \sqrt{\tfrac{\omega}{2\pi}}\tfrac{gB_0}{R}\int_{-R/2}^{R/2} dy' \mathrm{e}^{ik\theta y'} y' \mathrm{e}^{ig\frac{B_0 L}{2R}y'} \int_{-L/2}^{L/2} dx' \mathrm{e}^{ig\frac{B_0}{R}y'x'} = \\
&= 2\sqrt{\tfrac{\omega}{2\pi}}\int_{-R/2}^{R/2} dy' \mathrm{e}^{i(g\frac{B_0 L}{2R}+k\theta)y'} \sin(\tfrac{gB_0 L y'}{2R}) = \\
&= 2\sqrt{\tfrac{\omega}{2\pi}}\cdot i\cdot\left(\frac{\sin(\frac{1}{2}kR\theta)}{k\theta} - \frac{R\,\sin(\frac{1}{2}(gB_0L+kR\theta))}{kR\theta+gB_0L}\right) .
\end{aligned}
\tag{9.32}
$$

Therefore, using the optical theorem, we obtain the total cross section

$$
\sigma_{tot}^{quad} = \sqrt{\frac{8\pi}{k}}\mathrm{Im}\{f(0)\} = 2R\left(1-\frac{\sin(\frac{1}{2}gB_0L)}{\frac{1}{2}gB_0L}\right) . \tag{9.33}
$$

To get the probability, in this case we just divide by R (geometrical cross section $= R^2$)

$$
P_{quad} = 2(1-\frac{\sin(\frac{1}{2}gB_0L)}{\frac{1}{2}gB_0L}) \approx 2\frac{\frac{1}{8}(gB_0L)^3}{3gB_0L} = \frac{1}{3}\frac{g^2B_0^2L^2}{4} . \tag{9.34}
$$

Although, as was discussed before, this result may be different than the one that would be obtained by using Born's approximation (since the potential is not piecewise continuous), it coincides with a result that is obtained by using an optical analogue as was previously shown by J. Redondo [100]. However, Redondo's calculation is missing features of the 2D calculation (and is also computed in an unphysical setup), as we now show (and as will be discussed in the conclusions of this work).

The scattering from the z component of the magnetic was merely a matter of choice in the in the initial setup of our system. The Ψ field will scatter, of course, from the y component as well since this component of the magnetic is also perpendicular to the momentum of the incoming beam. The same process described above can be repeated by a $\pi/2$ rotation of the system in the yz plane. In this case, the ψ field would have been defined as $\tilde{\Psi} = (a + i\tilde{A})/\sqrt{2}$, where $\tilde{A}$ is the y-polarization of the photon this time. This will give the same expression for the cross-section and conversion probability and since these two processes are distinguishable we can sum incoherently the two probabilities.

Hence, in order to get the complete probability we have to multiply Eq. (9.34) by a factor of two and thus

$$P_{quad}^{total} = 2 \cdot P_{quad} = \frac{2}{3}\frac{g^2 B_0^2 L^2}{4} = \frac{g^2 s^2 R^2 L^2}{24} \ . \tag{9.35}$$

9.4. Conclusions

In this section we have calculated the axion-photon conversion probability from a quadrupole magnetic field. We have used the eikonal approximation to calculate the scattering from the quadrupole magnet which simplifies the calculations compared to the Born approximation and verified this approximation by comparing to known results obtained with the Born approximation. The comparison to the step function and Gaussian distributed fields shows that the eikonal approximation and the Born's approximation give reasonably close answers.

In a previous letter by J. Redondo [100], a related analysis concerning the evolution of an axion-photon field in the presence of a magnetic field with a constant gradient over the entire space, was studied. In our case, however, the constant gradient field exists only in a finite region of space. This boundary condition for the magnetic field contributes in an essential way to the scattering amplitude since, as was explained in [84], even for the case of a strictly constant magnetic field living in a finite region of space one gets a non trivial scattering amplitude due to these boundary conditions. Thus, we conclude that the boundary effects can be as important as the gradient of magnetic field inside the finite scattering region. This is a significant difference between our treatment and that of reference [100]. In Redondo's letter, the applied magnetic field does not satisfy Maxwell's equations without sources since, in his letter, $\vec{\nabla} \times \vec{B} = \partial_x B_y = B_1 = J_z$ (where in Redonodo's notations $B_y = B_1 x$). Therefore, in his analysis there is an infinite extent of currents along the z axis which can simply not represent a physical situation. In conclusion, the work of Redondo is not a scattering problem and therefore

cannot incorporate all the physical aspects of an experimental set-up as opposed to the work presented here. This is most easily seen by comparing Eq. (9.35) with equation 3 in Redondo's letter. This comparison unveils the fact that the different approaches lead to different results.

Moreover, it may sometimes be tempting to believe that the 2D results can be obtained by averaging over 1D conversion probabilities. As we have already discussed here, a general prescription to find a 1D analogue to the 2D calculation may be obtained by using the magnetic flux as the averaging measure

$$P_{1D}^{avg} = \frac{\int_{-\infty}^{\infty}\int_{-\infty}^{\infty}\frac{1}{4}g^2|\int_{-\infty}^{\infty}B(x',y)dx'|^2B(x,y)dxdy}{\int_{-\infty}^{\infty}\int_{-\infty}^{\infty}B(x,y)dxdy}\ . \tag{9.36}$$

However, since the quadrupole magnetic flux is zero, this method will not work this time. Of course, it is possible to find an averaging process that will produce the 2D result, but it cannot be done a-priori with certainty. Eq. (9.36) is an example for a legitimate choice of measure that cannot produce a result at all. It is clear that there is no way to avoid the real calculation and obtain results in higher dimensions from averaging on lower dimension estimations. This shows that 2D processes cannot be reduced to a 1D calculation. The scattering process from a quadrupole field is intrinsically 2D since the scattered photon may have two different polarizations: Considering a magnetic field produced by a *physical* localized current naturally makes a significant difference. In particular, it shows that any attempt to say that the problem can be deduced from a 1D analogue is untenable and, in fact, will fail since the magnetic field produced by a physical current will necessarily have at least two components (in the source free region). Hence, in the process of photon production from the scattering of axions, the photon will have two distinguished polarizations. In addition, in the source free regions, a non-uniform field pointing in one direction, of the form $\vec{B} = B(x,y)\hat{l}$, will not be able to satisfy the source free Maxwell's equations, $\vec{\nabla}\times\vec{B} = \vec{\nabla}B(x,y)\times\hat{l} = 0$ and $\vec{\nabla}\cdot\vec{B} = \vec{\nabla}B(x,y)\cdot\hat{l} = 0$, since the solution requires that $\vec{\nabla}B(x,y) = 0$. Therefore, a

one directional magnetic field cannot solve these equations and the problem cannot be reduced to 1D.

We can, however, compare the scattering from a quadrupole to the scattering from a solenoid, which can represent a dipole accelerator magnet (with a different geometry of course). The result obtained here shows that it will be preferable to have a constant magnetic field distributed over the scattering region aperture (like, for example, the field of a solenoid) rather than having an inhomogenous field (as the quadrupole field). This comes from the fact that the magnetic field energy will be higher in the first case (when the maximal magnetic field strength B_0 is equal for both cases and both fields are distributed over the same scattering region). Since B_0 is an intrinsic property of the superconducting material, comparing a quadrupole magnet to a dipole magnet of the same length and aperture and made with the same superconductor, the dipole will yield a higher conversion rate.

One can also observe that the magnetic field parameter that determines the conversion rate is actually the global maximum value of the magnetic field in the scattering region. This feature appears as well in other calculations of the conversion probability from inhomogeneous fields, like, for example, the Gaussian distributed field in Sec. 8.2.1.

Part IV

The Next Generation Axion Helioscope

As we have seen, axions have very low interaction cross-sections with ordinary matter which practically makes them "invisible" particles. However, axions are predicted to convert to and from photons in the presence of strong magnetic fields. This property is used to detect axions in terrestrial experiments. It is the aim of this part of the research to define a new superconducting toroidal detector magnet that will be specifically designed for axions detection and will constitute the backbone of a Next Generation Axion Helioscope (NGAH). The NGAH project will be an immense upgrade of axion detection experiments, relative to the current state-of-the-art which is represented by the CAST experiment at CERN. This will lead to a significant expansion of the present limits on axions search.

For terrestrial axion search experiments, it is especially promising to use the sun as a source for axions produced in its hot interior. Directing a strong magnet toward the sun allows one to search for keV-range X-rays produced by axion-photon conversion, a process best visualized as a particle oscillation phenomenon [57] in analogy to neutrino flavor oscillations. Three such helioscopes were built, in Brookhaven [101], Tokyo [102] and at CERN [103]. The CERN Axion Solar Telescope (CAST) is currently finishing an 8-year long data taking period, having strongly improved on previous experiments and even surpassed astrophysical limits for some range of parameters, although axions have not been found.

In this part, we show that large improvements to the magnetic field volume with respect to the current state-of-the-art, represented by CAST, are possible and much needed.

Based on these improvements, a New Generation Axion Helioscope (NGAH) could search for axions that are 1–1.5 orders of magnitude more weakly interacting than those allowed by the current CAST constraints. If these ambitious goals will be achieved, a much larger range of realistic axion models can be probed and it is even conceivable that one can reach a sensitivity corresponding to m_a in the 10 meV range. This mass range would be significant in several ways: The energy-loss limit from SN 1987A suggests that QCD axions have $f_a \gtrsim 10^9$ GeV or $m_a \lesssim$ 10–20 meV as mentioned earlier. Moreover, if axions also interact with electrons, axions nearly saturating the SN 1987A limit could explain the apparent anomalous energy loss of white dwarfs [75–78]. For the first time, it appears conceivable to surpass the SN 1987A constraint, test the white-dwarf cooling hypothesis, and begin to explore entirely uncharted axion territory experimentally.

10. AN ENHANCED AXION HELIOSCOPE

As we have seen, the axion-photon interaction is given by the Lagrangian $\mathcal{L}_{a\gamma} = g_{a\gamma}\mathbf{E}\cdot\mathbf{B}\ a$, where a is the axion field and $g_{a\gamma}$ is the axion-photon coupling constant. The probability that an axion going through the transverse magnetic field B over a length L will convert to a photon is then given by [56, 104, 105]:

$$P_{a\gamma} = 2.6\times10^{-17}\left(\frac{B}{10\ \mathrm{T}}\right)^2\left(\frac{L}{10\ \mathrm{m}}\right)^2\left(g_{a\gamma}\times10^{10}\ \mathrm{GeV}\right)^2\mathcal{F}\ , \tag{10.1}$$

where the form factor $\mathcal{F} = \frac{2(1-\cos qL)}{(qL)^2}$ accounts for the coherence of the process and q is the momentum transfer.

The basic layout of an axion helioscope requires a powerful magnet coupled to x-ray detectors. When the magnet is aligned with the sun, an excess of x-rays at the ends of the magnet is expected, over the background measured at non-alignment periods. During the last decade, the same basic concept has been used by CAST [86, 103–105] with some innovations that provide a considerable step forward in sensitivity to solar

axions. Moreover, during its last years of operation, CAST has also improved on the original concept of an axion helioscope and developed the expertise that will be crucial for a marked gain in sensitivity, as envisioned with a NGAH.

The CAST experiment is the most powerful axion helioscope ever constructed. It has provided the best experimental limit on $g_{a\gamma}$ for a wide range of axion masses, up to ~ 1 eV. As the conversion magnet is the main driver of a helioscope's sensitivity, the CAST collaboration has harnessed the most advanced superconducting magnet technology of CERN. Specifically, CAST uses a decommissioned LHC test magnet that provides a magnetic field of 9 Tesla along its two parallel pipes of $2{\times}14.5$ cm^2 area and 10 m length, increasing the corresponding axion-photon conversion probability by a factor 100 with respect to the previous implementation of the helioscope concept [104]. The magnet is able to track the Sun for ~ 3 hours per day. The rest of the day is used for background measurements.

10.1. Figures of Merit

In this section we work out the dependence of the sensitivity to the axion couplings $g_{a\gamma}$ and g_{ae} (where g_{ae} is the dimensionless axion-electorn Yukawa coupling) on each of the experimental parameters, concentrating on the magnet parameters, in order to discuss the basis for our proposed improvements. The axion signal counts N_γ and background counts N_b in an enhanced axion helioscope can be written as: $N_\gamma \propto N^* \times g^4 \equiv B^2\, L^2\, A\, \epsilon\, t \times g^4$ and $N_b = b\, a\, \epsilon_t\, t$, where B, L and A are the magnet field, length and cross sectional area, respectively. The efficiency $\epsilon = \epsilon_d\, \epsilon_o\, \epsilon_t$, ϵ_d being the detectors' efficiency, ϵ_o the optics throughput or focusing efficiency (it is assumed the optics covers all the magnet cross section area A), and ϵ_t the data-taking efficiency, i. e. the fraction of time the magnet tracks the sun. Finally, b is the normalized (in area and time) background of the detector, a the total focusing spot area and t the duration of the data taking campaign. The relevant coupling constant g, is $g_{a\gamma}$ for hadronic axions and

$(g_{a\gamma}g_{ae})^{1/2}$ for non-hadronic axions.

Assuming that the measurement is dominated by backgrounds ($N_b > N_\gamma$) but these can be estimated and subtracted through independent measurements, the discovery potential of the experiment depends upon $N_\gamma/\sqrt{N_b}$. The sensitivity on the relevant coupling g will be given by $g \sim (N^*/\sqrt{N_b})^{-1/4}$. It is useful to rewrite the previous expression in terms of a figure of merit (FOM) $f \equiv N^*/\sqrt{N_b} = f_M\, f_{DO}\, f_T$, where we write f as a product of 3 factors to explicitly show the contributions of the various experimental parameters: magnet, detectors and optics and tracking (i.e. effective exposure time of the experiment)

$$f_M = B^2\, L^2\, A \qquad f_{DO} = \frac{\epsilon_d\, \epsilon_o}{\sqrt{b\, a}} \qquad f_T = \sqrt{\epsilon_t\, t}\ . \tag{10.2}$$

10.2. A New Magnet For the NGAH

We shall not elaborate here on f_{DO} and f_T, as these are not part of our scope. However, it was shown in [106] that the FOM clearly demonstrates the importance of the magnet parameters when computing the sensitivity of an axion helioscope. It is difficult to considerably increase the B or L parameters of CAST's magnet as 9 T is close to the maximum field one can get in current large-size magnets, while the length scale of 10 m is considerable for any structure that needs to be moved with precision.

Hence, the most significant improvement may come in the cross section area. Substantially larger cross sections, of up to several m^2, can be achieved, although one needs to consider a different magnet configuration. It is the motivation for our proposal that a new magnet must be designed and built specifically for this application, if one aims at a substantial step forward in sensitivity. These improvements could lead to sensitivities, in terms of detectable signal counts, up to 10^6 better than CAST, which corresponds to 1.5 orders of magnitude in g, as seen from the FOMs of equation (10.2).

All the above, corroborates the importance of the magnet for a competitive axion he-

lioscope. In order to achieve the stated step forward in sensitivity, the design and construction of a new magnet is mandatory. Moreover, accelerator dipole magnets, like the one CAST is currently using, have additional design constraints that are not required by a NGAH use, with the most important constraint being the extraordinary quality of the magnetic field (i.e. the field is required to be extremely uniform within the accelerator's aperture). Of course, the design of the new magnet must be done with the FOM for an NGAH in mind already at the design stage. We have seen that the magnet's aperture is the only parameter left that can be significantly enhanced and thus our design of the magnet focuses on it. We must stress that the use of x-ray optics at the end of the magnet's bore allows the enlargement of the magnet's aperture do enhance the expected signal without necessarily implying an increased background. Indeed, as was shown before, the overall FOM of the axion helioscope is proportional to the magnet bore area $f \propto A$ (which means that the sensitivity to the coupling constant goes as $g_{\alpha\gamma} \propto A^{-1/4}$). It should also be noted here that only the perpendicular components of B, with respect to the axion beam momentum, will contribute to the conversion probability.

11. THE NGAH MAGNET

The previous analysis corroborates the importance of the magnet for a competitive axion helioscope. As previously anticipated, in order to achieve the stated step forward in sensitivity, the design and construction of a new magnet is mandatory. Of course, this must be done with the FOM for an NGAH in mind already at design time. The latest magnet technology allows for the magnetic strength and length to be improved with respect to CAST. However, the needed margin for the required improvement in the magnet FOM can still not be reached. Therefore, the magnet's aperture is the only parameter left that can be significantly enhanced and thus we shall base our possible magnet design by concentrating on it. We must stress that thanks to the use of X-ray optics at the end of the magnet bore, the enlargement of the magnet aperture do

imply an enhancement of the expected signal without necessarily implying an increase of background. Indeed, as was shown before, the overall FOM of the axion helioscope goes directly proportional to the magnet bore area $f \propto A$ (which means that the sensitivity to the coupling constant goes as $g_{\alpha\gamma} \propto A^{-1/4}$). Needless to say, for this relation to hold, one assumes the optics size is enlarged accordingly to couple the magnet bore down to the stated focal spot size. It should also be noted here that the magnetic field B in an axion helioscope magnet must be perpendicular to the longitudinal (axion incoming) direction. More correctly, only the perpendicular components of B, with respect to the axion beam momentum, will contribute to the conversion probability.

Accelerator dipole magnets, like the one CAST is currently using (see Fig. 8), have additional design constraints that are not required by a NGAH use, with the most important constraint being the extraordinary quality of the magnetic field (i.e the field is required to be extremely uniform within the accelerator's aperture). Moreover, accelerator type magnets cannot reach apertures wide enough to improve the magnet FOM significantly. For example, a CAST like magnet with a 9 T magnetic field and 9.26 m length will need a 620 mm aperture ,which is clearly not achievable in the near future, in order to improve the relative FOM by a factor of just 100. However, by considering different designs of detector magnets (e.g the ATLAS and the AMS experiments), which are characterized by a very large volume and a lower field (compared to accelerator magnets), relaxing those constraints and, in principal, conceiving the magnet design from the beginning by addressing specifically our requirements, it seems feasible to reach the required FOM, in particular regarding apertures of up to several meters with rather intense fields.

A complete feasibility study is currently in progress to define the simplest magnet design that satisfies the requirements of a NGHA and optimizes the FOM within the use of current magnet technologies at CERN. In the light of the difficulties with achieving the required FOM by using an accelerator type magnets, this study concentrates on the approach of scaling an existing model of a detector magnet like, for example, ATLAS or AMS.

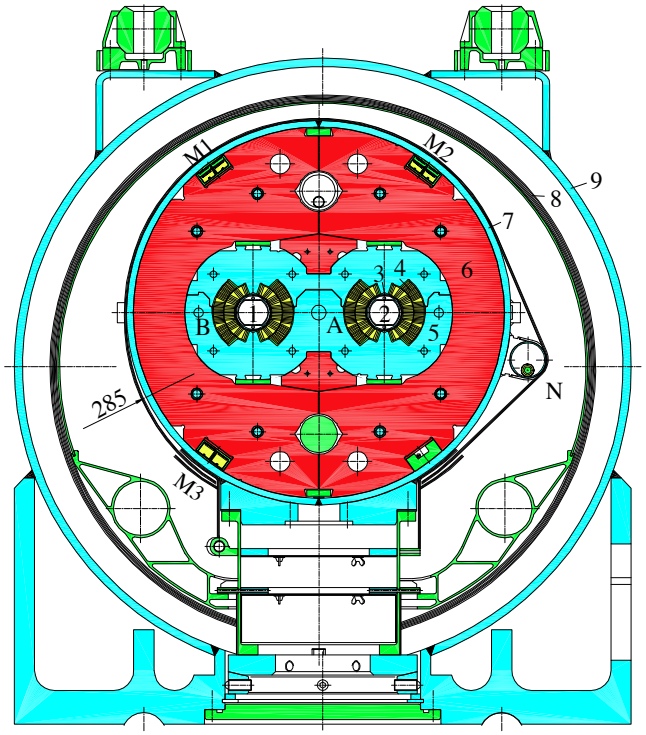

FIG. 8: A cross-section of the LHC main dipoles. 1: Aperture 1 (outer ring). 2: Aperture 2 (inner ring). 3: Cold-bore and beam screen. 4: Superconducting coil. 5: Austenitic steel collar. 6: Iron yoke. 7: Shrinking cylinder. 8: Super-insulation. 9: Vacuum vessel. M1-M3: Busbars for the powering of the main dipole and quadrupole circuits. N: Auxiliary busbar for the powering of arc-corrector magnets. CAST is currently using a twin dipole LHC magnet prototype with a design similar to the one shown here and with a total aperture of 2×15 cm^2. Courtesy of Stephan Russenschuck.

The ATLAS experiment at CERN is using an enormous central toroid magnet [107] (known as the barrel toroid) of 25.3 m in length with 20.1 m and 9.4 in outer and inner diameters, respectively (see Fig. 9) . This toroid has a peak field of 3.9 T at the coils which generates an average field of about 0.8 T in the useful aperture (that is, the aperture that would have been used for solar axions search) for a current of 20.5 kA. The NGAH can rely on this numbers and the barrel toroid design in order to scale it down and optimize it for axions search. Since the useful diameter for the optics detector is not more than 1 m, the NGAH has the advantage of having a smaller width and hence maintaining a higher useful field in the aperture. First considerations seem to favor a

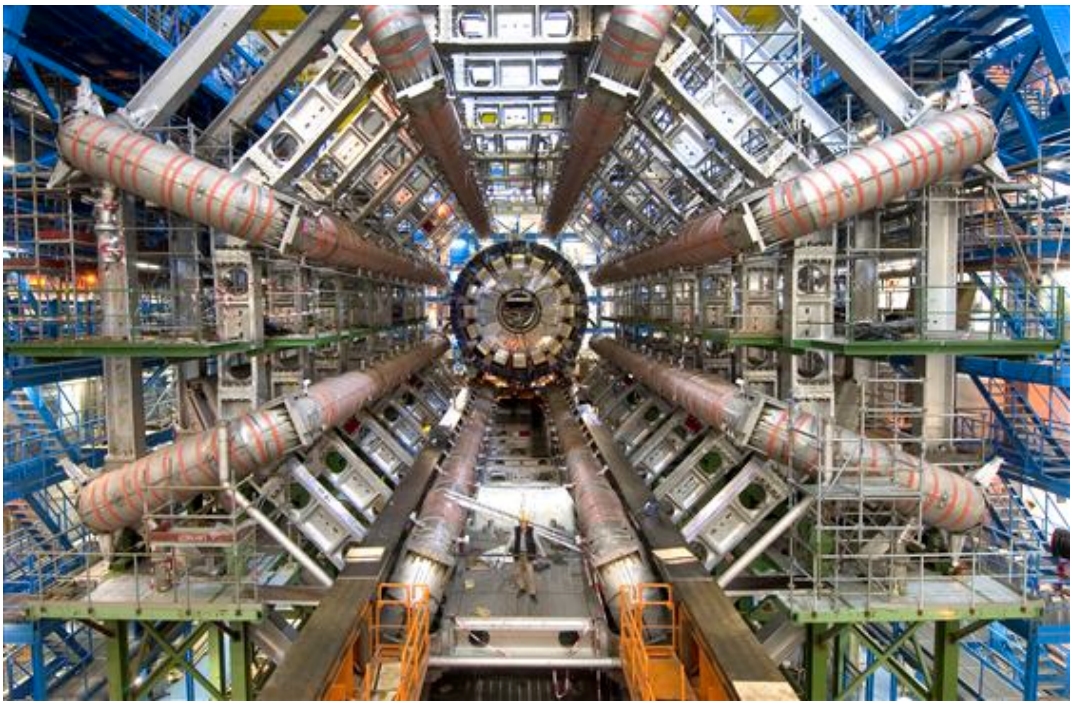

FIG. 9: The barrel toroid of the ATLAS experiment at CERN. The huge dimensions of the magnet can be appreciated by a comparison to the man standing at the bottom of the photo. The NGAH magnet's volume will be about 1-2 % of this enormous magnet. Courtesy of the ATLAS experiment.

configuration in which 8 vacuum bores, of relatively large size (0.5 - 1 m diameter), are placed between the coils and are available to couple optics and detectors. This configuration is demonstrated in Fig. 10, where a cross-section of the geometry is shown. The magnetic field in the bores, although not homogeneous, is largely perpendicular to the axion directions. With this type of configuration, it appears possible to reach a magnet length similar or somewhat longer than CAST (15 - 20 m), with B peak fields not much less (about 6 T) and a total effective cross section of around 1 - 3 m^2. The average field in the aperture (i.e the vacuum bores) is about 2.5 - 3 T, thus providing a FOM in the range of 100-350 relative to CAST, matching the requirements exposed in previous sections.

As mentioned above, also in this class of magnets is the super-conducting shielded dipole magnet design, which was designed by the AMS mission [108]. This NGAH design will have a dipole field in its center, where the dipole is surrounded by a 8 coils, semi-toroidal, geometry (see Fig. 11). The dipole bore can contain 6-8 apertures with an average field of about 1.5 T, while the peripheral shielding coils coils give additional 2 apertures with an average field of 2.5 - 3 T and 4 apertures (when using 4 shielding coils and not 6 as in the original AMS design) with an average field of 2.5 T. Overall, this geometry will not yield a higher FOM than the one that can be gained with the toroidal design and will also have the disadvantage of using more cable, which increases the overall costs of the NGAH. Moreover, another disadvantage of the AMS geometry is that it sustains higher stress than the ATLAS geometry since the toroidal geometry is self supported thanks to its symmetry. The bigger stress serves as an additional limitation on the maximal current and hence on the magnetic field.

Another option for the NGAH will be to consider a solenoidal magnetic field. These kind of magnets have the advantage of being the easiest to design and manufacture. However, since in a CAST like experiment the axion beam has to be perpendicular to the magnetic field, the solenoid must be transparent to x-ray photons, which limits the magnetic field strength and the radius of the solenoid and makes achieving the FOM goal very difficult.

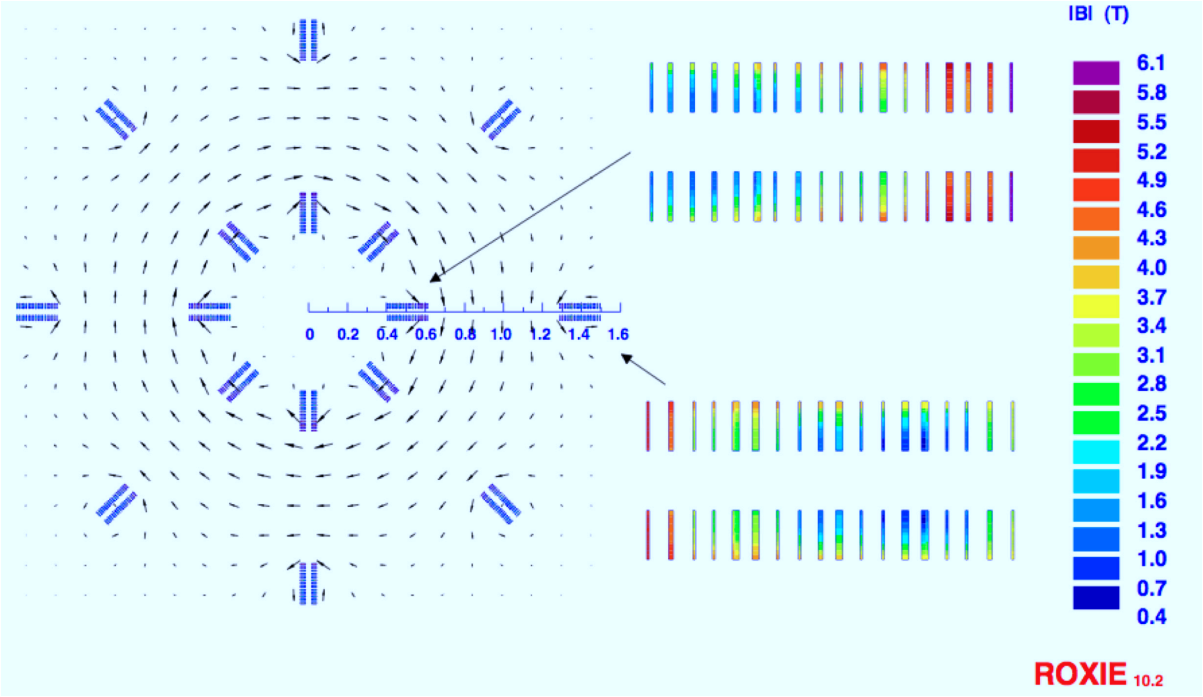

FIG. 10: An example for a possible toroidal NGAH magnet design. The cross-section of the toroidal magnet with 8 racetrack coils (with a double pancake configuration), where the magnetic field lines and the field modulus inside the coils are represented. In this possible design, the coils have a double layer geometry with 18 turns in each layer. The peak field is 6.1 T. This calculation was done with the CERN field computation program ROXIE 10.2 .

On top of that, a solenoid magnet with the parameters needed for the NGAH (i.e large diameter and very high field) will suffer from very large fringe fields which will restrict the possibility for easy approach and access to detectors, optics, cryogenics, etc.
The possibility of using a new and more advanced superconductor (SC) such as Nb3Sn

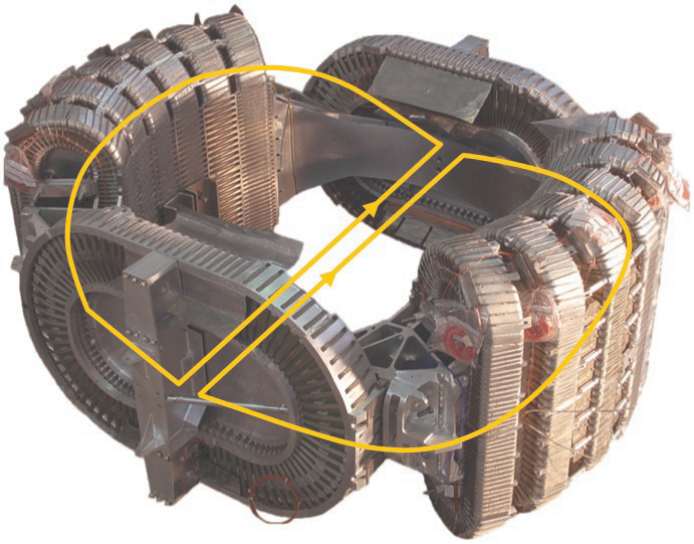

FIG. 11: The AMS superconducting magnet. The two largest coils generate the dipolar field while the 2 × 6 shielding coils close the magnetic flux and reduce considerably the fringe fields. Source: http://www.ams02.org/what-is-ams/tecnology/magnet/scmagnet/

was also considered. Nb3Sn may increase the magnetic (peak) field up to 15-16 T in an accelerator type magnet (for the same amount of SC). However, such an increase will double the stress applied to the coils, which is already close to the limit at the 9 T dipole. In addition, this material is about 5 times more expensive than NbTi and, moreover, these magnets are still in a R&D stage. The use of Nb3Sn has also a limitation since it is strain sensitive and very brittle. Thus, it practically ceases operating when the stress is above 150 MPa.

The major efforts when coming to engineer the NGAH magnet, will focus on the mechanical structure, cryogenics and (quench) protection of such a machine. Since the required increase of the present FOM is of a large factor, which will be challenging to achieve, the new design will have to stretch the limits of the design factors (i.e operating current, operational margin, cable design, inductance, etc.). Nonetheless, it will be more

efficient to follow known designs and by that reduce the need for building and designing new tooling and assembly machines.

In this context, it is important to emphasize that the NGAH magnet requires a very large aperture while still maintaining the highest possible magnetic field. To understand the difficulties in achieving this, two definitions are required: The so-called operational margin of the magnet and the magnet's load line (see Fig. 12).

For a superconducting magnet, the magnetic field is limited by the critical surface, which is determined by the properties of the superconducting material. This means that for a given temperature and current density there is a critical magnetic field limiting the superconducting performance. Hence, for the sake of proper magnet operation, the magnetic field should be low enough to avoid frequent quenching of the machine but, at the same time, for the efficiency and the purpose for which the machine is being built in the first place, the magnetic field should be as high as possible. This choice of the operating envelope of the magnet determines the operational margin of the magnet.

The operational margin is defined by means of the load line: For a given configuration of the magnet (at a constant temperature), the Bio-Savart law gives the (linear) relation between the current density J and the magnetic field strength B. This relation yields a straight line in the (B, J) phase space. The portion of this line, which extends from the origin of the (B, J) space to the critical surface is called the 'load line' of the magnet. In the magnet designers' jargon, it is common to refer to the operational margin by the so called percentage on the load line. For example, the operational margin of the LHC main dipoles is set at 20% on the load line [109]. This expression means that the magnet's operating values, namely the current density and the magnetic field, are those given by the point (called the magnet's working point) in the (B, J) phase space which will mark 0.8 of the magnet's load line length, for a given temperature (1.9 K for the LHC). The smaller the operational margin is, the closer the magnet is to its quench point.

Most detector type magnets usually work at lower fields and hence have a relatively large

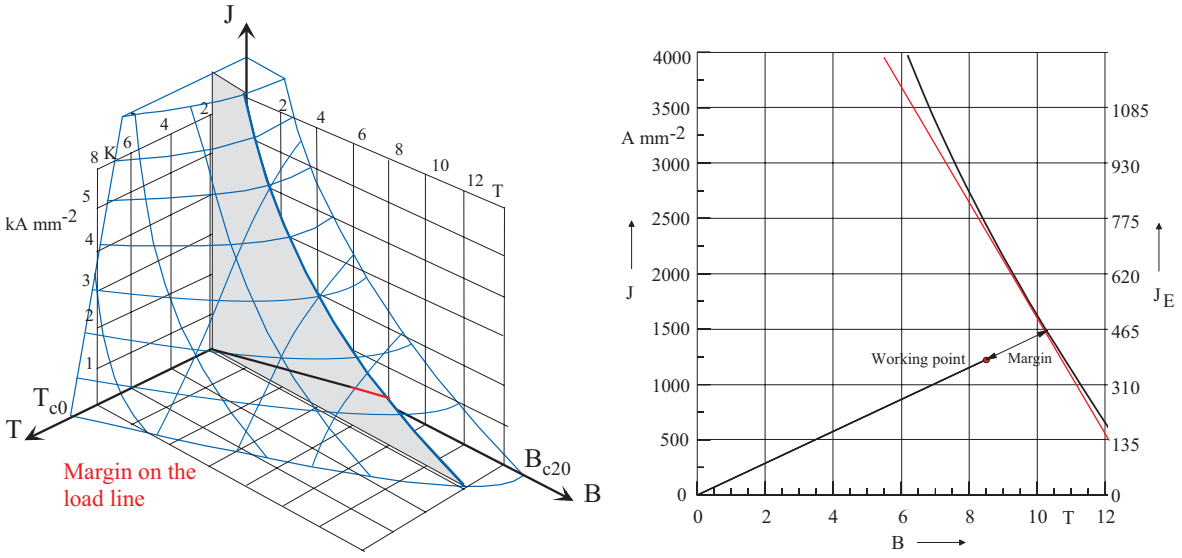

(a)Critical surface and load line.

(b)Critical current density and load line.

FIG. 12: Left: Critical surface of NbTi superconductor. Also shown are the load line (continuous straight line, divided to two parts). The operational margin at a constant temperature is the red portion of the load line, while the working point is at the end of the black portion of the load line. Right: Critical current density of NbTi at 1.9 K (black line), together with the linear approximation for the critical current density (red line), the load line and the working point. These images represent data taken from the LHC main dipoles. Courtesy of Stephan Russenschuck.

operational margin. However, as mentioned, the NGAH magnet will have to sustain the highest possible fields. Thus, the operational margin will inevitably be reduced and the NGAH will have to combine the protection techniques commonly used for both detector and accelerator magnets. Consequently, the protection of the NGAH magnet may be the most challenging part of the design.

An efficient magnet design will be the one which yields a load line with a slope as small as possible since the smaller the load line's slope is, the lower the current density needed

to generate a specific magnetic field. A possible way to increase the operational margin, for a given temperature, is by adding more SC to the magnet while at the same time reducing the current density. Thus, by increasing the number of current sources, the same field can be maintained for a lower current density. This can be done in two ways: the straightforward way will be to increase the number of turns in the coil, or more simply, using more cable. However, additional turns make the magnet's coil, and hence the cold mass (i.e the coils and their supporting structure) as well, bigger. Therefore, the resulting magnet will have an aperture bigger than the area that can be covered by the optics and this might result in a less efficient machine (depending on the gain in the magnetic field). Another way to increase the SC amount is to use larger strands in the cable and by that not effecting considerably the geometry of the magnet.

It is important to notice, however, that even increasing the amount of SC in the coils has a limited influence on the magnet's performance, since, at some point, adding more SC to the coil will increase the cost of the machine without adding significantly to its capabilities. Moreover, the magnetic field is always constrained by the critical field at zero current density, which is an internal property of the superconducting material.

For example, for a dipole magnet as the one used by CAST, the relation between the modulus of the magnetic field B to the critical current density J_c of the SC is given by [99]

$$B = \frac{\mu_0}{2}\lambda_{\text{tot}} J_c W \ , \tag{11.1}$$

where μ_0 is the vacuum permeability, λ_{tot} is the total superconducting filling factor (the ratio between the engineering current density to the critical current density) and W is the width of the coil. Using the linear approximation of the critical current density J_c for NbTi

$$J_c = d(\tilde{B}_{c2} - B) \ , \tag{11.2}$$

valid for the high field region (i. e. for magnetic fields larger than 5 T at 1.9 K and 2 T at 4.2 K) and for $\tilde{B}_{c2} > B$, where $d = -\frac{dJ_c}{dB}|_{\tilde{B}_{c2}}$ is the negative slope in the high field region of the critical surface at constant temperature and $\tilde{B}_{c2}$ is the critical field at zero current density according to the fit [110], we get the relation between the modulus of the magnetic field B and the critical field $\tilde{B}_{c2}$

$$B = \frac{\mu_0}{2}\lambda_{\mathrm{tot}}(\tilde{B}_{c2} - B)Wd \ . \tag{11.3}$$

By obtaining an expression for the width of the coil from the latter

$$W = \frac{2B}{\mu_0\lambda_{tot}d(\tilde{B}_{c2} - B)} \ , \tag{11.4}$$

one immediately notices that $W \to \infty$ as $B \to \tilde{B}_{c2}$. Therefore, when increasing the coil's width W the magnetic field B will rise and at the same time the critical current density ($J_c = (\tilde{B}_{c2} - B)d$) will have to be decreased (in order to stay below the critical surface). By linearity of the Bio-Savart law, this implies that the slope of the load line will be smaller.

From Eq. (11.3) we can also derive an explicit expression for the magnetic field

$$B = \frac{\frac{\mu_0}{2}\lambda_{tot}Wd}{1 + \frac{\mu_0}{2}\lambda_{tot}Wd}\tilde{B}_{c2} \ , \tag{11.5}$$

from which it is seen that the relations $\tilde{B}_{c2} > B$ and $\partial B/\partial W > 0$ hold for any $W > 0$. Hence, adding current sources to the coil will loose its efficiency at some point since the $B(W)$ curve is asymptotically approaching the limit value $\tilde{B}_{c2}$. Similarly, the same conclusions of the last paragraph hold for detector type magnets as well.

Work is still ongoing to further define the geometry, dimensions and final magnetic field strength, as well as the technical issues and cost. Preliminary results, however, indicate that the toroid geometry and design, inspired by ATLAS, is the favorable choice for

the NGAH. The toroid design seems to be the simplest and cheapest way to achieve the required FOM. Also, we can base most of the design on the existing and proven technology and the R&D that was carried out in order to be used in the ATLAS experiment. Moreover, there are certain points of this design option that represent important qualitative advantages with respect to the current CAST experience:

- The CAST magnet needs a heavy iron yoke around its bore and coils to let the magnetic field lines close, and by thus to prevent the field from leaking out of the magnet (i.e. fringe field). The coil arrangement in a toroidal geometry is such that they lead the field on a closed compact path and there is no need for an iron yoke. Hence, almost all the ?magnetic volume? produced by the magnet can effectively be used for axion conversion. This is not the case in the CAST magnet, in which part of the magnetic flux is lost for axion-detection purposes inside the iron yoke. This leads to a more efficient use of the magnet's strength.

- For the same reason (no need for an iron yoke), the weight of the magnet compared to its volume is much lower than in the current CAST magnet. For example, a toroid magnet will weight about 10 times more than the CAST magnet, but will have an effective useful volume (i.e volume used for data taking) of 700 - 1100 times (depending on the length) more than the twin dipoles of CAST.

- The cryogenics to cool down the superconducting coils are confined around the coils themselves, independent of the vacuum pipes (i.e the magnet's apertures) which lie in between the coils, thus leaving them at room temperature. This arrangement, unlike the CAST one in which the magnet bore was cooled down to cryogenic temperatures together with the coils, results in a more practical operation in several aspects: no big cryostat enclosing all the magnet, easier access to the magnet bores (pumps, sensors, etc.), no cryogenic pumping effects in the vacuum system, no need to use 3He in a possible second phase with buffer gas

(4He at room temperature can go to the required pressures, while in CAST 3He is needed as 4He would condense at 1.8 K).

[1] M.Y. Khlopov, *Cosmoparticle Physics*, (World Scientific, 1997).

[2] A. Vilenkin, *Cosmic strings and domain walls*, Phys. Rep. **121**, 263 (1985).

[3] W. Israel, *Singular hypersurfaces and thin shells in general relativity*, Nouvo Cimento **44B**, 1 (1966); **48B**, 463(E) (1967).

[4] S.K. Blau, E.I. Guendelman and A.H. Guth, *Dynamics of false vacuum bubbles*, Phys. Rev. **D 35**, 1747 (1987).

[5] S. Ansoldi, A. Aurilia, R. Balbinot and, E. Spallucci, *Effective dynamics of self-gravitating extended objects*, Phys. Essays **9**, 556 (1996); arXiv: gr-qc/9707001.

[6] A. Borde, M. Trodden and T. Vachaspati, *Creation and structure of baby universes in monopole collisions*, Phys. Rev. **D 59**, 043513 (1999); arXiv: gr-qc/9808069.

[7] E. Farhi, A. H. Guth and J. Guven, *Is it possible to create a universe in the laboratory by quantum tunneling?*, Nucl. Phys. **B339**, 417 (1990).

[8] E.I. Guendelman and A. Rabinowitz, *The gravitational field of a hedgehog and the evolution of vacuum bubbles*, Phys. Rev. **D 44**, 3152 (1991).

[9] For a general discussion about topological defects and inflation see: N. Sakai, H. Shinkai, T. Tachizawa and K. Maeda, *Dynamics of topological defects and inflation*, Phys. Rev. **D 53**, 655 (1996); **D 54**, 2981(E) (1996); arXiv: gr-qc/9506068.

[10] N. Sakai, K. Nakao, H. Ishihara and M. Kobayashi, *The universe out of a monopole in the laboratory?* Phys. Rev. D **74** ,024026 (2006); arXiv: gr-qc/0602084.

[11] E.I. Guendelman and J. Portnoy, *The universe out of an elementary particle?* Class. Quant. Grav. **16**, 3315 (1999); arXiv: gr-qc/9901066.

[12] A. Davidson and E.I. Guendelman, *Electric monopole with internal magnetic monopole-like structure*, Phys. Lett. **B 251**, 250 (1990).

[13] K. Kuchar, Czech. J. Phys. B **18**, 435 (1968).

[14] A.T. Barnaveli and M.Ya. Gogberashvili, *Antigravitating bubbles with the non-*

Minkowskian asymptotics, Theor. and Math. Phys. **113**, 2 (1997).

[15] A. Einstein, *Do gravitational fields play an essential part in the structure of the elementary particles of matter?* Sitzungsber. Preuss. Akad. Wiss. Berlin (Math.Phys.) **1919**, 433 (1919).

[16] P.A.M. Dirac, *An Extensible model of the electron*, Proc. Roy. Soc. Lond. **A 238**, 57 (1962).

[17] A. Davidson and U. Paz, *Threefold family of charged spin 1/2 Dirac bubbles*, Phys. Lett. B **300**, 234 (1993).

[18] S. Coleman, *The Fate of the False Vacuum. 1. Semiclassical Theory*, Phys. Rev. D **15**, 2929 (1977).

[19] J.C.G Callan and S. Coleman, *The Fate of the False Vacuum. 2. First Quantum Corrections*, Phys. Rev. D **16**, 1762 (1977).

[20] S. Coleman and F. De Luccia, *Gravitational Effects on and of Vacuum Decay*, Phys. Rev. D **21**, 3305 (1980).

[21] K. Sato, M. Sasaki, H. Kodama and K. Maeda, *Creation of Wormholes by First-Order Phase Transition of a Vacuum in the Early Universe*, Progr. Theor. Phys. **65**, 1443 (1981).

[22] H. Kodama, M. Sasaki, K. Sato, and K. Maeda, *Fate of Wormholes Created by First-Order Phase Transition in the Early Universe*, Progr. Theor. Phys. **66** 2052 (1981).

[23] H. Kodama, M. Sasaki and K. Sato, *Abundance Of Primordial Holes Produced By Cosmological First Order Phase Transition*, Progr. Theor. Phys. **68**, 1979 (1982).

[24] K. Sato, H. Kodama, M. Sasaki and K. Maeda, *Multiproduction Of Universes By First Order Phase Transition Of A Vacuum*, Phys. Lett. B **108**, 103 (1982).

[25] A. Tomimatsu, *Collapse of wormhole space and the baby universe production*, Mod. Phys. Lett. A **6** 1535 (1991).

[26] For a review see: S. Coleman, *The Magnetic Monopole, 50 Years Later*, in unity of Fundamental Interactions, Proc. of *the International school of Subnuclear Physics*, Erice,

1981; ed. A. Zichichi (Plenum, New York, 1983).

[27] C.W. Misner, K.S. Thorne and J.A. Wheeler, *Gravitation* (Freeman, San Francisco, 1973).

[28] S. Ansoldi, E.I. Guendelman and I. Shilon, *Stability, Singularities and Mass Thresholds in Child Universe Production*, Proceedings of *BH2, Dynamics and Thermodynamics of Black Holes and Naked Singularities*, Milano, Italy (2007). arXiv: 0711.2198 [gr-qc].

[29] V.A. Berezin, V.A. Kuzmin, and I.I. Tkachev, *Dynamics of bubbles in general relativity*, Phys. Rev. D **36** 2919 (1987).

[30] S. Ansoldi, Proccedings of *From quantum to emergent gravity: theory and phenomenology*, Trieste, Italy (2007).

[31] S. W. Hawking, *Occurrence of singularities in open universes*, Phys. Rev. Lett., **15** 689 (1965).

[32] S. W. Hawking, *The occurrence of singularities in cosmology*, Proc. Roy. Soc. Lon. A **294** 511 (1966).

[33] S. W. Hawking, *The occurrence of singularities in cosmology. II*, Proc. Roy. Soc. Lon. A **295** 490 (1966).

[34] S. W. Hawking, *The occurrence of singularities in cosmology. III. Causality and singularities*, Proc. Roy. Soc. Lon. A **300** 187 (1967).

[35] S. W. Hawking and R. Penrose, *The singularities of gravitational collapse and cosmology*, Proc. Roy. Soc. Lon. A **314** 529, (1970).

[36] S.W. Hawking and G.F.R. Ellis, *The Large Scale Structure of Space-Time* (Cambridge University Press, 1973).

[37] R. M. Wald, *General Relativity* (The University of Chicago Press, 1984).

[38] E. Farhi and A. A. Guth, *An obstacle to creating a universe in the laboratory*, Phys. Lett. B **183** 149 (1987).

[39] E.I. Guendelman and Idan Shilon, *Stabilization of neutral thin shells by gravitational effects from electric fields*, Class. Quantum Grav. **26** 045007 (2009).

[40] E.W. Kolb, *A coasting cosmology*, Astroph. J. **344**, 543 (1989).

[41] S. Alexander, R.H. Brandenberger and D. Easson, *Brane gases in the early universe*, Phys. Rev. D **62**, 103509 (2000).

[42] S. Ansoldi, *Vacuum and semiclassical gravity: a difficulty and its bewildering significance*, PoS(QG-Ph), 004 (2007); arXiv: 0709.2741 [gr-qc].

[43] For another example of breathing bubble see: E.I. Guendelman and N. Sakai, *The universe out of a breathing bubble*, Phys. Rev. D **77**, 125002 (2008); arXiv: 0803.0268 [gr-qc].

[44] J. Kijowski, G. Magli ang D. Malafarina, Gen. Rel. Grav. **38**, 1697 (2006).

[45] S. Ansoldi and E.I. Guendelman, *Universes out of almost empty space*, Prog. Theor. Phys. **120**, 985 (2007); arXiv: 0706.1233 [gr-qc].

[46] E.I. Guendelman, *Child universes UV regularization?*, Int. J. Modern Physics D **17** (2008); arXiv: gr-qc/0703105.

[47] R. D. Peccei and H. R. Quinn, *CP Conservation in the Presence of Pseudoparticles*, Phys. Rev. Lett. **38**, 1440 (1977).

[48] R. D. Peccei and H. R. Quinn, *Constraints Imposed By CP Conservation in the Presence of Pseudoparticles*, Phys. Rev. D **16**, 1791 (1977).

[49] S. Weinberg, *A New Light Boson?*, Phys. Rev. Lett. **40**, 223 (1978).

[50] F. Wilczek, *Problem of Strong p and t Invariance in the Presence of Instantons*, Phys. Rev. Lett. **40**, 279 (1978).

[51] R.D. Peccei, *The strong CP problem and axions*, Lect. Notes Phys. **741**, 3 (2008); arXiv: [hep-ph/0607268].

[52] J. E. Kim and G. Carosi, *Axions and the strong CP problem*, Rev. Mod. Phys. **82**, 557 (2010); [arXiv:0807.3125].

[53] G. G. Raffelt, *Astrophysical axion bounds*, Lect. Notes Phys. **741**, 51 (2008); arXiv: [hep-ph/0611350].

[54] P. Sikivie, *Axion cosmology*, Lect.Notes Phys. **741**, 19 (2008); arXIv: [astro-ph/0610440].

[55] O. Wantz and E. P. S. Shellard, *Axion Cosmology Revisited*, Phys. Rev. D **82**, 123508

(2010); [arXiv:0910.1066].

[56] P. Sikivie, *Experimental tests of the "invisible" axion*, Phys. Rev. Lett. **51**, 1415 (1983); *Detection rates for "invisible" axion searches*, Phys. Rev. D **32**, 2988 (1985) [Erratum ibid. D 36 (1987) 974]

[57] G. Raffelt and L. Stodolsky, *Mixing of the photon with low mass particles*, Phys. Rev. D **37**, 1237 (1988).

[58] M.E. Peskin and D.V. Schroeder, *An Introduction to quantum field theory* (Westview Press, 1995).

[59] S. Adler and W.A. Bardeen, *Absence of higher order corrections in the anomalous axial vector divergence equation*, Phys. Rev. **182**, 1517 (1969); S. Adler, in Deser et. al. (1970).

[60] G. 't Hooft, *Symmetry Breaking Through Bell-Jackiw anomalies*, Phys. Rev. Lett. **37**, 8 (1976).

[61] G. 't Hooft, *Computation of the Quantum Effects Due To a Four-dimensional Pseudoscalar*, Phys. Rev. D **14**, 3432 (1976); E. ibid. D **18**, 2199 (1978).

[62] R.J. Crewther, *Effects Of Topological Charge In Gauge Theories*, Acta Phys. Austriaca Suppl. **19**, 47 (1978).

[63] C.P. Burgess and Guy D. Moore, *The Standard Model: A Primer*, (Cambridge University Press, 2007).

[64] C.A. Baker et. al. *An Improved Experimental Limit On the Electric Dipole Moment of the Neutron*, Phys. Rev. Lett. **97**, 131801 (2006); arXiv: [hep-ex/0602020].

[65] J.E. Kim, *Light pseudoscalars, particle physics and cosmology*, Phys. Rep. **150** (1-2):1-177, (1987).

[66] W.A, Bardeen, S.H. Tye and J.A.M. Vermaseren, *Phenomenology of the New Light Higgs Boson Search*, Phys. Lett. B **76**, 580 (1978).

[67] W.A. Bardeen, R.D. Peccei and T. Yanagida, *Constraints On Variant Axion Models*, Nucl. Phys. B **279**, 401 (1987).

[68] J.E. Kim, *Weak Interaction Singlet and Strong CP invariance*, Phys. Rev. Lett. **43**, 103

(1979).

[69] M.A. Shifman, A.I. Vainshtein and V.I. Zakharov, *Can Confinement Ensure Natural CP Invariance of Strong Interactions?*, Nucl. Phys. B **166**, 493 (1980).

[70] M. Dine, W. Fischler and M. Srednicki, *A Simple Solution To the Strong CP Problem With a Harmless Axion*, Phys. Lett. B **104**, 199 (1981).

[71] A.R. Zhitnisky, *On Possible Suppression of the Axion Hadron Interactions*, Sov. J. Nucl. Phys. **31**, 260 (1980); (Yad. Fiz. **31**, 497 (1980).

[72] Particle Data Group Collaboration, K. Nakamura et. al., J. Phys. G **G37**, 075021 (2010).

[73] G.G. Raffelt, *Stars As Laboratories for Fundamental Physics*, (Chicago University Press, Chicago 1996).

[74] M.S. Turner, *Windows on the Axion*, Phys. Rept. **197**, 67 (1990).

[75] J. Isern, E. Garcia-Berro, L. Althaus, and A. Corsico, *Axions and the pulsation periods of variable white dwarfs revisited*, Astron. Astrophys. **512** (2010), no. A86 86, [arXiv:1001.5248].

[76] J. Isern, M. Hernanz, and E. Garcia-Berro, *Axion cooling of white dwarfs*, Astrophys.J **392** (1992) L23.

[77] J. Isern, E. Garcia-Berro, S. Torres, and S. Catalan, *Axions and the cooling of white dwarf stars*, arXiv:0806.2807.

[78] J. Isern, S. Catalan, E. Garcia-Berro, and S. Torres, *Axions and the white dwarf luminosity function*, J.Phys.Conf.Ser. **172** (2009) 012005, [arXiv:0812.3043].

[79] E.I. Guendelman, *Continuous axion photon duality and its consequences*, Mod. Phys. Lett. A **23** 191 (2008), arXiv: 0711.3685 [hep-th]; E.I. Guendelman, *Localized Axion Photon States in a Strong Magnetic Field*, Phys. Lett. B **662** 227 (2008), arXiv: 0801.0503 [hep-th].

[80] E.I. Guendelman, *Photon and Axion Splitting in an Inhomogeneous Magnetic Field*, Phys. Lett. B **662**, 445 (2008); arXiv: 0802.0311 [hep-th].

[81] D. Chelouche and E.I. Guendelman, *Cosmic Analogues of the Stern-Gerlach Experiment*

and the Detection of Light Bosons, Astrophys. J. **699**, L5 (2009); arXiv: 0810.3002 [astro-ph].

[82] E.I. Guendelman and I. Shilon, *Axions and Photons In Terms of "Particles" and "Anti-Particles"*, arXiv: 0808.2572 [hep-th] (2008).

[83] W. Gerlach, O. Stern, *Experimental proof of the magnetic moment of the silver atom*, *Z. Phys.* **8**, 110 (1922); W. Gerlach, O. Stern, *Experimental test of the applicability of the quantum their to the magnetic field*, *Z. Phys.* **9**, 349 (1922).

[84] E.I. Guendelman, I. Shilon, G. Cantatore and K. Zioutas, *Photon production from the scattering of axions out of a solenoidal magnetic field*, JCAP **06**, 031 (2010); arXiv: 0906.2537 [hep-ph].

[85] Y. Inoue, Y. Akimoto, R. Ohta, T. Mizumoto, A. Yamamoto and M. Minowa, *Search for solar axions with mass around 1 eV using coherent conversion of axions into photons*, Phys. Lett. B **668** 93 (2008); arXiv: astro-ph/0806.2230.

[86] CAST Collaboration, E. Arik et. al., *Probing eV-scale axions with CAST*, JCAP **02**, 008 (2009); [arXiv:0810.4482].

[87] K. van Bibber, P.M. McIntyre, D.E. Morris and G.G. Raffelt, *A Practical Laboratory Detector For Solar Axions*, Phys. Rev. D **39** 2089 (1989). See also: R. Rabadan, A. Ringwald, K. Sigurson, Phys. Rev. Lett. **96** 110407 (2006).

[88] G.G. Raffelt, *Stars as Laboratories For Fundamental Physics* (The University of Chicago Press, Chicago, 1996).

[89] K. van Bibber, N.R. Dagdeviren, S.E. Koonin, A.K. Kerman and H.N. Nelson, *Proposed experiment to produce and detect light pseudoscalars*, Phys. Rev. Lett. **59** 759 (1987).

[90] R.D. Woods and D.S. Saxon, *Diffuse Surface Optical Model for Nucleon-Nuclei Scattering*, Phys. Rev. **95** 577 (1954).

[91] A. Mirizzi, G.G. Raffelt and P.D. Serpico, *Signatures of axion-like particles in the spectra of TeV gamma-ray sources*, Phys. Rev. D **76**, 023001 (2007) [arXiv:0704.3044]; D. Hooper and P.D. Serpico, *Detecting axion-like particles with gamma ray telescopes*, Phys.

Rev. Lett. **99**, 231102 (2007) [arXiv:0706.3203]; M. Simet, D. Hooper and P.D. Serpico, *The milky way as a kiloparsec-scale axionscope*, Phys. Rev. D **77**, 063001 (2008) [arXiv:0712.2825] [SPIRES].

[92] S.L. Adler, J. Gamboa, F. Mendez and J. Lopez-Sarrion, *Axions and 'Light Shining Through a Wall': A Detailed Theoretical Analysis*, Annals. Phys. **323** 2851 (2008); arXiv:0801.4739 [hep-ph].

[93] P.W. Milonni, *Fast Light, Slow Light and Left-Handed Light* (IOP publishing, London, 2005).

[94] R.A. Shelby, D.R. Smith and S. Schultz, Science **292** 77 (2001).

[95] K. Zioutas, M. Tsagri, Y. Semertzidis, T. Papaevangelou, T. Dafni and V. Anastassopoulos, *Axion Searches with Helioscopes and astrophysical signatures for axion(-like) particles*, New J. Phys. **11** 105020 (2009).

[96] Eduardo I. Guendelman, Shay Leizerovitch and Idan Shilon, *Axions scattering from a quadrupole magnetic field*, Int. J. of Mod. Phys. A **27**, 3n04 (2012); arXiv:1010.4239 [hep-ph].

[97] Charles J. Joachain, *Quantum Collision Thoery*, North Holland, Amsterdam, Holland (1975).

[98] F. W. Byron Jr. and C. J. Joachain, Physica **66** 33 (1973).

[99] For details on magnetic field harmonics see: S. Russenschuck, *Field Computation for Accelerator Magnets*, Wiley-VCH, Weinheim, Germany (2010).

[100] J. Redondo, *Photon-Axion conversions in transversely inhomogeneous magnetic fields*, Proceedings of Durham 2009, Patras Workshop on Axions, WIMPs and WISPs; arXiv: 1003.0410 [hep-ph].

[101] D. M. Lazarus et. al., *A Search for solar axions*, Phys. Rev. Lett. **69** (1992) 2333.

[102] S. Moriyama et. al., *Direct search for solar axions by using strong magnetic field and X-ray detectors*, Phys. Lett. B **434** (1998) 147, [hep-ex/9805026].

[103] K. Zioutas et. al., *A decommissioned LHC model magnet as an axion telescope*, Nucl.

Instrum. Meth. A **425** 480 (1999); arXiv: astro-ph/9801176.

[104] CAST Collaboration, K. Zioutas et. al., *First results from the CERN Axion Solar Telescope (CAST)*, Phys. Rev. Lett. **94** (2005) 121301, [hep-ex/0411033].

[105] CAST Collaboration, S. Andriamonje et. al., *An improved limit on the axion-photon coupling from the CAST experiment*, JCAP 0704 (2007) 010, [hep-ex/0702006].

[106] Igor G. Irastorza et. al., *Towards a new generation axion helioscope*, JCAP **06**, 013 (2011); arXiv: 1103.5334.

[107] The ATLAS collaboration , *ATLAS Manget System: Technical Design Report*, ATLAS TDR 06, CERN/LHCC 97-18 (1997).

[108] B. Blau *et al.*, *The superconducting magnet system of AMS-02 - a particle physics detector to be operated on the International Space Station*, IEEE Trans. Applied Superconductivity **12**, 349 (2002).

[109] O. Brüning, P. Collier, P. Lebrun, S. Myers, R. Ostojic, J. Poole and P. Proudlock, *LHC Design Report*, CERN-2004-003-V-1 (2004).

[110] L. Rossi and E. Todesco, *Electromagnetic design of superconducting dipoles based on sector coils*, Phys. Rev. ST AB **10**, 112401 (2007).